Blood Biochemical Responses to Acute Exercise: Findings from the Molecular Transducers of Physical Activity Consortium (MoTrPAC)

Jeremy M. Robbins, MD[1,2,*†], Daniel H. Katz, MD[3*], Gina M. Many, PhD[4*], Prashant Rao, MD[1,2*], Gregory R. Smith, PhD[5*], Gaurav Tiwari, MS[2], Christopher Jin, BS[3], Guillaume Spielmann, PhD[6], Samuel Montalvo, PhD[3], Gayatri Iyer, PhD[7], David Amar, PhD[3], Damon Leach, MS[4], Brian J. Coyne, MEd[8], Malene E. Lindholm, PhD[3], Bret Goodpaster, PhD[9], Martin J. Walsh, PhD[10], Clary B. Clish, PhD[11], Charles F. Burant, MD, PhD[12**], Robert E. Gerszten, MD[1,2,11**†], MoTrPAC Study Group

[1]Division of Cardiovascular Medicine, Beth Israel Deaconess Medical Center, Boston, MA;

[2]CardioVascular Institute, Beth Israel Deaconess Medical Center, Boston, MA;

[3]Department of Medicine, Stanford University School of Medicine, CA;

[4]Biological Sciences Division, Pacific Northwest National Laboratory, Richland, WA;

[5]Department of Neurology, Icahn School of Medicine at Mount Sinai, NY;

[6]Department of Kinesiology, Louisiana State University, Baton Rouge, LA;

[7]Department of Computational Medicine and Bioinformatics, University of Michigan, Ann Arbor, MI;

[8]Division of Cardiology, Department of Medicine, Duke University School of Medicine, Durham, NC;

[9]Translational Research Institute, AdventHealth, Orlando, FL;

[10]Department of Pharmacological Sciences, Icahn School of Medicine at Mount Sinai, New York, NY

[11]Broad Institute of MIT and Harvard, Cambridge, MA;

[12]Division of Metabolism, Endocrinology, and Diabetes, Department of Internal Medicine, University of Michigan, Ann Arbor, MI.

*; ** These authors contributed equally

†Corresponding Authors:
Jeremy M. Robbins, MD,

Robert E. Gerszten, MD,
Division of Cardiovascular Medicine
Beth Israel Deaconess Medical Center,
185 Pilgrim Road,
Boston, MA 02215
Email: jrobbin1@bidmc.havard.edu
Email: rgerszte@bidmc.harvard.edu

Abstract: Exercise benefits numerous organ systems and tissues, however limited knowledge exists about its underlying molecular pathways. Identifying the exercise-induced biochemical changes that occur in the circulation may provide further insights into how exercise confers systemic health changes. Here, we perform large-scale plasma proteomic, metabolomic, and whole blood transcriptional profiling in sedentary human participants undergoing acute endurance exercise (EE), resistance exercise (RE), or a non-exercise control (CON) in up to 7 timepoints over a 24 hour period. We observe 7066 transcript, 189 protein, and 448 metabolite changes in response to EE or RE compared to CON. Our analyses reveal numerous shared biochemical responses between EE and RE modes, but also differences in immune cell responses, lipid metabolism, and pathways reflective of tissue repair and angiogenesis. Taken together, our findings highlight novel temporal and exercise mode-specific blood-based molecular responses to acute exercise, and provide a new resource for the scientific community.

Keywords: exercise physiology; multi-omics; skeletal muscle; adipose tissue; biomarkers; endurance exercise; resistance exercise; physical activity; proteomics; metabolomics; transcriptomics; exerkines; systems biology; precision medicine; acute exercise response; molecular mechanisms; cross-tissue analysis

Introduction:

Exercise's health benefits are uniquely expansive, leading to improvements in cardiorespiratory fitness (CRF) and metabolism, muscle strength, mood and cognition, healthy aging, and a lower risk of chronic diseases including cancer, obesity, diabetes and cardiovascular disease.[1-7] It is unsurprising then, that exercise is among the most robust physiologic stimuli, affecting a network of cellular processes and organ systems spanning the cardiovascular, pulmonary, musculoskeletal, neurologic, and endocrine systems among others.[8, 9] While exercise is widely regarded as beneficial, its effects are heterogeneous and vary according to both its exposure (i.e., mode and duration of exercise) as well as host factors such as age, training background, nutritional status, and the presence or absence of underlying pathologic conditions. Furthermore, there is increasing recognition that genetic and genomic heterogeneity play a role in inter-individual differences in the response to exercise.[10, 11] Despite this, our understanding of the biochemical pathways that underlie the physiologic effects of exercise and exercise-response traits is incomplete, providing strong rationale to investigate its molecular transducers, a principal goal of the Molecular Transducers of Physical Activity Consortium (MoTrPAC).[12]

The blood as a "highway" of whole-body physiology is particularly relevant to the study of how exercise mediates its systemic effects through inter-organ cross-talk. Indeed, exercise induces widespread molecular changes even in tissues not directly involved in locomotor activity.[9] These concepts are underscored by the emerging paradigm of "exerkines", or exercise-stimulated soluble biochemicals that can act in autocrine, paracrine, or endocrine fashion to confer exercise's health benefits.[13, 14] A growing list of small molecule metabolites, lipids, peptides and nucleic acids in the plasma have been identified as candidate exerkines,[15-24] yet even among these known biochemicals there is limited knowledge about their temporal changes during acute exercise, their responses to distinct exercise modes, and their tissue source(s). While the exerkine paradigm reflects beneficial actors, exercise can also improve health through the downregulation or increased clearance of deleterious, circulating factors - an understudied area of investigation.[25] In addition to its application in studying exercise's integrative physiology, molecular profiling in the blood offers a practical means to identify biochemical signatures of a health or disease state. Prior works have shown that blood-based signatures can identify differential health responses to an exercise intervention,[26] reflect CRF,[27, 28] and that these signatures may in turn predict long-term human health outcomes.[29] Prior studies leveraging blood biochemical profiling have used either a lone molecular profiling method, focused on either a select group of analytes, a single time point and/or an individual exercise mode, or have

lacked a non-exercise control arm, motivating a more comprehensive, multi-omic examination of blood in response to exercise that leverages a control group.[28, 30-34]

Here, we describe large-scale whole-blood transcriptomic, plasma proteomic and metabolomic profiling in well-phenotyped sedentary adults from the MoTrPAC study to characterize the multi-omic responses to acute exercise in the circulation. We compare and contrast biochemical responses to bouts of endurance exercise (EE) and resistance exercise (RE) at up to 7 different time points over the course of 24 hours using a non-exercise control (CON) group to rigorously isolate the effects of exercise from those driven by time of day, fasting, and biospecimen collection. We further integrate the biochemical responses across the three profiling techniques and relate blood-based biochemical features across a range of cardiorespiratory, muscle strength and metabolic phenotypes assessed in MoTrPAC.

Results:

Research design and clinical characteristics

A total of 175 sedentary adult participants underwent baseline clinical phenotyping and blood biochemical profiling during and after an acute bout of endurance or resistance exercise or a control period of non-exercise and are included in this study. The individuals were enrolled prior to suspension of MoTrPAC enrollment due to the SARS-CoV-2 pandemic and are further detailed here (*Clinical Landscape*, in submission, REF). A detailed description of the human studies design and protocol including group assignment, exercise familiarization protocols, clinical phenotyping, biospecimen collection, and acute exercise sessions has been published.[35] Briefly, healthy but sedentary participants were randomized to endurance exercise (EE), resistance exercise (RE), and non-exercise control (CON) arms. EE subjects underwent a 40-minute exercise session using cycle ergometry at a power output estimated to elicit ~65% VO_2peak, and RE subjects underwent eight upper and lower body exercises, each for 3 sets of 8-12 repetitions to volitional fatigue. CON participants did not perform exercise but underwent the same biospecimen collection as the EE group. Prior to the acute exercise bouts, both EE and RE underwent 2 and 3 exercise familiarization sessions, respectively, to establish the appropriate exercise workloads for each participant's exercise session. The blood biospecimen sampling schedule by group assignment is shown in **Figure 1A.** Participants also underwent skeletal muscle and adipose tissue sampling before and after exercise; the analysis of data from

these tissues is presented elsewhere (*Multi-Omic Landscape, Skeletal Muscle companion, Adipose tissue companion, Clinical Landscape*, all in submission, REF).

The number of participants who underwent molecular profiling varied across each -ome due to study interruption from the SARS-CoV-2 shutdown. Nearly all participants underwent plasma metabolomic and blood transcriptomic profiling (N=175 and 173, respectively), whereas 44 participants underwent plasma proteomic profiling using Olink® technology. The clinical characteristics of the full cohort as well as those profiled by each -omic method are described in **Table 1** and **Supplemental Table 1 (Table S1)**, respectively. The mean age and BMI of the full cohort was 41±15 years and 26.9±4.0 kg/m^2, respectively, and 72% were female. The majority of participants achieved a maximal effort during cardiopulmonary exercise testing (CPET): the peak respiratory exchange ratio was 1.16±0.08. Peak maximal oxygen uptake (VO_2peak) was 24±7 $ml*kg^{-1}*min^{-1}$. Descriptive characteristics by sex are shown in **Table S2**.

A total of 23,082 analytes across antibody-based plasma proteomics (N=1,417 proteins), liquid-chromatography mass spectrometry (LC-MS)-based plasma metabolomics (N=1,141 plasma metabolites across 4 targeted and 6 untargeted platforms) and transcriptomics from PAXgene whole blood (N=20,524 transcripts) were included for analyses after quality control and data annotation (detailed in **STAR Methods**). Differential abundance (DA) analysis identified molecular features that are differentially regulated by EE or RE compared to CON. We identified 7703 unique features that changed in the plasma or blood at any time point after acute exercise, including 7066 blood transcripts (34% of platform), 189 plasma proteins (13%), and 448 plasma metabolites (39% of the annotated features across the multiple platforms). After excluding features that were differentially abundant at 20 or 40 minutes during EE (as only this mode underwent sampling during exercise due to experimental feasibility), a greater number of features were found to be differentially regulated by RE compared to EE across the 3 plasma/blood -omes (2644 versus 349 features for RE versus EE, respectively, with 2945 shared DA features; **Figure 1C and S1A**). The number of overlapping, DA features between EE and RE by each -ome across all time points are shown in the UpSet plots in **Figure 1D** and further discussed in each -omic section below; overlap among each -ome and mode at the individual time points is shown in **Figure S1A**. Notably, there were numerous plasma protein, metabolite, and blood transcript changes that occurred within the CON group over the 24 h period (**Figure S1B**). CON changes in the plasma and blood featured analytes that likely reflect a combination of factors, including fasting effects (e.g., plasma IL-6 increases at 3.5 hours[36];

decreases in triglycerides) and responses from the biopsy collections (e.g., increases in monoethylglycinexylidide, a lidocaine derivative; **Figures S1C-D**).

Plasma metabolomic changes in response to acute endurance and resistance exercise reflect distinct physiologic demands

We observed extensive plasma metabolite changes in response to both EE and RE that highlight both the breadth of metabolic pathways affected by exercise and the shared and exercise mode-specific metabolic responses. In two general patterns that were similar to plasma proteomic findings, we observed that: 1) more DA plasma metabolites in the early post-exercise time points that returned to baseline levels within 30 min of exercise completion and contrasted the fewer metabolites that only became differentially abundant at post 3.5 h and 24 h, and 2) under the exercise intensities employed, RE generally induced metabolite changes that were of greater magnitude and more sustained than EE (**Figures 2A-B)**. We took two approaches to further evaluate plasma metabolic class responses to each exercise modality. First, we performed enrichment analyses using RefMet annotations (**Figure S2)**. These demonstrated RE-specific enrichment (all p-adj<0.05) of xanthines within 30 minutes of the acute bout (including post 10 min: hypoxanthine, logFC: 4.75, p-adj=1.61e-86; xanthosine, logFC: 2.05, p-adj=5.7e-80; inosine, logFC: 4.85, p-adj=2.82e-52), findings that are consistent with previously described increases in nucleotide turnover with RE.[34] In addition, we found persistent changes in phosphatidylinositols (PIs) and C24 Bile acids in RE post 24 h (**Figure S2**). Both groups of compounds - and their derivatives - are increasingly recognized as important signaling molecules in glucose and lipid metabolism.[37]

RE also led to decreases in branched-chain amino acids and other key metabolites involved in anabolic signaling and nitrogen metabolism that persisted late into exercise recovery (post 3.5 h). In addition to alterations in purine and amino acid metabolism, RE elicited sustained steroid hormonal responses with changes in androgens seen up to 24 h post RE (post 24 h: Dehydroepiandrosterone sulfate (DHEA-S), logFC: -0.22, p-adj=7.25e-3; 5alpha-Androstane-3alpha-ol-17-one sulfate, logFC: -0.23, p-adj=0.04). Notably, RE elicited a distinct biphasic response in circulating pregnenolone sulfate levels, with an initial increase, followed by a decrease below baseline levels at the later time points (post 10 min: logFC: 0.42, p-adj=0.004; post 30 mins: logFC: 0.32, p-adj=0.028; post 3.5 h: logFC: -0.56, p-adj=0.009; post 24 h: logFC: -0.52, p-adj=0.01). Although only a subset of steroids were profiled, our findings align with and extend prior observations that acute RE induces an immediate rise in circulating steroids

followed by a progressive decline below baseline levels within 48-72 h post exercise, possibly reflecting increased tissue uptake and/or utilization.[38, 39] Notably, hydroxyproline, a marker of collagen turnover and connective tissue remodeling, was one of the most significantly upregulated metabolites in RE post 24 h (post 24 h: logFC: 0.45, p-adj=1.81e-10), possibly reflecting musculoskeletal remodeling and repair processes further described in immune analyses below.

We next performed c-means clustering to further characterize temporal metabolite class changes in each exercise mode.[40] Four distinct patterns in EE and RE underwent enrichment analyses using CAMERA-PR (**Figures 2C-D and Table S3**). In EE, Cluster 1 is enriched in metabolites that acutely decreased post-EE and returned to baseline levels within 3.5 h, (p-adj<0.05) and include triglycerides (TG), lysophosphatidylethanolamines (LPE) and lipophosphatidylcholines (LPC) reflecting their well-described role as a fuel source during submaximal aerobic exercise (**Table S3**).[41, 42] Cluster 4 featured transient increases in tricarboxylic acid (TCA) intermediates (including during 40 min: succinic acid, logFC: 1.57, p-adj=1.52e-60; fumaric acid, logFC: 0.33, p-adj=1.82e-7; and malic acid, logFC: 0.93, p-adj=8.83e-32), diglycerides (DG), and acylcarnitines, consistent with an increased mitochondrial lipid oxidation during EE (**Table S3**). Clusters 2 and 3 showed delayed changes in recovery and contained lipid species, including sphingomyelins (SM), ether-phosphatidylethanolamines (O-PE), and ether-phosphatidylcholines (O-PC).

In contrast, RE revealed a distinct set of temporal signatures. While Cluster 1 RE metabolites resembled Cluster 4 EE metabolites with a rapid increase and sustained elevations in TCA intermediates, Cluster 2 analytes peaked by 10 min post-RE, before falling below baseline levels and were enriched for DG, SM, and phosphatidylcholines. Cluster 3 RE metabolites, similar in trajectory to EE Cluster 1, included C24 bile acids that specifically decreased in the post RE period and remained suppressed. Cluster 4 analytes demonstrated a biphasic profile, with an early decrease followed by a late increase and comprised unsaturated fatty acids and acylcarnitines (including CAR 8:0;OH: post 10 min, logFC: - 0.61, p-adj=6.19e-8; post 24 h, logFC: 0.36, p-adj=0.068).

Taken together, these analyses reveal both shared temporal dynamics of metabolite classes (e.g., rapid elevations in TCA intermediates, decreases of dipeptides and amino fatty acids) as well as distinct metabolite class trajectories in circulating lipids and bile acids that likely reflect different energetic demands and anabolic responses of EE and RE.

RE and EE lead to divergent lipid responses in early and late exercise recovery

Enrichment analyses identified divergent early temporal responses in acylcarnitines and free fatty acids between the two exercise modes at the first comparative time point (post 10 min, p-adj<0.05, **Figure S2A**). Plasma levels of several medium- and long-chain acylcarnitines increased during and immediately after EE but decreased after RE (**Figures 3A and S3A-B**). While acylcarnitine responses after both acute EE and RE in human plasma,[34, 43] and EE in murine skeletal muscle[44] have been described, we sought to better understand the possible tissue origins and regulation of these features by leveraging MoTrPAC's simultaneous assessment of both plasma and skeletal muscle metabolomics and transcriptomics. We first observed that the divergent acylcarnitine responses in plasma were broadly mirrored in the skeletal muscle (**Figure 3A**) (*Skeletal muscle* REF). This likely reflects enhanced mitochondrial fatty acid oxidation in the skeletal muscle during EE with the exit of partially oxidized fatty acids by exchange of the acyl group for carnitine.[45] In contrast, RE results in significant hypoxia by severely limiting blood flow during concentric exercise (ref), relying on muscle glycogen mobilization and anaerobic glycolysis to supply ATP resulting in increased lactate production.[46]

We next examined skeletal muscle gene expression changes in the key regulators of lipid and acylcarnitine metabolism and found that EE induced a delayed (post 24 h) increase in skeletal muscle expression of genes involved in lipid oxidation including carnitine palmitoyltransferases (CPT1B, CPT2) and the very long chain acyl-CoA dehydrogenase (ACADVL), that were either unique or of greater magnitude than RE (**Figure 3B)**. Although previous studies of endurance training have shown increased expression of genes involved in fatty acid metabolism and transport in skeletal muscle, the transcriptional effects of a single acute bout have been less consistent.[47, 48] Notably, this gene expression pattern was not evident in the Meta-analysis of Skeletal Muscle Response to Exercise (MetaMEx) database of publicly available acute exercise transcriptomic responses.[49] Collectively, our findings highlight both the likely tissue source of circulating acylcarnitines during acute exercise and provide new evidence that even a single bout of EE, and to a lesser extent RE, is sufficient to increase transcription of genes involved in lipid oxidation.

Canonical Correlation Analysis Identifies Multivariate Associations Between Baseline Plasma Metabolites and Exercise Traits

To integrate blood biochemical features with physiological exercise and metabolic traits, we applied canonical correlation analysis (CCA) using pre-exercise (rest) plasma metabolomics. CCA identifies shared axes of variation between two high-dimensional datasets by maximizing the correlation between linear combinations of features from each domain.[50]

The plasma metabolomic data was selected given that it was performed in all participants and because it reflects metabolic processes involved in energy utilization, substrate turnover, and hormonal regulation, and may provide insight into the biochemical underpinnings of exercise capacity and muscle strength. The top three primary canonical variates highlighted distinct domains of physiologic function and underlying metabolic patterns (**Figure 4A**). The first canonical variate was predominantly driven by metrics of aerobic fitness and endurance performance, including VO_2peak (both absolute and relative), O_2 pulse, and peak workload. This axis of metabolite variation was positively weighted on creatinine, dipeptides (Pro-Phe, Leu-Pro), ethanolamine, and branched chain amino acids (e.g., leucine/isoleucine), and negatively weighted on sphingomyelin species (e.g., SM 32:2;O2, SM 39:2;O2) (**Figure 4B**). The second canonical variate identified associations with vascular and hemodynamic traits, including systolic and diastolic blood pressure at peak exercise and during recovery, heart rate at peak exercise, BMI, and age. This variate was positively weighted on long-chain triglycerides and ceramides (e.g., Cer 20:1;O2/24:0), a subclass of sphingolipids that have previously been implicated in insulin resistance, cardiovascular disease and mortality. [51-54] Collectively, this variate captures a metabolite signature of subclinical vascular and metabolic health (**Figure 4C**). The third canonical variate mapped strongly to age, body weight, and strength, and was most strongly weighted on steroid hormone derivatives including pregnenolone sulfate and DHEA-S, as well as a broad panel of phosphatidylcholine species (**Figure 4D**). Taken together, unbiased, multivariate integration of baseline plasma metabolomics with important exercise traits using CCA revealed distinct biochemical profiles reflecting unique physiological domains of i) cardiorespiratory fitness ii) vascular and metabolic health, and iii) strength and age, many of which have not previously been described. Further work will be needed to assess for causal relationships.

Resistance and endurance exercise elicit distinct plasma proteomic kinetic responses

We identified numerous plasma proteomic changes that occur during the acute endurance bout (**Figures 5A-B**), with a large overlap between the 20 min and 40 min time points in the EE group; 14 of 16 proteins with DA changes during 20 min also change with the same direction of effect at the 40 min time point; **Figure 5A**). By 40 minutes of EE, 95 plasma proteins changed

with the overwhelming majority (97%) increasing. The relatively few protein decreases included kallikrein-related peptidase 6 (KLK6), neuronal pentraxin receptor (NPTXR), and protein tyrosine phosphatase receptor type N2 (PTPRN2), a protein involved in regulating insulin storage and secretion in response to glucose (logFC=-0.65, -0.59, and -0.68, p-adj=5.3e-3, 1.24e-2, 1.21e-2, respectively).[55] Our findings reflected both known plasma proteomic changes that occur during acute aerobic exercise, including increases in tissue-type plasminogen activator (PLAT; logFC=1.92, p-adj=4.07e-4), granulysin (GNLY; logFC=0.82, p-adj=8.90e-3), fractalkine (CX3CL1; logFC=0.50, p-adj=2.87e-3), and the myogenic factor, hepatocyte growth factor (HGF; logFC=0.49, p-adj=2.36e-2),[32, 33, 56-58] as well as newly identified protein changes including increases in neprilysin (MME; logFC=0.33, p-adj=3.68e-2) - an endopeptidase that degrades vasoactive peptides and is a major pharmacologic target in the treatment of heart failure[59], angiopoietin-related protein 7 (ANGPTL7), and CCN family member 1 (CCN1; highlighted as a candidate exerkine in a companion paper (*Multi-Omic Landscape* REF). Further, the immediate plasma proteomic response to EE suggests early immune cell mobilization and activation through the increase in chemokine levels including C-X-C motif chemokine 17 [CXCL17], C-C motif chemokine 16 [CCL16], and C-X-C motif chemokine 16 [CXCL16]; monocyte chemoattractant interleukins (e.g., Interleukin-16 [IL16], Interleukin-18 receptor 1 [IL18R1], as well as the anti-inflammatory and putative exerkine IL1R1 [IL1RA],[13] and cluster of differentiation [CD] proteins. By post 30 min, nearly all the DA plasma proteins during EE returned to their baseline levels.

Plasma protein levels are affected by renal function, which dynamically changes during acute exercise – decreasing during acute bouts and normalizing in recovery.[60-62] Thus, we tested the baseline (resting) relationship between renal function and exercise-responsive plasma protein levels. Interestingly, many (91%) of the plasma proteins that increased during 40 min and rapidly returned to baseline levels demonstrated an inverse association with renal function (estimated glomerular filtration; eGFR) (**Figure S5A**). In contrast, fewer exercise-responsive proteins at the later, post-exercise time points were inversely associated with baseline eGFR, suggesting lesser impact of renal clearance on these protein changes (**Table S4**).

In contrast to the protein changes observed during the acute bout, all of the DA plasma proteins at 3.5 h post EE decreased (**Figures 5A-B**). While growth hormone's (GH1) sustained decrease in exercise recovery (post 3.5 h logFC=-5.18, p-adj=1.11e-2) follows its known trajectory,[63] other DA proteins observed at post 3.5 h were not differentially regulated at other time points.

Similar to the transient proteomic changes seen within and immediately after the acute EE bout, all plasma proteins that increased in the immediate post-RE recovery period (post 10 min) demonstrated a smaller magnitude of increase by the subsequent time point (post 30 min), highlighting their rapid return to baseline levels following exercise. However, in contrast to EE, several proteins that decreased in the early RE recovery period (post 10-30 min) demonstrated sustained decreases of greater magnitude through the post 3.5 h time point, including the secreted serine protease, kallikrein-related peptidase 8 (KLK8), soluble receptor for advanced glycation end products (AGER or RAGE), and Thy-1 membrane glycoprotein (THY1 or CD90) (**Figure 5B**). Overall, and in a pattern that largely mirrored the plasma metabolome, while RE and EE led to similar directional effects in terms of plasma protein changes, RE led to more extensive decreases in plasma proteins (both number and magnitude of effect) compared to EE (**Figures S5B-D**), with 88% (53/60) and 98% (42/43) of the plasma proteins decreasing at the post 30 min and 3.5 h time points, respectively. The underlying mechanisms for RE-induced plasma protein decreases in late recovery require further study, however one potential contributor could be the relatively greater hypoxia exposure during RE, leading to altered protein localization and/or transcriptional repression via HIF1 and related pathways.[64-66]

We next used the Human Protein Atlas (HPA) secretome database to annotate exercise-responsive, secreted plasma proteins given that they represent an important group of physiologic signaling molecules.[67-69] Among the 189 unique proteins that were responsive to either exercise mode (N=103 in EE, N=109 in RE with 23 proteins overlapping), 94 (~50%) were secreted. The group of RE-responsive proteins at the post 30 min and post 3.5 h time points were more likely to be secreted (~63%) than EE-responsive proteins (20-45% for a given time point) or those in the immediate post-RE time point (post 10 min, 44%) (**Figure 5C**). Late (post 3.5 h) responsive proteins included a group of hormones and hormonal binding proteins with sustained decreases (e.g., fibroblast growth factor 21 [FGF21]; adrenomedullin [ADM], galanin [GAL], and corticotropin-releasing factor-binding protein [CRHBP]; **Figure 5D**) that contrast the transient rise and fall of within exercise protein changes during EE.

Plasma protein tissue sources may differ in the exercised and rested states

The plasma secretome reflects a heterogeneous group of proteins that span both different secretory processes (e.g., “classically” secreted proteins with signal peptide sequences, leakage proteins) as well numerous tissue sources.[70] Thus, we sought to characterize the putative tissue sources of exercise-responsive plasma proteins using the largest human plasma

secretome atlas[44] as well as MoTrPAC human adipose and skeletal muscle data (*Multi-omic, Skeletal muscle companion, adipose tissue companion*, REF). We first assigned all of the EE and RE responsive plasma proteins (N=189) from our dataset to their putative tissue source, as well as the certainty of a given tissue assignment based on data from 4 tissue- and 2 cell-type atlases across 21 tissues and 8 blood cells across the Genotype-Tissue Expression (GTEx) project, European Molecular Biology Laboratory (EMBL)-EBI Expression Atlas, and the recently published human protein distribution atlas (HATLAS resource).[71-73] We found tissue assignments for all 21 tissues, 7 cell types, as well as proteins with similar abundance in multiple tissues/cells (common), with brain, spleen and adipose tissue representing the largest putative tissue sources (**Figures 6A-B**). This included well-described protein-tissue source relationships (e.g., FGF21-liver, ghrelin [GHRL]-stomach, and neurocan [NCAN]-brain).

To investigate whether a protein's annotated tissue source(s) in the resting condition informs its potential tissue source(s) during exercise, we focused on a subset of 23 proteins that mapped to either adipose and/or skeletal muscle in HATLAS, and then compared their transcriptional and global proteomic responses in MoTrPAC adipose and skeletal muscle samples (adipose and skeletal muscle global proteomics did not detect 8 of these proteins). We found that among this subset of DA plasma proteins, there were not directionally concordant, significant changes in the respective adipose or skeletal muscle transcripts and/or proteins, either at the same time point or at an earlier time point (**Figures 6C-D**). Given that exercise regulation of protein translation occurs on the order of hours,[74] we subsequently tested all of the plasma proteins that were DA at the post 3.5 h time point (no proteins were DA at 24 h) for transcriptional and global proteomic changes at or prior to that time point. We found that TNFRSF8 (CD30), a protein annotated to adipose tissue (GLS 2) in HATLAS[71] demonstrated concordant decreases in skeletal muscle gene expression (post 30 min) and plasma protein levels (post 3.5 h) (**Figures S6A-B)**. Collectively, these analyses suggest that a plasma protein's tissue source in response to exercise may differ from its source in the rested state and/or its transcriptional regulation following acute exercise.

Whole blood transcriptional responses to acute exercise

We used CAMERA-PR to identify pathways enriched by differentially expressed genes following the exercise bouts (Figure 7A) (**STAR Methods**). The immediate response to acute exercise was dominated by changes in immune-related pathways, many of which were enriched in response to both exercise modes. Natural killer (NK) and CD8+ T cells were upregulated during

and remained elevated 10 minutes post-EE, and 30 minutes post-RE (p-adj<0.05, **Figures 7A-C**). Both exercise modes led to upregulation in neutrophil-related terms and broader immune effector terms such as IL-4, IL-6 and IL-17, IL-8, IFNγ, Toll-like receptor signaling, and CXCR4 signaling in the early post-exercise period (post 10 or 30 min) with more sustained changes after RE (up to 24 h). Additionally, platelet activation occurred in a similar temporal pattern, with a prolonged response following RE, as compared to EE (**Figure 7C**).

Whole blood transcriptional profiling may also provide insights into gene expression in additional tissues.[75] In enrichment analyses, we identified blood transcriptional responses in both exercise modes that reflect well-established exercise-responsive processes including angiogenesis and tissue remodeling (VEGF, IL-6, and EGFR signaling; **Figure 7C**) that occur in multiple tissues, including skeletal muscle. Key features, including VEGFA, IL6R, and AKT1 demonstrated consistent transcriptional responses across blood and skeletal muscle (**Figure S7A**) but not adipose (data NS). We found an enrichment for the heat shock protein (HSP) 90 chaperone system which shares molecular coordination with the HSP70 system—both well-known pathways involved in immune regulation and tissue regeneration after exercise that are regulated across multiple tissues including skeletal and cardiac muscle, liver, brain and blood, which increases after both EE and RE (**Figure 7C**). Several HSP90 and the closely related HSP70 pathway members, including HSP90AA1, STIP1, TUBA4A, and HSPA1A (HSP72) increased in the blood either prior to or at the same time as corresponding skeletal muscle transcriptional changes, (**Figures 7D-E**), highlight shared transcriptional responses to acute exercise across these tissues.[76-79] Further, we identified increased enrichment in heat shock transcription factor 1 (HSF1) activation, a key regulator of HSPs that has been shown to modulate physiologic cardiac remodeling to exercise[80] and angiogenesis[81] (**Figure S7B**).

Resistance exercise leads to greater innate immune cellular responses

To assess shifts in either immune cellular populations and/or their level of activation, we first performed gene set enrichment analysis using the human CellMarker 2.0 database given that its curations primarily contain traditional flow cytometry cellular and activation markers.[82]

Enrichment analyses demonstrated early induction and recovery of cytotoxic effector cells in response to both EE and RE (e.g., NK cells, cytotoxic CD8+ and CD4+ T cells, (γδ) T cells, and nonspecific innate lymphoid cells; all **Figure 8A**). Plasma proteomic profiling also revealed an increase in several proteins involved in cytotoxic processes (e.g. GNLY and GZMB), most pronounced during EE, suggesting their early activation and potential shedding of cellular

receptors or extracellular vesicle release (**Figure 8B**).[83] Broadly, the CD8+ T cell and NK cell response either returned to baseline by 30 min or 3.5 h post-exercise (**Figure 8A**). While within exercise time points were only assessed in EE, top pathway feature enrichments including granzyme A, B, and H [GZMA, GZMB, GZMH] and NK cell markers including KLRC1, CD94 [KLRD1]), and KLRK1 (KLRC2) revealed similar trajectories between exercise modes at the first shared time point (post 10 min) (**Figures 8C-D; Figure S8D**). Similarly, the T cell marker of differentiation, KLRG1, demonstrated early upregulation in both modes (**Figure 8D**) in the absence of significant responses in markers of other T cell subsets (**Figure S8E**). In contrast, CD274 (PDL1) another marker of differentiation in T cells also expressed on antigen presenting cells (APCs), increased post 24 h in RE only (**Figure 8D**). RE also induced unique enrichment in antigen presenting cell (APC) subtypes including eosinophils and a general granulocyte subclass post 30 min. Further, RE led to increases in M1 (proinflammatory) macrophages post 3.5 h, likely reflecting mobilization of non-classical monocytes given increases in CD14 and CD16 (FCGR3A & FCGR3B) without corresponding increases in CCR2 (**Figures 8A, S8A-C**).[84] Exercise intensity is positively associated with mobilization of non-classical monocyte subsets,[85] which may facilitate tissue reparative processes. Further examination of the top features leading these mode differential pathway enrichments demonstrated that RE uniquely induced CD44 increases (**Figures S8A-B**), a key regulator of immune cell homing in response to tissue injury that facilitates extracellular matrix repair.[86] Interestingly, CD44 expression displayed a delayed, yet coordinated increase in the skeletal muscle in response to RE, increasing at 3.5 h, and suggestive of potential CD44+ immune cell infiltration (*Skeletal muscle companion*, in preparation/submission REF). RE also induced greater mobilization of markers of platelet activation (**Figure S8F**), including CD63,[87] an additional cell type that can promote skeletal muscle regeneration.[88]

To further test immune cell type proportions in response to EE and RE, we performed cell deconvolution analyses among the whole blood samples using CIBERSORTx and the LM22 signature matrix.[89] Neutrophils accounted for the largest proportion of cells in baseline samples (~40% of all cells), consistent with established cell proportions in peripheral blood.[90] Monocytes were the second most abundant immune cell type in the whole blood at 20% (**Figure 8D**). We calculated changes in proportion for each cell type at each time point within EE, RE and CON, respectively, and found minimal changes in CON but significant changes in both exercise groups, suggesting that non-exercise factors, such as blood and tissue sampling, had small impact(s) on immune cell mobilization (**Figure 8D**).

Through cellular deconvolution, we observed decreases in the predicted proportion of blood monocytes post 3.5 h in RE (p-adj=8.8e-5) with a non-significant trend towards a decrease in EE. This was paralleled by increases in gene expression associated with M0 macrophages (post-3.5 h EE: p-adj=3.4e-5, post 3.5 h RE: p-adj=3.3e-7) and, in RE, M1 macrophages (post-3.5 h: p-adj=0.046) (**Figure 8E**), indicating a shift in monocytes relative to total blood cellular abundance that may suggest either: 1) M1-like macrophage differentiation in tissue, consistent with increases in M1 macrophage markers from enrichment analyses described above (**Figure 8A**); or 2) a more proinflammatory CD14+, CD16+, CCR2- monocyte subtype.[84] Neutrophil proportions increased up to 3.5 h following both exercise modes (post 30 m EE: p-adj=1.2e-5, post-3.5 h EE: p-adj=2.9e-5, post-30 m RE: p-adj = 2.6e-8, post-3.5 h RE: p-adj=2.8e-8), consistent with our enrichment analyses. The proportion of resting NK cells increased during EE (p-adj=1.3e-11) and immediately post-exercise across both modes (post 10 min EE: p-adj=0.067, RE: p-adj=4.1e-6), and was consistent with prior studies.[91] We further observed an acute decrease in the proportion of naïve B cells (EE during 40 min: p-adj=3.7e-4; RE post 10 min: p-adj=7e-5), coupled with an increased in memory B cells. T cells (EE during 20 min: p-adj=2.8e-5, RE post 10 min: p-adj=5.7e-5) and resting memory CD4+ T cells were predicted to decrease in both modes (EE during 40 min: p-adj=0.018, RE post-3.5 h: p-adj=0.18), findings that may reflect proportional shifts in immune cell populations (e.g., mobilization of cytotoxic cells and monocytes) following an acute exercise bout. Taken together, cell deconvolution findings were consistent with our enrichment analyses and highlight many shared immune responses after both exercise modes, with RE demonstrating greater innate immune cellular mobilization and/or homing.

Discussion

Blood biochemical profiling of exercise provides an opportunity to better understand its multi-organ effects and communication. While several prior studies have characterized the responses of single plasma and blood biochemical profiling technologies to acute exercise[30-32, 92], few have integrated multi-omic datasets[43] or compared multiple exercise modes.[34] Our work is, to our knowledge, the first large human study to simultaneously test the effects of acute aerobic and resistance exercise using large-scale plasma proteomics, metabolomics, and whole blood transcriptomics across a 24 h period leveraging a non-exercise control arm. We make several observations from these data. Using guideline recommended doses of endurance and resistance exercise in untrained individuals,[93, 94] we found that RE generally induces a more robust and sustained effect on plasma analytes in the post-exercise recovery period, while EE

elicited a rapid and transient rise and fall in circulating analytes during the exercise session. While we identified several mode-specific responses including among specific immune cell populations, analytes involved in or reflecting lipid metabolism, and features reflecting angiogenic/tissue repair processes, we note that EE and RE produced many shared molecular responses in the blood. We observed that exercise tissue sources of plasma proteins may diverge from their annotated, resting (non-exercise) tissue sources, at least among the human tissues directly profiled in MoTrPAC. Further, we highlight shared plasma metabolomic features that reflect different aspects of clinical and exercise physiology, including cardiorespiratory fitness, muscle strength, and anthropometrics.

These initial blood and plasma molecular data from MoTrPAC sedentary humans demonstrate notable individual -omic and acute exercise mode-specific differences. The transient rise in protein levels seen within or immediately after acute exercise appears to occur across both modes, and contrasts with the sustained plasma protein decreases after RE that reflect a greater percentage of secreted proteins. The biology underlying these differences remains to be explored. We hypothesize that in addition to exercise stimulating enhanced protein secretion during EE, non-specific cellular shedding during rapid changes in circulatory blood flow, hemoconcentration and/or rapid changes in renal clearance could contribute to the transient rise and fall in plasma protein levels seen during and immediately after acute exercise. Further, we observed unanticipated findings during EE, including increases in angiopoietin-2 (ANGPT2), a circulating factor that, during periods of VEGF inhibition, can also exert pro-angiogenic effects[95-97]; neprilysin, a potent degrader of the vasodilatory B-type and atrial natriuretic peptides and bradykinin[98]; and hypoxia-inducible factor prolyl hydroxylase 2 (EGLN1), a cellular oxygen sensor whose gene variants are associated with VO_2max and that demonstrates reduced activity during periods of hypoxia.[99] While the functional effects of these protein changes during exercise require further evaluation, we anticipate that specific findings may reflect context dependence, similar to IL-6's contrasting roles in exercise metabolism and cancer.[100, 101] Ultimately, further assessing these and other analyte's temporal changes after repeated bouts of exercise (i.e., training) and relating their levels to training-induced physiological adaptations will be crucial to their interpretation, work that is underway in the larger, post suspension MoTrPAC study.

We note several new, mode-specific findings among blood transcriptomics that both build upon limited existing data on whole blood transcriptional profiling in response to acute exercise[92] and integrate plasma proteomic data. Both EE and RE induced the rapid expression of cytotoxic (NK

and CD8+ T cell) cell markers in the early post-exercise period, and further, increased gene expression among serine proteases contained in cytotoxic granules in NK cells and CD8+ T cells, including granulysin and granzymes B, H and A during (during EE) and 10 min post exercise (in EE and RE). Taken together, these data offer novel mechanistic insights behind the increased NK cell and T-cell killing of target cells in health and disease reported elsewhere.[102-104] In contrast, only RE induced markers indicative of eosinophil and monocyte mobilization, and platelet activation, cell types that are critical to reparative processes in the skeletal muscle.[105-107] We found that increases in cell type marker expression translated to predicted increases in cell type proportion by deconvolution methods in general, but not always. While deconvolution serves as a strong predictive tool for shifts in cellular proportions in various resting physiological states, the dynamic state and molecular responses to acute exercise may differ from these reference data sets. These analyses highlight the important need for cellular phenotyping using flow cytometry and/or single cell profiling analyses to further inform of understanding of the exercise immune response.[108]

A larger body of work exists studying the effects of acute exercise on plasma proteins and metabolites, however the majority of these studies did not include a non-exercise control group[30-32, 34, 43, 109], a feature notable in light of the vast number of analytes that not only change during the 24 h period in the non-exercise control group but mimic the trajectories seen in the exercise groups. Along these same lines, our study design also highlights molecular features whose levels remain largely unchanged in response to acute exercise, but contrast a fall or rise in the non-exercise control group (*Multi-Omic Landscape* REF). Thus, the MoTrPAC study design and our analytic approach provide confidence that differentially changed features represent the effects of exercise, and not the influences of circadian rhythm, fasting, or procedural instrumentation (e.g., placement of intravenous catheters or tissue biopsies).

While there are notable examples of solid tissue transcriptional and/or proteomic changes that correlate with plasma protein levels (e.g. CCN1, highlighted in *Multi-Omic Landscape* REF), our in silico analyses of the exercise-responsive plasma secretome highlights the limitations of using resting tissue atlases to infer a plasma protein's putative exercise tissue source. Our findings support the concept that a plasma protein whose basal (resting) tissue gene and/or protein expression is low, may have significantly higher expression during or after an exercise stimulus, or that its secretory process may be distinct from tissue transcriptional regulation. Indeed, IL-6 serves as a classic example, with its resting tissue sources (adipose and genitourinary tissues[67]) contrasting its acute exercise tissue source (skeletal muscle).[110] Here,

we make a similar observation with TNFRSF8. A strength of the MoTrPAC study is the ability to relate temporal skeletal muscle, and adipose and blood tissue transcriptional and proteomics data with each other, however additional strategies, including leveraging data from an expanded repertoire of tissues in pre-clinical animal studies in MoTrPAC and/or the use of new proximity-labeling technologies[111, 112] will be needed to help draw a more comprehensive assessment of the tissue-specific contributions to the exercise secretome.

We note limitations to this work in addition to those described above. Because of the age and sex imbalances in enrollment at the time of study interruption (due to the SARS-CoV-2 pandemic), we were underpowered to perform age- and sex-specific analyses, work that we anticipate performing in the larger MoTrPAC post-suspension cohort. Similarly, the number of participants who completed the 12-week training intervention was small, limiting our ability to relate pre-training, acute exercise findings to exercise training adaptations. As described above, we cannot fully distinguish whether whole blood transcriptional changes are driven by shifts in cell proportions or changes in transcript abundance due to activation or inhibition, however we employed alternative strategies to analyze the acute exercise blood immune response including our use of plasma proteomics and gene set enrichment analyses that used a database enriched for flow cytometry markers of immune cell phenotype.[113] The targeted proteomics platform creates limited membership among curated gene set lists, thus we did not perform enrichment analysis to avoid overinterpretation of our data[114], but that may potentially limit our findings. Plasma proteomic profiling for the post-suspension MoTrPAC human subjects will be performed using an updated, ~5,000-protein assay that will facilitate expanded analyses. Further, plasma proteomics was performed on a more limited sample in this cohort due to the study interruption from the pandemic. Similarly, tissue and -omic coverage across this cohort was variable and led to different sample sizes for cross-tissue comparisons (*Multi-Omic Landscape* REF). Finally, while RE appears to elicit larger magnitude effects than EE across numerous circulating analytes in this study, our findings are specific to the relative intensities of the unaccustomed resistance and aerobic bouts in MoTrPAC and may not be more generalizable to other exercise interventions.

In summary, we identify novel patterns of blood and plasma biochemical responses after acute exercise according to temporal profile, -ome, and exercise mode in initial human findings from the MoTrPAC study. In addition to identifying new exercise-responsive analytes and pathways across our platforms, we provide all of these data in an accessible resource for the broader scientific and medical communities.

STAR Methods

Experimental model and study participant details

IRB

The Molecular Transducers of Physical Activity Consortium (MoTrPAC) (NCT03960827) is a multicenter study designed to isolate the effects of structured exercise training on the molecular mechanisms underlying the health benefits of exercise and physical activity. Methods are described here in sufficient detail to interpret results, with references to supplemental material and prior publications for detailed descriptions. The present work includes data from prior to the suspension of the study in March 2020 due to the Covid-19 pandemic. The study was conducted in accordance with the Declaration of Helsinki and approved by the Institutional Review Board of Johns Hopkins University School of Medicine (IRB protocol # JHMIRB5; approval date: 05/06/2019). All MoTrPAC participants provided written informed consent for the MoTrPAC study indicating whether they agreed to open data sharing and at what level of sharing they wanted. Participants could choose to openly share all de-identified data, with the knowledge that they could be reidentified, and they could also choose to openly share limited de-identified individual level data, which is lower risk of re-identification. All analyses and resulting data and results are shared in compliance with the NIH Genomic Data Sharing (GDS) policy and DSMB requirements for the randomized study.

Participant Characteristics

Volunteers were screened to: (a) ensure they met all eligibility criteria; (b) acquire phenotypic assessments of the study population; and (c) verify they were healthy and medically cleared to be formally randomized into the study (*Clinical Landscape*, in submission, REF).[35] Participants were then randomized into intervention groups stratified by clinical site and completed a pre-intervention baseline acute test. A total of 176 participants completed the baseline acute test (endurance exercise [EE]=66, resistance exercise [RE]=73, and control [CON]=37), and among those, 175 (99%) had at least one biospecimen sample collected. Participants then began 12 weeks of exercise training or control conditions. Upon completion of the respective interventions, participants repeated phenotypic testing and the acute test including biospecimen sampling. Due to the COVID-19 suspension, only 45 participants (26%) completed the post-intervention follow-up acute exercise test (some with less than 12 weeks of training), with 44

completing the post-intervention biospecimen collections. See *Clinical Landscape* (REF) for further detail.

Participant Assessments

As described in *Clinical Landscape* (REF), prior to randomization, participant screening was completed via questionnaires, and measurements of anthropometrics, resting heart rate and blood pressure, fasted blood panel, cardiorespiratory fitness, muscular strength, and free-living activity and sedentary behavior (*Clinical landscape* REF).[35] Cardiorespiratory fitness was assessed using a cardiopulmonary exercise test (CPET) on a cycle ergometer (Lode Excalibur Sport Lode BV, Groningen, The Netherlands) with indirect calorimetry. Quadriceps strength was determined by isometric knee extension of the right leg at a 60° knee angle using a suitable strength device.[35] Grip strength of the dominant hand was obtained using the Jamar Handheld Hydraulic Dynamometer (JLW Instruments, Chicago, IL). See *Clinical Landscape* (REF) for participant assessment results.

Acute Exercise Intervention

The pre-intervention baseline EE acute bouts (Figure 1) were composed of three parts: (1) a 5 minute (min) warm up at 50% of the estimated power output to elicit 65% VO_2peak, (2) 40 min cycling at ~65% VO_2peak, and (3) a 1 min recovery at ~25 W. The pre-intervention baseline RE acute bouts were composed of a 5 min warm-up at 50-60% heart rate reserve (HRR) followed by completion of three sets each of five upper (chest press, overhead press, seated row, triceps extension, biceps curl) and three lower body (leg press, leg curl, leg extension) exercises to volitional fatigue (~10RM) with 90 sec rest between each set. Participants randomized to CON did not complete exercise during their acute tests. Participants rested supine for 40 min to mirror the EE and RE acute test schedule. See *Clinical Landscape* (REF) for acute bout results (REF).

Biospecimen Collection

To standardize conditions prior to the acute test, participants were instructed to comply with a variety of controls related to COX-inhibitors, biotin, caffeine, alcohol, exercise, and final nutrition consumption.[35] Blood, muscle (SKM), and adipose (AT) samples were collected for the acute test at specific timepoints before, during, and after exercise (*Multi-Omic Landscape* REF).

Participants arrived fasted in the morning, and rested supine for at least 30 min prior to pre-exercise biospecimen collections. All participants had pre-exercise sampling from all three

tissues. After the pre-exercise biospecimen collections, the subsequent collection timepoints varied for each training group and their randomized temporal profile (early, middle, late, all). Temporal profiles were used to reduce the burden of repeat sampling while still maintaining biochemical coverage of the full post-exercise period (reference *Multi-Omic Landscape*). During and after exercise, biospecimen collection varied by randomized group, tissue, and temporal group. At 20 and 40 min of exercise, blood was collected from only EE and CON groups due to limitations in safely obtaining blood during RE. Immediately post exercise, at 10 minutes, a blood sample was collected in all three groups. Finally, samples from all three tissues were collected at early (SKM at 15, blood at 30, and AT at 45 min post-exercise), intermediate (blood and SKM at 3.5, and AT at 4 hour (h) post-exercise), and late (24 h post-exercise in all tissues) timepoints. The post-exercise timepoint began at the completion of the 40 minutes of cycling, third set of leg extension, or 40 minutes of rest, depending on the randomized group. Except for the EE blood collection timepoints during exercise, participants rested supine or seated for biospecimen collections. The collection and processing protocols for each tissue were previously described in the human clinical protocol design paper.[35] See *Clinical Landscape* (REF) for biospecimen collection success results.

The number of biospecimen samples that were profiled on any given assay varied by tissue, timepoint, and randomized intervention group for feasibility reasons. Multi-omic coverage is summarized in the *Multi-Omic Landscape* (REF).

Post training intervention data

As mentioned, 44 of the 175 individuals who began the trial did complete at least a portion of the training intervention period and the post-training acute bout session. These biospecimens were collected, and molecular data were generated for them. While these data are to be shared with the scientific community as detailed in the MoTrPAC Data Sharing Plan, the data are not analyzed here due to the low sample size and potential confounding between participant characteristics and groups of interest. Rather, the focus is on the baseline acute bout data. The full cohort dataset will allow exploration of multiple hypotheses related to training effects and is forthcoming.

Molecular Quantification Methods

Transcriptomics

RNA Sequencing (RNA-Seq) was performed at Stanford University and the Icahn School of Medicine at Mount Sinai. Processing randomization for blood, muscle was done according to https://github.com/MoTrPAC/clinical-sample-batching. See below for adipose randomization considerations.

Extraction of total RNA

Tissues (~10 mg for muscle, ~50 mgs for adipose) were disrupted in Agencourt RNAdvance tissue lysis buffer (Beckman Coulter, Brea, CA) using a tissue ruptor (Omni International, Kennesaw, GA, #19-040E). Total RNA was extracted in a BiomekFX automation workstation according to the manufacturer's instructions for tissue-specific extraction. Total RNA from 400 µL of blood collected in PAXgene tubes (BD Biosciences, Franklin Lakes, NJ, # 762165) was extracted using the Agencourt RNAdvance blood specific kit (Beckman Coulter). Two tissue-specific consortium reference standards were included to monitor the sample processing QC. The RNA was quantified by NanoDrop (ThermoFisher Scientific, # ND-ONE-W) and Qubit assay (ThermoFisher Scientific), and the quality was determined by either Bioanalyzer or Fragment Analyzer analysis.

mRNA Sequencing Library Preparation

Universal Plus mRNA-Seq kit from NuGEN/Tecan (#9133) were used for generation of RNA-Seq libraries derived from poly(A)-selected RNA according to the manufacturer's instructions. Universal Plus mRNA-Seq libraries contain dual (i7 and i5) 8 bp barcodes and an 8 bp unique molecular identifier (UMI), which enable deep multiplexing of NGS sequencing samples and accurate quantification of PCR duplication levels. Approximately 500ng of total RNA was used to generate the libraries for muscle, 300ng for adipose, and 250ng of total RNA was used for blood. The Universal Plus mRNA-Seq workflow consists of poly(A) RNA selection, RNA fragmentation and double-stranded cDNA generation using a mixture of random and oligo(dT) priming, end repair to generate blunt ends, adaptor ligation, strand selection, AnyDeplete workflow to remove unwanted ribosomal and globin transcripts, and PCR amplification to enrich final library species. All library preparations were performed using a Biomek i7 laboratory automation system (Beckman Coulter). Tissue-specific reference standards provided by the consortium were included with all RNA isolations to QC the RNA.

RNA Sequencing, quantification, and normalization

RNA sequencing, quantification, and normalization Pooled libraries were sequenced on an Illumina NovaSeq 6000 platform (Illumina, San Diego, CA, USA) to a target depth of 40 million read pairs (80 million paired-end reads) per sample using a paired-end 100 base pair run configuration. In order to capture the 8-base UMIs, libraries were sequenced using 16 cycles for the i7 index read and 8 cycles for the i5 index read. Reads were demultiplexed with bcl2fastq2 (v2.20.0) using options --use-bases-mask Y*,I8Y*,I*,Y* --mask-short-adapter-reads 0 --minimum-trimmed-read-length 0 (Illumina, San Diego, CA, USA), and UMIs in the index FASTQ files were attached to the read FASTQ files. Adapters were trimmed with cutadapt (v1.18),[115] and trimmed reads shorter than 20 base pairs were removed. FastQC (v0.11.8) was used to generate pre-alignment QC metrics. STAR (v2.7.0d)[116] was used to index and align reads to release 38 of the Ensembl Homo sapiens (hg38) genome and Gencode (Version 29). Default parameters were used for STAR's genomeGenerate run mode; in STAR's alignReads run mode, SAM attributes were specified as NH HI AS NM MD nM, and reads were removed if they did not contain high-confidence collapsed splice junctions (--outFilterType BySJout). RSEM (v1.3.1)[117] was used to quantify transcriptome-coordinate-sorted alignments using a forward probability of 0.5 to indicate a non-strand-specific protocol. Bowtie 2 (v2.3.4.3)[118] was used to index and align reads to globin, rRNA, and phix sequences in order to quantify the percent of reads that mapped to these contaminants and spike-ins. UCSC's gtfToGenePred was used to convert the hg38 gene annotation (GTF) to a refFlat file in order to run Picard CollectRnaSeqMetrics (v2.18.16) with options MINIMUM_LENGTH=50 and RRNA_FRAGMENT_PERCENTAGE=0.3. UMIs were used to accurately quantify PCR duplicates with NuGEN's "nodup.py" script (https://github.com/tecangenomics/nudup). QC metrics from every stage of the quantification pipeline were compiled, in part with multiQC (v1.6). The openWDL-based implementation of the RNA-Seq pipeline on Google Cloud Platform is available on Github (https://github.com/MoTrPAC/motrpac-rna-seq-pipeline). Filtering of lowly expressed genes and normalization were performed separately in each tissue. RSEM gene counts were used to remove lowly expressed genes, defined as having 0.5 or fewer counts per million in at least 10% of samples. These filtered raw counts were used as input for differential analysis with the variancePartition::dream,[119] as described in the statistical analysis methods section. To generate normalized sample-level data for downstream visualization, filtered gene counts were TMM-normalized using edgeR::calcNormFactors, followed by conversion to log counts per million with edgeR::cpm.

Principal Component Analysis and calculation of the variance explained by variables of interest were used to identify and quantify potential batch effects. Based on this analysis, processing batch (muscle and blood, see below for adipose), Clinical Site (all tissues), percentage of UMI duplication, and RNA Integrity Number (RIN) technical effects were regressed out of the TMM-normalized counts via linear regression using limma::RemoveBatchEffect function in R.[120] A design matrix including age, sex, and a combination of group and timepoint was used during batch effect removal to avoid removing variance attributable to biological effects.

Adipose tissue processing considerations

In the adipose tissue, RNA extraction was performed in separate batches according to exercise modality, so the extraction batch and exercise modality were perfectly collinear. This collinearity was identified at the RNA extraction step and samples were randomized prior to construction of cDNA libraries. Ultimately, under this processing implementation, differences in gene expression attributable to exercise group can be impossible to disentangle from RNA extraction batch effects, so the batch variable was not regressed out in the technical effect stage or included as a covariate in the differential analysis, and left as an experimental limitation.

RNA Quality Inclusion Criteria

In the blood transcriptomic data, 79/1032 processed adult-sedentary samples had RIN values under 5. Based on established guidelines and internal quality control assessments, any samples with a RIN score below 5 were excluded from further analysis due to concerns about potential degradation artifacts. Additional visualizations and summary figures supporting this decision are available in the quality control report at: https://github.com/MoTrPAC/precovid-analyses/tree/main/QC/

Proteomics

Plasma proteomics

Plasma proteomics profiling was performed using the Olink (Uppsala, Sweden) assay. The Proximity Extension Assay (PEA) technology has been described.[121] Briefly, a ~20µL plasma sample is first incubated with two distinct antibodies that bind proximal epitopes on the protein target. The two antibodies are conjugated with complementary DNA oligonucleotide sequences, which come in close proximity upon target binding and subsequently hybridize (immunoreaction). The sequence is then extended by DNA polymerase, creating a unique

amplicon (i.e., barcode) for each individual protein, which is then amplified by polymerase chain reaction. Every sample is spiked with three internal quality controls: (1) “Immuno controls” are non-human antigens measured by Olink that assess technical variation in all three steps of the reaction; (2) “extension controls” are composed of an antibody coupled to a unique pair of DNA-tags that are always in proximity, to produce a constant signal independent of the immunoreaction. This control is used to adjust the signal from each sample with respect to extension and amplification; (3) “amplification/detection” control is a complete double-stranded DNA amplicon that does not require either proximity binding or extension to generate a signal, specifically monitoring only the amplification/detection step. Additionally, eight external controls are added to separate wells on each sample plate. Two pooled plasma or “external sample” controls, generated by pooling several µL of plasma from samples from healthy volunteers, are used to assess potential variation between runs and plates (i.e. to calculate inter-assay and intra-assay CVs). Three negative controls (buffer only) per plate are used to monitor background noise generated when DNA-tags come in close proximity without prior binding to the appropriate protein. These negative controls set the background level for each protein assay in order to calculate the limit of detection (LOD). Finally, each plate includes a Plate Control (PC) of a separate pooled EDTA plasma sample plated in triplicate; the median of the PC triplicates is used to normalize each assay and to compensate for potential variation between runs and plates. Data values for measurements below LOD are reported for all samples.

Adipose and skeletal muscle LC-MS proteomics

LC-MS/MS analysis of 379 muscle samples encompassing baseline and 3 post-intervention timepoints from all three groups (EE, RE, CON) was performed at the Broad Institute of MIT and Harvard (BI) and Pacific Northwest National Laboratories (PNNL). Samples were split evenly across the two sites, and a total of 14 samples were processed and analyzed at both sites to serve as cross-site replicates for evaluation of reproducibility. Additionally, 46 adipose tissue samples representing baseline and 4-hours post-intervention from all three groups were analyzed at PNNL.

Generation of common reference

For both tissue types, a tissue-specific common reference material was generated from bulk human samples. The common reference sample for muscle consisted of bulk tissue digest from 5 individuals at 2/3 ratio of female/male. Samples were split equally between the Broad Institute

and PNNL, digested at each site following sample processing protocol described below, then mixed all digests from both sites and centrally aliquoted at PNNL. Common reference for adipose tissue was generated at PNNL using bulk tissue from 6 individuals representing a 4:2 ratio of female:male. 250 µg aliquots of both tissue specific common reference samples were made to be included in each multiplex (described below) and additional aliquots are stored for inclusion in future MoTrPAC phases to facilitate data integration.

Sample processing

Proteomics analyses were performed using clinical proteomics protocols described previously.[122, 123] Muscle and adipose samples were lysed in ice-cold, freshly-prepared lysis buffer (8 M urea (Sigma-Aldrich, St. Louis, Missouri), 50 mM Tris pH 8.0, 75 mM sodium chloride, 1 mM EDTA, 2 µg/ml Aprotinin (Sigma-Aldrich, St. Louis, Missouri), 10 µg/ml Leupeptin (Roche CustomBiotech, Indianapolis, Indiana), 1 mM PMSF in EtOH, 10 mM sodium fluoride, 1% phosphatase inhibitor cocktail 2 and 3 (Sigma-Aldrich, St. Louis, Missouri), 10 mM Sodium Butyrate, 2 µM SAHA, and 10 mM nicotinamide and protein concentration was determined by BCA assay. Protein lysate concentrations were normalized within samples of the same tissue type, and protein was reduced with 5 mM dithiothreitol (DTT, Sigma-Aldrich) for 1 hour at 37°C with shaking at 1000 rpm on a thermomixer, alkylated with iodoacetamide (IAA, Sigma-Aldrich) in the dark for 45 minutes at 25°C with shaking at 1000 rpm, followed by dilution of 1:4 with Tris-HCl, pH 8.0 prior to adding digestion enzymes. Proteins were first digested with LysC endopeptidase (Wako Chemicals) at a 1:50 enzyme:substrate ratio (2 hours, 25 °C, 850 rpm), followed by digestion with trypsin (Promega) at a 1:50 enzyme:substrate ratio (or 1:10 ratio for adipose tissue; 14 hours, 25 °C, 850 rpm). The next day formic acid was added to a final concentration of 1% to quench the reaction. Digested peptides were desalted using Sep-Pac C18 columns (Waters), concentrated in a vacuum centrifuge, and a BCA assay was used to determine final peptide concentrations. 250µg aliquots of each sample were prepared, dried down by vacuum centrifugation and stored at -80°C.

Tandem mass tag (TMT) 16-plex isobaric labeling reagent (ThermoFisher Scientific) was used for this study. Samples were randomized across the first 15 channels of TMT 16-plexes, and the last channel (134N) of each multiplex was used for a common reference that was prepared prior to starting the study (see above). Randomization of samples across the plexes within each site was done using https://github.com/MoTrPAC/clinical-sample-batching, with the goal to have all

timepoints per participant in the same plex, and uniform distribution of groups (EE, RE, CON), sex and sample collection clinical site across the plexes.

Peptide aliquots (250 µg per sample) were resuspended to a final concentration of 5 µg/µL in 200 mM HEPES, pH 8.5 for isobaric labeling. TMT reagent was added to each sample at a 1:2 peptide: TMT ratio, and labeling proceeded for 1 hour at 25°C with shaking at 400 rpm. The labeling reaction was diluted to a peptide concentration of 2 µg/µL using 62.5 µL of 200 mM HEPES and 20% ACN. 3 µL was removed from each sample to quantify labeling efficiency and mixing ratio. After labeling QC analysis, reactions were quenched with 5% hydroxylamine and samples within each multiplex were combined and desalted with Sep-Pac C18 columns (Waters).

Combined TMT multiplexed samples were then fractionated using high pH reversed phase chromatography on a 4.6mm ID x 250mm length Zorbax 300 Extend-C18 column (Agilent) with 5% ammonium formate/2% Acetonitrile as solvent A and 5% ammonium formate/90% acetonitrile as solvent B. Samples were fractionated with 96min separation gradient at flow rate of 1mL/min and fractions were collected at each minute onto a 96-well plate. Fractions are then concatenated into 24 fractions with the following scheme: fraction 1 = A1+C1+E1+G1, fraction 2 = A2+C2+E2+G2, fraction 3 = A3+C3+E3+G3, all the way to fraction 24 = B12+D12+F12+H12 following the same scheme. 5% of each fraction was removed for global proteome analysis, and the remaining 95% was further concatenated to 12 fractions for phosphopeptide enrichment using immobilized metal affinity chromatography (IMAC).

Data acquisition

Broad Institute: Both proteome and phosphoproteome samples were analyzed on 75um ID Picofrit columns packed in-house with ReproSil-Pur 120 Å, C18-AQ, 1.9 µm beads to the length of 20-24cm. Online separation was performed on Easy nLC 1200 systems (ThermoFisher Scientific) with solvent A of 0.1% formic acid/3% acetonitrile and solvent B of 0.1% formic acid/90% acetonitrile, flow rate of 200nL/min and the following gradient: 2-6% B in 1min, 6-20% B in 52min, 20-35% B in 32min, 35-60% B in 9min, 60-90% B in 1min, followed by a 5min hold at 90%, and 9min hold at 50%. Proteome fractions were analyzed on a Q Exactive Plus mass spectrometer (ThermoFisher Scientific) with MS1 scan across the 300-1800 m/z range at 70,000 resolution, AGC target of $3x10^6$ and maximum injection time of 5ms. MS2 scans of most

abundant 12 ions were performed at 35,000 resolution with AGC target of $1x10^5$ and maximum injection time of 120ms, isolation window of 0.7m/z and normalized collision energy of 27.

PNNL: For mass spectrometry analysis of the global proteome of muscle samples, online separation was performed using a nanoAcquity M-Class UHPLC system (Waters) and a 25 cm x 75 µm i.d. picofrit column packed in-house with C18 silica (1.7 µm UPLC BEH particles, Waters Acquity) with solvent A of 0.1% formic acid/3% acetonitrile and solvent B of 0.1% formic acid/90% acetonitrile, flow rate of 200nL/min and the following gradient: 1% B for 8min, 8-20% B in 90min, 20-35% B in 13min, 35-75% B in 5min, 75-95% B in 3min, followed by a 6min hold at 90%, and 9min hold at 50%. Proteome fractions were analyzed on a Q Exactive Plus mass spectrometer (ThermoFisher Scientific) with MS1 scan across the 300-1800 m/z range at 60,000 resolution, AGC target of $3x10^6$ and maximum injection time of 20ms. MS2 scans of most abundant 12 ions were performed at 30,000 resolution with AGC target of $1x10^5$ and maximum injection time of 100ms, isolation window of 0.7m/z and normalized collision energy of 30.

For MS analysis of the global proteome of adipose samples, online separation was performed using a Dionex Ultimate 3000 UHPLC system (ThermoFisher) and a 25 cm x 75 µm i.d. picofrit column packed in-house with C18 silica (1.7 µm UPLC BEH particles, Waters Acquity) with solvent A of 0.1% formic acid/3% acetonitrile and solvent B of 0.1% formic acid/90% acetonitrile, flow rate of 200nL/min and the following gradient: 1-8% B in 10min, 8-25% B in 90min, 25-35% B in 10min, 35-75% B in 5min, and 75-5% in 3min. Proteome fractions were analyzed on a Q Exactive HF-X Plus mass spectrometer (ThermoFisher Scientific) with MS1 scan across the 300-1800 m/z range at 60,000 resolution, AGC target of $3x10^6$ and maximum injection time of 20ms. MS2 scans of most abundant 12 ions were performed at 30,000 resolution with AGC target of $1x10^5$ and maximum injection time of 100ms, isolation window of 0.7m/z and normalized collision energy of 30.

Data searching

Proteome data from both the Broad Institute and PNNL were searched against a composite protein database at the Bioinformatics Center (BIC) using the MSGF+ cloud-based pipeline previously described.[124] This database comprised UniProt canonical sequences (downloaded 2022-09-13; 20383 sequences), UniProt human protein isoforms (downloaded 2022-09-13;

21982 sequences), and common contaminants (261 sequences), resulting in 42,626 sequences.

QC/Filtering/Normalization

Plasma proteomics: In total, 378 MoTrPAC sedentary adult samples were assayed across 9 plates in the same batch. No samples failed Olink standard quality control and median intra-assay and inter-assay CVs were 14.5% and 30.2%, respectively. Principal component analysis was performed and demonstrated minimal effects by plate and clinical site. Sample outliers were identified as those >3x the interquartile range for at least one of the first three principal components. Four samples (1.1%) from 3 different individuals were flagged as potential outliers and excluded from analyses. Final data are presented as NPX (normalized protein expression) values, Olink's relative protein quantification unit on a log2 scale.

LC-MS proteomics: The log2 Reporter ion intensity (RII) ratios to the common reference were used as quantitative values for all proteomics features. Datasets were filtered to remove features identified from contaminant proteins and decoy sequences. Datasets were visually evaluated for sample outliers by looking at top principal components, examining median feature abundance and distributions of RII ratio values across samples, and by quantifying the number of feature identifications within each sample. No outliers were detected in the muscle tissue dataset. In the adipose datasets, four samples were flagged as outliers based on inspection of the top principal components and evaluation of the raw quantitative results (median feature abundance <-1.0). These outlier samples were removed from the dataset, and the list of outlier samples can be found in the *Multi-Omic Landscape* (REF). The Log_2 RII ratio values were normalized within each sample by median centering to zero. Principal Component Analysis and calculation of the variance explained by variables of interest were used to identify and quantify potential batch effects. Based on this analysis, TMT plex (muscle and adipose), Clinical Site (muscle and adipose), and Chemical Analysis Site (muscle only, where samples were analyzed at both the Broad Institute and PNNL) batch effects were removed using Linear Models Implemented in the *limma::RemoveBatchEffect()* function in R.[120] A design matrix including age, sex, and group_timepoint was used during batch effect removal in order to preserve the effect of all variables included in later statistical analysis. Correlations between technical replicates analyzed within and across CAS (where applicable) were calculated to evaluate intra- and inter-site reproducibility; the data from technical replicates were then averaged for downstream

analysis. Finally, features with quantification in less of 30% of all samples were removed. For specific details of the process, see available code.

Metabolomics and Lipidomics

The metabolomic analysis was performed by investigators across multiple *Chemical Analysis Sites* that employed different technical platforms for data acquisition. At the highest level, these platforms were divided into two classes: *Targeted* and *Untargeted*. The data generated by the untargeted platforms were further divided into Named (confidently identified chemical entities) and Unnamed (confidently detected, but no chemical name annotation) compounds.

Targeted metabolomics data were generated at 3 analysis Sites: Duke University, the Mayo Clinic, and Emory University. Duke quantified metabolites belonging to the metabolite classes Acetyl-CoA, Keto Acids, and Nucleic Acids ("acoa", "ka", "nuc"), Mayo quantified amines and TCA intermediates (“amines” and “tca”), while Emory quantified Oxylipins (“oxylipneg”).

The untargeted metabolomics data were generated at 3 analysis Sites: the Broad Institute, the University of Michigan, and the Georgia Institute of Technology (Georgia Tech). The Broad Institute applied Hydrophilic interaction liquid chromatography (HILIC) in the positive ion mode (hilicpos), Michigan applied reverse phase liquid chromatography in both positive and negative ion modes (“rppos” and “rpneg”) and ion-pairing chromatography in the negative mode (“ionpneg”), and Georgia Tech performed lipidomics assays using reverse phase chromatography in both positive and negative ion modes (“lrppos” and “lrpneg”).

LC-MS/MS analysis of branched-chain keto acids

Duke University conducted targeted profiling of branched-chain keto acid metabolites. Plasma samples containing isotopically labeled ketoleucine (KIC)-d3, ketoisovalerate (KIV)-$^{13}C_5$ (from Cambridge Isotope Laboratories), and 3-methyl-2-oxovalerate (KMV)-d8 (from Toronto Research Chemicals, Canada) internal standards, were subjected to deproteinization with 3M perchloric acid. Tissue homogenates were prepared at 100 mg/ml in 3M perchloric acid and 200 µL was centrifuged.

Next, 200 µL of 25 M o-phenylenediamine (OPD) in 3M HCl were added to both the plasma and tissue supernatants. The samples were incubated at 80°C for 20 minutes. Keto acids were then extracted using ethyl acetate, following a previously described protocol.[125, 126] The extracts were dried under nitrogen, reconstituted in 200 mM ammonium acetate, and subjected to analysis on

a Xevo TQ-S triple quadrupole mass spectrometer coupled to an Acquity UPLC (Waters), controlled by the MassLynx 4.1 operating system.

The analytical column used was a Waters Acquity UPLC BEH C18 Column (1.7 µm, 2.1 × 50 mm), maintained at 30°C. 10 µL of the sample were injected onto the column and eluted at a flow rate of 0.4 ml/min. The gradient consisted of 45% mobile phase A (5 mM ammonium acetate in water) and 55% mobile phase B (methanol) for 2 minutes. This was succeeded by a linear gradient to 95% B from 2 to 2.5 minutes, holding at 95% B for 0.7 minutes, returning to 45% A, and finally re-equilibrating the column at initial conditions for 1 minute. The total run time was 4.7 minutes.

In positive ion mode, mass transitions of m/z 203 → 161 (KIC), 206 → 161 (KIC-d3), 189 → 174 (KIV), 194 → 178 (KIV-$^{5}C_{13}$), 203 → 174 (KMV), and 211 → 177 (KMV-d8) were monitored. Endogenous keto acids were quantified using calibrators prepared by spiking dialyzed fetal bovine serum with authentic keto acids (Sigma-Aldrich).

Flow injection MS/MS analysis of acyl CoAs

Duke University conducted targeted profiling of acyl CoAs. Here, 500 µL of tissue homogenate, prepared at a concentration of 50 mg/ml in isopropanol/0.1 M KH2PO4 (1:1), underwent extraction with an equal volume of acetonitrile. The resulting mixture was then centrifuged at 14,000 x g for 10 minutes, following a previously established procedure.[127, 128]

The supernatants were acidified with 0.25 ml of glacial acetic acid, and the acyl CoAs were subjected to additional purification through solid-phase extraction (SPE) using 2-(2-pyridyl) ethyl functionalized silica gel (Sigma-Aldrich), as outlined in Minkler et al. (2008). Prior to use, the SPE columns were conditioned with 1 ml of acetonitrile/isopropanol/water/glacial acetic acid (9/3/4/4 : v/v/v/v). After application and flow-through of the supernatant, the SPE columns underwent a washing step with 2 ml of acetonitrile/isopropanol/water/glacial acetic acid (9/3/4/4 : v/v/v/v). Acyl CoAs elution was achieved with 2 ml of methanol/250 mM ammonium formate (4/1 : v/v), followed by analysis using flow injection MS/MS in positive ion mode on a Xevo TQ-S triple quadrupole mass spectrometer (Waters). The mobile phase used was methanol/water (80/20, v/v) with 30 mM ammonium hydroxide. Spectra were acquired in the multichannel acquisition mode, monitoring the neutral loss of 507 amu (phosphoadenosine diphosphate) and scanning from m/z 750 to 1100. As an internal standard, heptadecanoyl CoA was employed.

Quantification of endogenous acyl CoAs was carried out using calibrators created by spiking tissue homogenates with authentic Acyl CoAs (Sigma-Aldrich) that covered saturated acyl chain lengths from C0 to C18. Empirical corrections for heavy isotope effects, particularly ^{13}C, to the adjacent m+2 spectral peaks in a specific chain length cluster were made by referring to the observed spectra for the analytical standards.

LC-MS/MS analysis of nucleotides

Duke University conducted targeted profiling of nucleotide metabolites. 300 µL of tissue homogenates, prepared at a concentration of 50 mg/ml in 70% methanol, underwent spiking with nine internal standards: $^{13}C^{10}$,$^{15}N^{5}$-adenosine monophosphate, $^{13}C^{10}$,$^{15}N^{5}$-guanosine monophosphate, $^{13}C^{10}$,$^{15}N^{2}$-uridine monophosphate, $^{13}C^{9}$,$^{15}N^{3}$-cytidine monophosphate, $^{13}C^{10}$-guanosine triphosphate, $^{13}C^{10}$-uridine triphosphate, $^{13}C^{9}$-cytidine triphosphate, $^{13}C^{10}$-adenosine triphosphate, and nicotinamide-1, N^{6}-ethenoadenine dinucleotide (eNAD) (all from Sigma-Aldrich).

Nucleotides were extracted using an equal volume of hexane, following the procedures previously outlines.[129, 130] After vortexing and centrifugation at 14,000 x g for 5 minutes, the bottom layer was subjected to another centrifugation. Chromatographic separation and MS analysis of the supernatants were performed using an Acquity UPLC system (Waters) coupled to a Xevo TQ-XS quadrupole mass spectrometer (Waters).

The analytical column employed was a Chromolith FastGradient RP-18e 50-2mm column (EMD Millipore, Billerica, MA, USA), that was maintained at 40°C. The injection volume was 2 µL. Nucleotides were separated using a mobile phase A consisting of 95% water, 5% methanol, and 5 mM dimethylhexylamine adjusted to pH 7.5 with acetic acid. Mobile phase B comprised 20% water, 80% methanol, and 10 mM dimethylhexylamine. The flow rate was set to 0.3 ml/min. The 22-minute gradient (t=0, %B=0; t=1.2, %B=0; t=22, %B=40) was followed by a 3-minute wash and 7-minute equilibration. Nucleotides were detected in the negative ion multiple reaction monitoring (MRM) mode based on characteristic fragmentation reactions. Endogenous nucleotides were quantified using calibrators prepared by spiked-in authentic nucleotides obtained from Sigma-Aldrich.

LC-MS/MS analysis of amino metabolites

The Mayo Clinic conducted LC-MS-based targeted profiling of amino acids and amino metabolites, as previously outlined (Gonsalves et al., 2020; Lanza et al., 2010). In summary, either 20 ml of plasma samples or 5 mg of tissue homogenates were supplemented with an internal standard solution comprising isotopically labeled amino acids (U-$^{13}C^4$ L-aspartic acid, U-$^{13}C_3$ alanine, U-$^{13}C_4$ L-threonine, U-^{13}C L-proline, U-$^{13}C_6$ tyrosine, U-$^{13}C_5$ valine, U-$^{13}C_6$ leucine, U-$^{13}C_6$ phenylalanine, U-$^{13}C_3$ serine, U-$^{13}C_5$ glutamine, U-$^{13}C_2$ glycine, U-$^{13}C_5$ glutamate, U-$^{13}C_6$,$^{15}N_2$ lysine, U-$^{13}C_5$,^{15}N methionine, 1,1U-$^{13}C_2$ homocysteine, U-$^{13}C_6$ arginine, U-$^{13}C_5$ ornithine, $^{13}C_4$ asparagine, $^{13}C_2$ ethanolamine, D_3 sarcosine, D_6 4-aminobutyric acid).

The supernatant was promptly derivatized using 6-aminoquinolyl-N-hydroxysuccinimidyl carbamate with a MassTrak kit (Waters). A 10-point calibration standard curve underwent a similar derivatization procedure after the addition of internal standards. Both the derivatized standards and samples were subjected to analysis using a Quantum Ultra triple quadrupole mass spectrometer (ThermoFischer) coupled with an Acquity liquid chromatography system (Waters). Data acquisition utilized selected ion monitoring (SRM) in positive ion mode. The concentrations of 42 analytes in each unknown sample were calculated against their respective calibration curves.

GC-MS analysis of TCA metabolites

The Mayo Clinic conducted GC-MS-targeted profiling of tricarboxylic acid (TCA) metabolites, as previously detailed (Dutta et al., 2016; Wilkins et al., 2019), with some modifications. In summary, 5 mg of tissue were homogenized in 1X PBS using an Omni bead ruptor (Omni International, Kennesaw, GA), followed by the addition of 20 µL of an internal solution containing U-^{13}C labeled analytes ($^{13}C_3$ sodium lactate, $^{13}C_4$ succinic acid, $^{13}C_4$ fumaric acid, $^{13}C_4$ alpha-ketoglutaric acid, $^{13}C_4$ malic acid, $^{13}C_4$ aspartic acid, $^{13}C_5$ 2-hydroxyglutaric acid, $^{13}C_5$ glutamic acid, $^{13}C_6$ citric acid, $^{13}C_2$,^{15}N glycine, $^{13}C_2$ sodium pyruvate). For plasma, 50 µL were used.

The proteins were precipitated out using 300 µL of a mixture of chilled methanol and acetonitrile solution. After drying the supernatant in the speedvac, the sample was derivatized first with ethoxime and then with MtBSTFA + 1% tBDMCS (N-Methyl-N-(t-Butyldimethylsilyl)-Trifluoroacetamide + 1% t-Butyldimethylchlorosilane) and then analyzed on an Agilent 5977B GC/MS (Santa Clara, California) under single ion monitoring conditions using electron ionization. Concentrations of lactic acid (m/z 261.2), fumaric acid (m/z 287.1), succinic acid (m/z

289.1), ketoglutaric acid (m/z 360.2), malic acid (m/z 419.3), aspartic acid (m/z 418.2), 2-hydroxyglutaratic acid (m/z 433.2), cis-aconitic acid (m/z 459.3), citric acid (m/z 591.4), isocitric acid (m/z 591.4), and glutamic acid (m/z 432.4) were measured against 7-point calibration curves that underwent the same derivatization procedure.

Targeted lipidomics of low-level lipids

Lipid targeted profiling was conducted at Emory University following established methodologies as previously described.[131, 132] In summary, 20 mg of powdered tissue samples were homogenized in 100 µL PBS using Bead Ruptor (Omni International, Kennesaw, GA). Homogenized tissue samples (or plasma samples) were diluted with 300 µL 20% methanol and spiked with a 1% BHT solution to a final BHT concentration of 0.1% and pH of 3.0 by acetic acid addition. After centrifugation (10 minutes, 14000 rpm), the supernatants were transferred to 96-well plates for further extraction.

The supernatants were loaded onto Isolute C18 solid-phase extraction (SPE) columns that had been conditioned with 1000 µL ethyl acetate and 1000 µL 5% methanol. The SPE columns were washed with 800 µL water and 800 µL hexane, and the oxylipins were then eluted with 400 µL methyl formate. The SPE process was automated using a Biotage Extrahera (Uppsala, Sweden). The eluate was dried with nitrogen and reconstituted with 200 µL acetonitrile before LC-MS analysis. Sample blanks, pooled extract samples used as quality controls (QC), and consortium reference samples were prepared for analysis using the same methods. All external standards were purchased from Cayman Chemical (Ann Arbor, Michigan) at a final concentration in the range 0.01-20 µg/ml and consisted of: prostaglandin E2 ethanolamide (Catalog No. 100007212), oleoyl ethanolamide (Catalog No. 90265), palmitoyl ethanolamide (Catalog No. 10965), arachidonoyl ethanolamide (Catalog No. 1007270), docosahexaenoyl ethanolamide (Catalog No. 10007534), linoleoyl ethanolamide (Catalog No. 90155), stearoyl ethanolamide (Catalog No. 90245), oxy-arachidonoyl ethanolamide (Catalog No. 10008642), 2-arachidonyl glycerol (Catalog No. 62160), docosatetraenoyl ethanolamide (Catalog No. 90215), α-linolenoyl ethanolamide (Catalog No. 902150), oleamide (Catalog No. 90375), dihomo-γ-linolenoyl ethanolamide (Catalog No. 09235), decosanoyl ethanolamide (Catalog No. 10005823), 9,10 DiHOME (Catalog No. 53400), prostaglandin E2-1-glyceryl ester (Catalog No. 14010), 20-HETE (Catalog No. 10007269), 9-HETE (Catalog No. 34400), 14,15 DiHET (Catalog No. 10007267), 5(S)-HETE (Catalog No. 34210), 12(R)-HETE (Catalog No. 10007247), 11(12)-DiHET (Catalog No. 10007266), 5,6-DiHET (Catalog No. 10007264), thromboxane B2 (Catalog

No. 10007237), 12(13)-EpOME (Catalog No. 52450), 13 HODE (Catalog No. 38600), prostaglandin F2α (Catalog No. 10007221), 14(15)-EET (Catalog No. 10007263), 8(9)-EET (Catalog No. 10007261), 11(12)-EET (Catalog No. 10007262), leukotriene B4 (Catalog No. 20110), 8(9)-DiHET (Catalog No. 10007265), 13-OxoODE (Catalog No. 38620), 13(S)-HpODE (Catalog No. 48610), 9(S)-HpODE (Catalog No. 48410), 9(S)-HODE (Catalog No. 38410), resolvin D3 (Catalog No. 13834), resolvin E1 (Catalog No. 10007848), resolvin D1 (Catalog No. 10012554), resolvin D2 (Catalog No. 10007279), 9(S)HOTrE (Catalog No. 39420), 13(S)HOTrE (Catalog No. 39620), 8-iso Progstaglandin F2α (Catalog No. 25903), maresin 1 (Catalog No. 10878), maresin 2 (Catalog No. 16369).

LC-MS data were acquired using an Agilent 1290 Infinity II chromatograph from Agilent (Santa Clara, CA), equipped with a ThermoFisher Scientific AccucoreTM C18 column (100 mm × 4.6, 2.6 µm particle size), and coupled to Agilent 6495 mass spectrometer for polarity switch multiple reaction monitoring (MRM) scan. The mobile phases consisted of water with 10 mM ammonium acetate (mobile phase A) and acetonitrile with 10 mM ammonium acetate (mobile phase B). The chromatographic gradient program was: 0.5 minutes with 95% A; 1 minute to 2 minutes with 65% A; 2.1 minutes to 5.0 minutes with 45% A; 7 minutes to 20 minutes with 25% A; and 21.1 minutes until 25 minutes with 95% A. The flow rate was set at 0.40 ml/min. The column temperature was maintained at 35°C, and the injection volume was 6 µL. For MS analysis, the MRM analysis is operated at gas temperature of 290 °C, gas flow of 14 L/min, Nebulizer of 20 psi, sheath gas temperature of 300 °C, sheath gas flow of 11 L /min, capillary of 3000 V for both positive and negative ion mode, nozzle voltage of 1500 V for both positive and negative ion mode, high pressure RF of iFunnel parameters of 150V for both positive and negative ion mode, and low pressure of RF of iFunnel parameters of 60 V for both positive and negative ion mode. Skyline (version 25.1.0.142)[133] was utilized to process raw LC-MS data. Standard curves were constructed for each oxylipin/ethanolamide and scrutinized to ensure that all concentration points fell within the linear portion of the curve with an R-squared value not less than 0.9. Additionally, features exhibiting a high coefficient of variation (CV) among the quality control (QC) samples were eliminated from the dataset. Pearson correlation among the QCs for each tissue type was computed using the Hmisc R library, and the figures documented in the QC report were generated and visualized with the corrplot R library.[134, 135]

Hydrophilic interaction LC-MS metabolomics

The untargeted analysis of polar metabolites in the positive ionization mode was conducted at the Broad Institute of MIT and Harvard. The LC-MS system consisted of a Shimadzu Nexera X2 UHPLC (Shimadzu Corp., Kyoto, Japan) coupled to a Q-Exactive hybrid quadrupole Orbitrap mass spectrometer (Thermo Fisher Scientific). Plasma samples (10 µL) were extracted using 90 µL of 74.9/24.9/0.2 v/v/v acetonitrile/methanol/formic acid containing valine-d8 and phenylalanine-d8 internal standards. Following centrifugation, the supernatants were directly injected onto a 150 x 2 mm, 3 µm Atlantis HILIC column (Waters). Tissue (10 mg) homogenization was performed at 4°C using a TissueLyser II (QAIGEN) bead mill set to two 2 min intervals at 20 Hz in 300 µL of 10/67.4/22.4/0.018 v/v/v/v water/acetonitrile/methanol/formic acid valine-d8 and phenylalanine-d8 internal standards. The column was eluted isocratically at a flow rate of 250 µL/min with 5% mobile phase A (10 mM ammonium formate and 0.1% formic acid in water) for 0.5 minute, followed by a linear gradient to 40% mobile phase B (acetonitrile with 0.1% formic acid) over 10 minutes, then held at 40% B for 4.5 minutes. MS analyses utilized electrospray ionization in the positive ion mode, employing full scan analysis over 70-800 m/z at 70,000 resolution and 3 Hz data acquisition rate. Various MS settings, including sheath gas, auxiliary gas, spray voltage, and others, were specified for optimal performance. Data quality assurance was performed by confirming LC-MS system performance with a mixture of >140 well-characterized synthetic reference compounds, daily evaluation of internal standard signals, and the analysis of four pairs of pooled extract samples per sample type inserted in the analysis queue at regular intervals. One sample from each pair was used to correct for instrument drift using “nearest neighbor” scaling while the second reference sample served as a passive QC for determination of the analytical coefficient of variation of every identified metabolite and unknown. Raw data processing involved the use of TraceFinder software (v3.3, Thermo Fisher Scientific) for targeted peak integration and manual review, as well as Progenesis QI (v3.0, Nonlinear Dynamics, Waters) for peak detection and integration of both identified and unknown metabolites. Metabolite identities were confirmed using authentic reference standards.

Reversed Phase-High Performance & Ion-pairing LC metabolomics

Reversed-phase and ion pairing LC-MS profiling of polar metabolites was conducted at the University of Michigan. LC-MS grade solvents and mobile phase additives were procured from Sigma-Aldrich, while chemical standards were obtained from either Sigma-Aldrich or Cambridge Isotope Labs. Plasma (50 µL aliquot) was extracted by addition of 200 µL of 1:1:1 v:v methanol:acetonitrile:acetone containing the following internal standards diluted from stock

solutions to yield the specified concentrations: D_4-succinic acid, 12.5 µM; :D_3-malic acid,12.5 µM; D_5 -glutamic acid,12.5 µM; D_{10} -leucine,12.5 µM; D_5-tryptophan,12.5 µM;D_5-phenylalanine,12.5 µM; D_3-caffeine,12.5 µM; D_8-lysine,12.5 µM; D_4-chenodeoxycholic acid,12.5 µM; phosphatidylcholine(17:0/17:0),2.5 µM; phosphatidylcholine(19:0/19:0),2.5 µM; D_{31}-palmitic acid,12.5 µM; D_{35}-stearic acid,12.5 µM; gibberellic acid, 2.5 µM; epibrassinolide, 2.5 µM. The extraction solvent also contained a 1:400 dilution of Cambridge Isotope carnitine/acylcarnitine mix NSK-B, resulting in the following concentrations of carnitine/acylcarnitine internal standards: D_9-L-carnitine, 380 nM; D_3-L-acetylcarnitine, 95 nM; D_3-L-propionylcarnitine, 19 nM; D_3-L-butyrylcarnitine, 19 nM; D_9-L-isovalerylcarnitine, 19 nM; D_3-L-octanoylcarnitine, 19 nM; D_9-L-myristoylcarnitine, 19 nM; D_3-L-palmitoylcarnitine, 38 nM. After addition of solvent, samples were vortexed, incubated on ice for 10 minutes, and then centrifuged at 15,000 x g for 5 minutes. 150 µL supernatant were retrieved from the pellet, transferred to a glass autosampler vial with a 250 uL footed insert, and dried under a constant stream of nitrogen gas at ambient temperature. A QC sample was created by pooling residual supernatant from multiple samples. This QC sample underwent the same drying and reconstitution process as described for individual samples. Dried supernatants were stored at -80 C until ready for instrumental analysis. On the day of analysis, dried samples were reconstituted in 37.5 µL of 8:2 v:v water:methanol, vortexed thoroughly, and submitted for LC-MS.

Frozen tissue samples (skeletal muscle and adipose) were rapidly weighed into pre-tared, pre-chilled Eppendorf tubes and extracted in 1:1:1:1 v:v methanol:acetonitrile:acetone:water containing the following internal standards diluted from stock solutions to yield the specified concentrations: $^{13}C_3$-lactic acid, 12.5 µM; $^{13}C_5$-oxoglutaric acid, 125 nM;$^{13}C_5$-citric acid,1.25 µM; $^{13}C_4$-succinic acid,125 nM; $^{13}C_4$-malic acid, 125 nM; U-^{13}C amino acid mix (Cambridge Isotope CLM-1548-1), 2.5 µg/mL; $^{13}C_5$-glutamine, 6.25 µM;$^{15}N_2$-asparagine, 1.25 µM;$^{15}N_2$-tryptophan, 1.25 µM; $^{13}C_6$-glucose, 62.5 µM; D_4-thymine, 1 µM; ^{15}N-anthranillic acid, 1 µM; gibberellic acid,1 µM; epibrassinolide, 1 µM. The extraction solvent also contained a 1:400 dilution of Cambridge Isotope carnitine/acylcarnitine mix NSK-B, resulting in the following concentrations of carnitine/acylcarnitine internal standards: D_9-L-carnitine, 380 nM; D_3-L-acetylcarnitine, 95 nM; D_3-L-propionylcarnitine, 19 nM; D_3-L-butyrylcarnitine, 19 nM; D_9-L-isovalerylcarnitine, 19 nM; D_3-L-octanoylcarnitine, 19 nM; D_9-L-myristoylcarnitine, 19 nM; D_3-L-palmitoylcarnitine, 38 nM. Sample extraction was performed by adding chilled extraction solvent to tissue sample at a ratio of 1 ml solvent to 50 mg wet tissue mass. Immediately after solvent addition, the sample was homogenized using a Branson 450 probe sonicator. Subsequently, the tubes were mixed

several times by inversion and then incubated on ice for 10 minutes. Following incubation, the samples were centrifuged and 300 µL of the supernatant was carefully transferred to two autosampler vials with flat-bottom inserts and dried under a constant stream of nitrogen gas. A QC sample was created by pooling residual supernatants from multiple samples. This QC sample underwent the same drying and reconstitution process as described for individual samples. Dried supernatants were stored at -80 C until ready for instrumental analysis. On the day of analysis, samples were reconstituted in 60 µL of 8:2 v:v water:methanol and then submitted to LC-MS.

Reversed phase LC-MS samples were analyzed on an Agilent 1290 Infinity II / 6545 qTOF MS system with a JetStream electrospray ionization (ESI) source (Agilent Technologies, Santa Clara, California) using a Waters Acquity HSS T3 column, 1.8 µm 2.1 x 100 mm equipped with a matched Vanguard precolumn (Waters Corporation). Mobile phase A was 100% water with 0.1% formic acid and mobile phase B was 100% methanol with 0.025% formic acid. The gradient was as follows: Linear ramp from 0% to 100% B from 0-10 minutes, hold 100% B until 17 minutes, linear return to 0% B from 17 to 17.1 minutes, hold 0% B until 20 minutes. The flow rate was 0.45 ml/min, the column temperature was 55°C, and the injection volume was 5 µL. Each sample was analyzed twice, once in positive and once in negative ion mode MS, scan rate 2 spectra/sec, mass range 50-1200 m/z. Source parameters were: drying gas temperature 350°C, drying gas flow rate 10 L/min, nebulizer pressure 30 psig, sheath gas temperature 350°C and flow 11 L/minute, capillary voltage 3500 V, internal reference mass correction enabled. A QC sample run was performed at minimum every tenth injection.

Ion-pair LC-MS samples were analyzed on an identically-configured LC-MS system using an Agilent Zorbax Extend C18 1.8 µm RRHD column, 2.1 x 150 mm ID, equipped with a matched guard column. Mobile phase A was 97% water, 3% methanol. Mobile phase B was 100% methanol. Both mobile phases contained 15 mM tributylamine and 10 mM acetic acid. Mobile phase C was 100% acetonitrile. Elution was carried out using a linear gradient followed by a multi-step column wash including automated (valve-controlled) backflushing, detailed as follows: 0-2min, 0%B; 2-11 min, linear ramp from 0-99%B; 12-16 min, 99%B, 16-17.5min, 99-0%B. At 17.55 minutes, the 10-port valve was switched to reverse flow (back-flush) through the column. From 17.55-20.45 min the solvent was ramped from 99%B to 99%C. From 20.45-20.95 min the flow rate was ramped up to 0.8 mL/min, which was held until 22.45 min, then ramped down to 0.6mL/min by 22.65 min. From 22.65-23.45 min the solvent was ramped from 99% to 0% C while flow was simultaneously ramped down from 0.6-0.4mL/min. From 23.45 to

29.35 min the flow was ramped from 0.4 to 0.25mL/min; the 10-port valve was returned to restore forward flow through the column at 25 min. . Column temperature was 35°C and the injection volume was 5 µL. MS acquisition was performed in negative ion mode, scan rate 2 spectra/sec, mass range 50-1200 m/z. Source parameters were: drying gas temperature 250°C, drying gas flow rate 13 L/min, nebulizer pressure 35 psig, sheath gas temp 325°C and flow 12 L/min, capillary voltage 3500V, internal reference mass correction enabled. A QC sample run was performed at minimum every tenth injection.

Iterative MS/MS data was acquired for both reverse phase and ion pairing methods using the pooled sample material to enable compound identification. Eight repeated LC-MS/MS runs of the QC sample were performed at three different collision energies (10, 20, and 40) with iterative MS/MS acquisition enabled. The software excluded precursor ions from MS/MS acquisition within 0.5 minute of their MS/MS acquisition time in prior runs, resulting in deeper MS/MS coverage of lower-abundance precursor ions.

Feature detection and alignment was performed utilizing a hybrid targeted/untargeted approach. Targeted compound detection and relative quantitation was performed by automatic integration followed by manual inspection and correction using Profinder v8.0 (Agilent Technologies, Santa Clara, CA.) Non-targeted feature detection was performed using custom scripts that automate operation of the “find by molecular feature” workflow of the Agilent Masshunter Qualitative Analysis (v7) software package. Feature alignment and recursive feature detection were performed using Agilent Mass Profiler Pro (v8.0) and Masshunter Qualitative Analysis (“find by formula” workflow), yielding an aligned table including m/z, RT, and peak areas for all features.

Data Cleaning and Degeneracy Removal: The untargeted features and named metabolites were merged to generate a combined feature table. Features missing from over 50% of all samples in a batch or over 30% of QC samples were then removed prior to downstream normalization procedure. Next, the software package Binner was utilized to remove redundancy and degeneracy in the data.[136] Briefly, Binner first performs RT-based binning, followed by clustering of features by Pearson’s correlation coefficient, and then assigns annotations for isotopes, adducts or in-source fragments by searching for known mass differences between highly correlated features.

Normalization and Quality Control: Data were then normalized using a Systematic Error Removal Using Random Forest (SERRF) approach,[137] which helps correct for drift in peak

intensity over the batch using data from the QC sample runs. When necessary to correct for residual drift, peak area normalization to closest-matching internal standard was also applied to selected compounds. Both SERRF correction and internal standard normalization were implemented in R. Parameters were set to minimize batch effects and other observable drifts, as visualized using principal component analysis score plots of the full dataset. Normalization performance was also validated by examining relative standard deviation values for additional QC samples not included in the drift correction calculations.

Compound identification: Metabolites from the targeted analysis workflow were identified with high confidence (MSI level 1)[138] by matching retention time (+/- 0.1 minute), mass (+/- 10 ppm) and isotope profile (peak height and spacing) to authentic standards. MS/MS data corresponding to unidentified features of interest from the untargeted analysis were searched against a spectral library (NIST 2020 MS/MS spectral database or other public spectral databases) to generate putative identifications (MSI level 2) or compound-class level annotations (MSI level 3) as described previously.[139]

LC-MS/MS untargeted lipidomics

Sample preparation: Non-targeted lipid analysis was conducted at the Georgia Institute of Technology. Powdered tissue samples (10 mg) were extracted in 400 µL isopropanol containing stable isotope-labeled internal standards (IS) with bead homogenization with 2mm zirconium oxide beads (Next Advance) using a TissueLyser II (10min, 30 Hz). Samples were then centrifuged (5 min, 21,100xg), and supernatants were transferred to autosampler vials. Plasma samples (25 µL) were extracted by mixing with 75 µL isopropanol containing the IS mix followed by centrifugation. Sample blanks, pooled extract samples used as quality controls (QC), and consortium reference samples, were prepared for analysis using the same methods. The IS mix consisted of PC (15:0-18:1(d7)), Catalog No. 791637; PE (15:0-18:1(d7)), Catalog No. 791638; PS (15:0-18:1(d7)), Catalog No. 791639; PG(15:0-18:1(d7)), Catalog No. 791640; PI(15:0-18:1(d7)), Catalog No. 791641; LPC(18:1(d7)), Catalog No. 791643; LPE(18:1(d7)); Catalog No. 791644; Chol Ester (18:1(d7)), Catalog No. 700185; DG(15:0-18:1(d7)), Catalog No. 791647; TG(15:0-18:1(d7)-15:0), Catalog No. 791648; SM(18:1(d9)), Catalog No. 791649; Cholesterol (d7), Catalog No. 700041. All internal standards were purchased from Avanti Polar Lipids (Alabaster, Alabama) and added to the extraction solvent at a final concentration in the 0.1-8 µg/ml range.

Data collection: Lipid LC-MS data were acquired using a Vanquish (ThermoFisher Scientific) chromatograph fitted with a ThermoFisher Scientific AccucoreTM C30 column (2.1 × 150 mm, 2.6 µm particle size), coupled to a high-resolution accurate mass Q-Exactive HF Orbitrap mass spectrometer (ThermoFisher Scientific) for both positive and negative ionization modes. For positive mode analysis, the mobile phases were 40:60 water:acetonitrile with 10 mM ammonium formate and 0.1% formic acid (mobile phase A), and 10:90 acetonitrile:isopropyl alcohol, with 10 mM ammonium formate and 0.1% formic acid (mobile phase B). For negative mode analysis, the mobile phases were 40:60 water:acetonitrile with 10 mM ammonium acetate (mobile phase A), and 10:90 acetonitrile:isopropyl alcohol, with 10 mM ammonium acetate (mobile phase B). The chromatographic method used for both ionization modes was the following gradient program: 0 minutes 80% A; 1 minute 40% A; 5 minutes 30% A; 5.5 minutes 15% A; 8 minutes 10% A; held 8.2 minutes to 10.5 minutes 0% A; 10.7 minutes 80% A; and held until 12 minutes. The flow rate was set at 0.40 ml/min. The column temperature was set to 50°C, and the injection volume was 2 µL.

For analysis of the organic phase the electrospray ionization source was operated at a vaporizer temperature of 425°C, a spray voltage of 3.0 kV for positive ionization mode and 2.8 kV for negative ionization mode, sheath, auxiliary, and sweep gas flows of 60, 18, and 4 (arbitrary units), respectively, and capillary temperature of 275°C. The instrument acquired full MS data with 240,000 resolution over the 150-2000 m/z range. LC-MS/MS experiments were acquired using a DDA strategy. MS2 spectra were collected with a resolution of 120,000 and the dd-MS2 were collected at a resolution of 30,000 and an isolation window of 0.4 m/z with a loop count of top 7. Stepped normalized collision energies of 10%, 30%, and 50% fragmented selected precursors in the collision cell. Dynamic exclusion was set at 7 seconds and ions with charges greater than 2 were omitted.

Data processing: Data processing steps included peak detection, spectral alignment, grouping of isotopic peaks and adduct ions, drift correction, and gap filling. Compound Discoverer V3.3 (ThermoFisher Scientific) was used to process the raw LC-MS data. Drift correction was performed on each individual feature, where a Systematic Error Removal using Random Forest (SERRF) method builds a model using the pooled QC sample peak areas across the batch and was then used to correct the peak area for that specific feature in the samples. Detected features were filtered with background and QC filters. Features with abundance lower than 5x the background signal in the sample blanks and that were not present in at least 50% of the QC pooled injections with a coefficient of variance (CV) lower than 80% (not drift corrected) and

50% (drift corrected) were removed from the dataset. Lipid annotations were accomplished based on accurate mass and relative isotopic abundances (to assign elemental formula), retention time (to assign lipid class), and MS2 fragmentation pattern matching to local spectral databases built from curated experimental data. Lipid nomenclature followed that described previously.[140]

Quality control procedures: System suitability was assessed prior to the analysis of each batch. A performance baseline for a clean instrument was established before any experiments were conducted. The mass spectrometers were mass calibrated, mass accuracy and mass resolution were checked to be within manufacturer specifications, and signal-to-noise ratios for the suite of IS checked to be at least 75% of the clean baseline values. For LC-MS assays, an IS mix consisting of 12 standards was injected to establish baseline separation parameters for each new column. The performance of the LC gradient was assessed by inspection of the column back pressure trace, which had to be stable within an acceptable range (less than 30% change). Each IS mix component was visually evaluated for chromatographic peak shape, retention time (lower than 0.2 minute drift from baseline values) and FWHM lower than 125% of the baseline measurements. The CV of the average signal intensity and CV of the IS (<=15%) in pooled samples were also checked. These pooled QC samples were used to correct for instrument sensitivity drift over the various batches using a procedure similar to that described by the Human Serum Metabolome (HUSERMET) Consortium (ref). To evaluate the quality of the data for the samples themselves, the IS signals across the batch were monitored, PCA modeling for all samples and features before and after drift correction was conducted, and Pearson correlations calculated between each sample and the median of the QC samples.

Metabolomics/Lipidomics Data filtering and normalization

The untargeted metabolomics datasets were categorized as either “named”, for chemical compounds confidently identified, or “unnamed”, for compounds with specific chemical properties but without a standard chemical name. While the preprocessing steps were performed on the named and unnamed portions together, only the named portions were utilized for differential analysis. For each dataset i.e. each assay for each tissue type, the following steps are performed:

- Average rows that have the same metabolite ID.
- Merge the “named” and “unnamed” subparts of the untargeted datasets.

- Convert negative and zero values to NAs.
- Remove features with > 20% missing values.
- Features with < 20% missing values are imputed either using K-Nearest Neighbor imputation (for datasets with > 12 features) or half-minimum imputation (for datasets with < 12 features).
- All data are log2-transformed, and the untargeted data are median-MAD normalized if neither sample medians nor upper quartiles were significantly associated with sex or sex-stratified training group (Kruskal-Wallis p-value < 0.01). Note that for all log2 calculations, 1 is added to each value before log-normalization. This allows metabolite values that fall between 0 and 1 to have a positive log2 value.

Outlier detection was performed by examining the boxplot of each Principal Component and extending its whiskers to the predefined multiplier above and below the interquartile range (5x the IQR). Samples outside this range are flagged. All outliers were reviewed by Metabolomics CAS, and only confirmed technical outliers were removed.

Redundant Metabolite/Lipid Management

To address metabolites measured on multiple platforms (e.g. a metabolite measured on the HILIC positive and RP positive platforms), and metabolites with the same corresponding RefMet ID (e.g. alpha-Aminoadipic-acid, Aminoadipic acid both correspond to RefMet name ‘Aminoadipic acid’), we utilize the set of internal standards described above to make a decision on which platform’s measurement of a given feature to include in further analysis. For each tissue, based on whichever platform has the lowest coefficient of variation across all included reference standards for a given refmet id, that metabolite was chosen. The other platforms or metabolites, for this tissue, corresponding to this refmet id were removed from further downstream analysis. Data for all metabolites removed, including information about the coefficient of variation in the standards, normalized data, or differential analysis results, is available in the R Package *MotrpacHumanPreSuspensionData*, but is not loaded by default.

Statistical analysis

Differential analysis

To model the effects of both exercise modality and time, relative to non-exercising control, each measured molecular feature was treated as an outcome in a linear mixed effects model accounting for fixed effects of exercise group (RE, EE, or CON), timepoint, as well as demographic and technical covariates (see covariate selection below for more info). Participant identification was treated as a random effect. For each molecular feature, a cell-means model is fit to estimate the mean of each exercise group-timepoint combination, and all hypothesis tests are done comparing the means of the fixed effect group-timepoint combinations. In order to model the effects of exercise against non-exercising control, a difference-in-changes model was used which compared the change from pre-exercise to a during or post-exercise timepoint in one of the two exercise groups to the same change in control. This effect is sometimes referred to as a "delta-delta" or "difference-in-differences" model.

Model selection via simulation

In order to determine the optimal statistical package/model for these data – given MoTrPAC's unique sampling design (see 'acute exercise intervention' above) – a simulation study was conducted to determine the impact of various approaches to account for correlation in repeated measurements. The simulation evaluated type 1 error, power, and bias for multiple plausible modeling approaches, to identify those that would obtain higher power while maintaining nominal type 1 error rates. For a subset of molecular features in the datasets, mean, covariance, skew, and kurtosis were summarized over the relevant timepoints in the acute exercise bout within subgroups defined by sex and exercise type. Then, these summary values were used in combination with the "covsim" R package to generate non-normally distributed simulated data.[141] Additionally, sample size and missingness patterns were aligned in the simulated data to match those of the observed data. Using a total of 5 million simulated instances where data were generated under the null hypothesis (i.e., no change in the mean values of the outcome over the exercise timepoints) or alternative hypothesis (i.e., the mean value of the outcome differs between at least two timepoints), type 1 error rate and power, respectively, were evaluated for seven analytic strategies: (1) pairwise t-tests between timepoints of interest, (2) ordinary least squares regression, (3) differential expression for repeated measures (i.e., dream) with random intercepts,[119] (4) linear mixed models with random intercepts, (5) mixed models for repeated measures using an unstructured covariance matrix, and (6) generalized linear models using generalized estimating equations (GEEs) and a first degree autoregressive correlation structure. These analyses were replicated for adipose, blood, and muscle samples. The dream function obtained type 1 error rates 5.2, 5.4, and 5.2% for

adipose, blood, and muscle analyses, respectively, with higher power than all other methods apart from generalized linear models with GEEs. Although generalized linear models with GEEs had higher power than dream, they also had higher type 1 error with 7.7%, 6.0%, and 6.5% type 1 error rates for adipose, blood, and muscle analyses, respectively. Therefore, due to stability of type 1 error and relatively high power compared to other approaches, the *dream* function from the variancePartition R package was selected for the primary analyses for every omic platform except Methyl-Cap (see methylation capture sequencing methods above for more details).[119]

Covariate selection

Covariates were selected through a combination of a priori knowledge about factors influencing molecular levels as well through empiric screening. Factors were considered for model inclusion by correlating the principal components of each tissue-ome feature set to demographic and technical factors using variancePartition::canCorPairs.[119] Visualizations and computational analysis that describe this process for the decisions for covariate selection can be found at: https://github.com/MoTrPAC/precovid-analyses/tree/main/QC. Ultimately, the following fixed effect covariates were included in the models for every omic platform: group and timepoint in a cell means model, clinical site, age, sex, and BMI. 'Participant id' was included as a random effect in every model. Each -ome then had ome-specific covariates selected as described in prior sections.

A targeted analysis was conducted to assess whether and how race, ethnicity, and genetic ancestry could be incorporated, given prior evidence that these factors can influence omic data.[142, 143] We evaluated multiple models that included patient-reported race and/or ethnicity, as well as principal components derived from whole-genome sequencing (WGS), to determine their impact on model fit using the BIC. However, no combinations of individual or joint inclusion of race, ethnicity, or WGS-derived principal components led to an improvement in average model BIC across all features for a platform.

The final set of covariates included in each model for each tissue and ome can be found in the R Package *MotrpacHumanPreSuspensionData*, and the *Multi-Omic Landscape* (REF).

Missingness

Data missingness varied for multiple reasons including experimental design (i.e. temporal randomization which randomized some participants to have samples obtained at a subset of

timepoints, see assay limitations (metabolomics and proteomics can have missingness as described in their individual sections). For some omic sets, imputation to alleviate missingness could be performed (metabolomics) but for others was not, including proteomics. Analysis demonstrated proteomics missingness was approximately at random (data not shown).

Given the above issues affecting the ultimate sample size for effect estimation, for a feature to be included in the analysis, a minimum number of 3 participants were required to have a paired pre-exercise sample for all groups and all during/post-exercise timepoints. Thus, all group comparisons (e.g. RE vs CON at 3.5 h post-exercise) required 3 participants with matched pre- and post-exercise samples in each group. This requirement was satisfied in all omes and tissues except a subset of MS-acquired proteomics features in SKM and AT. Features not meeting this criterion in any group-timepoint set were excluded from differential analysis entirely, though raw and QC-normalized values are available.

Specific omic-level statistical considerations

Models for all omes were fit using 'variancePartition::dream'.[119] For the transcriptomics, which are measured as numbers of counts, the mean-variance relationship was measured using 'variancePartition::voomWithDreamWeights' as previously described.[119] For all other omes the normalized values were used directly as input to the statistical model.

The full implementation of the statistical models for each dataset can be found in the R Package *MotrpacHumanPreSuspensionData*.

Contrast types

The specific contrasts made in the statistical analysis include three categories of comparison: difference-in-changes relative to control, group-specific, and resistance vs endurance. All comparisons were structured using 'variancePartition::makeContrastsDream'.[119]

The difference-in-changes model as described at the opening of this section represents the primary DA analysis, and any individual feature mentioned as statistically significantly changing due to exercise will be referring to the difference-in-changes results unless otherwise specifically stated.

The next category of contrasts is a group-specific comparison, which compares a given post-intervention timepoint to pre-exercise within a given group, without comparing to the control

group. This contrast was implemented to more easily quantify effect sizes within each group independently, but are not used as a general endpoint.

Significance thresholds

For each of the above contrasts, p-values were adjusted for multiple comparisons for each unique contrast-group-tissue-ome-timepoint combination separately using the Benjamini-Hochberg method to control False Discovery Rate (FDR).[144] Features were considered significant at a FDR of 0.05 unless otherwise stated.

Human feature to gene mapping

The feature-to-gene map links each feature tested in differential analysis to a gene, using Ensembl version 105 (mapped to GENCODE 39) as the gene identifier source.[145] Proteomics feature IDs (UniProt IDs) were mapped to gene symbols and Entrez IDs using UniProt's mapping files.[146] Gene symbols, Entrez IDs, and Ensembl IDs were assigned to features using biomaRt version 2.58.2 (Bioconductor 3.18).[147, 148]

Metabolite features were mapped to KEGG IDs using KEGGREST, RefMet REST API, or web scraping from the Metabolomics Workbench.[149, 150]

Enrichment analysis

Preparation of differential analysis results

The differential analysis results tables for each combination of tissue and ome were converted to matrices of z-scores with either gene symbols, RefMet metabolite/lipid IDs, or phosphorylation flanking sequences as rows and contrasts as columns. These matrices serve as input for the enrichment analyses. For the transcriptomics, transcripts were first mapped to gene symbols. To resolve cases where multiple features mapped to a single gene, only the most extreme z-score for each combination of tissue, contrast, and gene was retained. Metabolite and lipid identifiers were standardized using the Metabolomic Workbench Reference List of Metabolite Names (RefMet) database.

Gene set selection

Gene sets were obtained from the MitoCarta3.0 database, CellMarker 2.0 database,[82] and the C2-CP (excluding KEGG_LEGACY) and C5 collections of the human Molecular Signatures

Database (MSigDB; v2023.2.Hs).[82, 151, 152] Metabolites and lipids were grouped according to chemical subclasses from the RefMet database.[153] This includes subclasses such as “Acyl carnitines” and “Saturated fatty acids”.

For each combination of tissue and ome, molecular signatures were filtered to only those genes and metabolites/lipids that appeared in the differential analysis results. After filtering, all molecular signatures were required to contain at least 5 features, with no restriction on the maximum size of sets. Additionally, gene sets were only kept if they retained at least 70% of their original genes to increase the likelihood that the genes that remain in a given set are accurately described by the set label. Gene set enrichment was thus not performed among plasma proteomics given limited membership among the targeted platform.

Analysis of Molecular Signatures

Analysis of molecular signatures was carried out with the pre-ranked Correlation Adjusted MEan RAnk (CAMERA-PR) gene set test using the z-score matrices described in the “Preparation of differential analysis results” section to summarize the differential analysis results for each contrast at the level of molecular signatures.[154] Z-scores were selected as the input statistics primarily to satisfy the normality assumption of CAMERA-PR, and the analysis was carried out with the *cameraPR.matrix* function from the TMSig R/Bioconductor package.[155, 156]

Over-representation analysis (ORA)

Over-representation analysis (ORA) was conducted using the run_ORA function from the *MotrpacHumanPreSuspension* R package (v0.0.1.53) which uses the hypergeometric test for statistical significance. The input consisted of differentially expressed genes (adjusted p-value < 0.05) identified from one or more omic layers in a particular tissue. The background gene set included all genes detected in each of the ome(s) and tissue(s) under consideration.

Statistical significance thresholds

For both CAMERA-PR and ORA results, p-values were adjusted within each combination of tissue, ome, contrast, and broad molecular signature collection (MitoCarta3.0, CellMarker 2.0, C2, C5, RefMet, PSP, and PTMsigDB) using the Bejamini-Hochberg method. Gene sets and RefMet subclasses were declared significant if their adjusted p-values were less than 0.05.

Visualization methods

Bubble heatmaps were generated from the enrichment analysis results using the *enrichmap* function from the TMSig R/Bioconductor package.[155]

C-means clustering

Fuzzy c-mean clustering was performed using the Mfuzz R package[40] after log2-transformation and Z-score scaling of the filtered and normalized plasma metabolite data. We calculated the minimum centroid distance for a range of cluster numbers and the final cluster numbers were determined through manual inspection after using the 'elbow' method.

In silico plasma secretome analyses

Published atlases of human plasma protein tissue and/or cellular sources were used to map the putative location of exercise-responsive plasma proteins. Briefly, these resources used MS proteomic and/or RNA data across 29 tissues and 8 cell types from three separate human studies, EMBL-EBI, GTEx, and HATLAS to infer the tissue source for a given plasma protein; detailed descriptions of these datasets are found here.[71-73] Protein-tissue relationships were categorized according to: single tissue- or cell-enriched; multiple tissues or cell-types; or common; and subsequently assigned a confidence score (global label score, GLS) based on tissue labels across the three atlases.[71] Proteins were then assigned to the tissue or cell labels with the highest GLS on a 0-4 scale, with increasing score reflecting increasing confidence in a given tissue assignment. Using these methods, we subsequently mapped the 189 unique DA plasma proteins in EE and/or RE in MoTrPAC to their annotated tissue source and by GLS. MoTrPAC participants' adipose and skeletal muscle transcriptional and global proteomic responses to exercise for a given DA plasma protein were then compared to evaluate the plasma protein's putative tissue source during exercise.

Cell deconvolution

We used the program CIBERSORTx[89] to conduct cell type deconvolution operations. The normalized blood RNAseq data across all control and exercise samples were used as input and the LM22 leukocyte cell type signature matrix was used as the reference.[113] CIBERSORTx generated as output a predicted cell type composition for each sample. Mean cell type proportion was displayed for each cell type across all pre-exercise samples to present a

baseline estimate for cell type composition. T tests measuring the statistical significance of differences in cell type composition for each cell type at each time point within each exercise mode and control were calculated with the *compare_means* R function.

Canonical Correlation Analysis

To identify metabolite signatures associated with variation across cardiorespiratory fitness, muscle strength, and metabolic phenotypes, we applied sparse CCA to baseline plasma metabolomic profiles and exercise-related clinical traits. This multivariate approach identifies shared axes of variation between two high-dimensional datasets by maximizing the correlation between linear combinations of features from each domain.[50] Unlike principal component analysis or traditional regression, CCA jointly optimizes associations between domains without predefining one as explanatory and the other as outcome.

We used pre-exercise plasma metabolomics data and a curated set of exercise phenotypes spanning aerobic fitness (e.g. VO_2peak, O_2 pulse, ventilatory threshold), hemodynamic responses (e.g. exercise systolic/diastolic blood pressure), and muscular strength (e.g. handgrip and isokinetic torque). Sparse penalized CCA was implemented using the *PMA* R package, with optimal regularization parameters for each domain selected via 1,000 permutations. The final model retained the top three canonical variates for interpretation. Canonical weights were visualized using clustered heatmaps to highlight metabolite-trait associations for each variate. Each canonical variate was visualized based on the strongest exercise trait loadings and the associated top metabolite contributors.

QUANTIFICATION AND STATISTICAL ANALYSIS

Statistical parameter reporting

All relevant statistical parameters for the analyses performed in this study such as sample size (*N*), center and spread (e.g. mean/median, standard deviation/error), statistical methodology (e.g. mixed-effects linear model) and significance cutoffs (e.g. adjusted *p*-value < 0.05) are reported in the main text, figure legends, STAR Methods, and/or supplementary information.

Where appropriate, methods used to determine the validity of certain statistical assumptions are discussed.

Statistical limitations

This report presents analyses and results for 206 participants randomized before the suspension of the MoTrPAC study due to the COVID-19 pandemic. The main post-suspension MoTrPAC study will include over 1,500 participants randomized under a slightly modified protocol.[35] The current paper focuses on evaluating feasibility and generating hypotheses for the main study. Results should be interpreted with caution for several reasons: 1) small sample sizes reduce the power to detect even moderate effects;[157] 2) simple randomization of small groups can create imbalances in both known and unknown confounders;[158, 159] and 3) NIH initiatives have long emphasized caution in interpreting small studies to enhance reproducibility.[160]

Although blocked randomization with site-based stratification was employed, discrepancies in regulatory approvals, start-up times, and pandemic-related interruptions resulted in imbalanced and small sample sizes. Specific limitations in the baseline (pre-intervention) data include: 1) subgroup sample sizes based on intervention group, sex, and timepoint as small as 4 participants; 2) limited generalizability, as 50% of controls with biosamples were randomized at two of the ten sites, and 74% of participants at four sites; and 3) "sex differences" may reflect "body composition differences" due to insufficient data to disentangle sex from body composition, and variations in DXA machine operators and brands across sites.

Testing for heterogeneity of response in small subgroups was largely avoided. As Brookes et al. show,[161] interaction effects must be at least double the main effect to achieve 80% power. While the EE and RE groups each had around 70 participants with biosamples, providing 80% power to detect a 0.5 effect size (difference in means/SD) using a two-sample t-test (alpha = 0.05, two-sided), for tests of interaction effects to have 80% power an interaction effect size > 1 would be required, which is considered large.[162] Consequently, heterogeneity of response was explored only descriptively within the larger randomized groups (EE/RE), with some inferential statistics (e.g., confidence intervals, p-values) emphasizing interval estimation. Our aim was to present the results from a hypothesis-generating perspective, following Ioannidis's cautionary guidance,[157] and to lay a solid foundation for future analyses in the main MoTrPAC study.

Additional resources

Package assembly and distribution

The MotrpacHumanPreSuspensionData R package (https://github.com/MoTrPAC/MotrpacHumanPreSuspensionData) contains data objects that correspond to the products of the normalized data analysis, differential abundance analysis, enrichment analysis, feature to gene mapping, and molecular signature datasets as described in the methods.

Data used in the preparation of this article were obtained from the Molecular Transducers of Physical Activity Consortium (MoTrPAC) database, which is available for public access at motrpac-data.org. Specific datasets used are human-precovid-sed-adu-v1.2.

The MotrpacHumanPreSuspension R package (https://github.com/MoTrPAC/MotrpacHumanPreSuspension) contains functions to generate visualizations, using the objects in the MotrpacHumanPreSuspensionData package.

Lastly, the precovid-analyses GitHub repository (https://github.com/MoTrPAC/precovid-analyses) contains code and individual parameters for each figure panel, utilizing the MotrpacHumanPreSuspension and MotrpacHumanPreSuspensionData packages

Acknowledgements

The MoTrPAC Study is supported by NIH grants U24OD026629 (Bioinformatics Center), U24DK112349, U24DK112342, U24DK112340, U24DK112341, U24DK112326, U24DK112331, U24DK112348 (Chemical Analysis Sites), U01AR071133, U01AR071130, U01AR071124, U01AR071128, U01AR071150, U01AR071160, U01AR071158 (Clinical Centers), U24AR071113 (Consortium Coordinating Center), U01AG055133, U01AG055137, U01AG055135, U01AG070959, U01AG070960, and U01AG070928 (Pre-Clinical Animal Sites). JMR is supported by NIH K23 HL150327; R03OD038387. MEL is supported by Wu Tsai Human Performance Alliance.

Author information

MoTrPAC Study Group

Bioinformatics Center: David Amar, Trevor Hastie, David Jimenez-Morales, Daniel H. Katz, Malene E. Lindholm, Samuel Montalvo, Robert Tibshirani, Jay Yu, Jimmy Zhen, Euan A. Ashley, Matthew T. Wheeler

Biospecimens Repository: Sandra T. May, Jessica L. Rooney, Russell Tracy

Data Management, Analysis, and Quality Control Center: Catherine Gervais, Fang-Chi Hsu, Byron C. Jaeger, David Popoli, Joseph Rigdon, Courtney G. Simmons, Cynthia L. Stowe, Michael E. Miller

Exercise Intervention Core: W. Jack Rejeski

NIH: Ashley Y. Xia

Preclinical Animal Study Sites: Sue C. Bodine, R. Scott Rector

Chemical Analysis Sites: Hiba Abou Assi, Mary Anne S. Amper, Brian J. Andonian, Isaac K. Attah, Jacob L. Barber, Kevin Bonanno, Clarisa Chavez Martinez, Natalie M. Clark, Johanna Y. Fleischman, David A. Gaul, Yongchao Ge, Marina A. Gritsenko, Joshua R. Hansen, Patrick Hart, Zhenxin Hou, Chelsea M. Hutchinson-Bunch, Olga Ilkayeva, Gayatri Iyer, Pierre M. Jean-Beltran, Christopher A. Jin, Maureen T. Kachman, Hasmik Keshishian, Damon T. Leach, Minghui Lu, D. R. Mani, Gina M. Many, Nada Marjanovic, Nikhil Milind, Matthew E. Monroe, Ronald J. Moore, Venugopalan D. Nair, German Nudelman, Nora-Lovette Okwara, Vladislav A. Petyuk, Paul D. Piehowski, Hanna Pincas, Wei-Jun Qian, Prashant Rao, Abraham Raskind, Alexander Raskind, Stas Rirak, Jeremy M. Robbins, Margaret Robinson, Tyler J. Sagendorf, James A. Sanford, Gregory R. Smith, Kevin S. Smith, Yifei Sun, Mital Vasoya, Nikolai G. Vetr, Alexandria Vornholt, Yilin Xie, Xuechen Yu, Elena Zaslavsky, Zidong Zhang, Bingqing Zhao, Joshua N. Adkins, Charles F. Burant, Steven A. Carr, Clary B. Clish, Facundo M. Fernandez, Robert E. Gerszten, Stephen B. Montgomery, Christopher B. Newgard, Eric A. Ortlund, Stuart C. Sealfon, Michael P. Snyder, Martin J. Walsh

Clinical Sites: Cheehoon Ahn, Alicia Belangee, Bryan C. Bergman, Daniel H. Bessesen, Gerard A. Boyd, Anna R. Brandt, Nicholas T. Broskey, Toby L. Chambers, Clarisa Chavez Martinez, Maria Chikina, Alex Claiborne, Zachary S. Clayton, Paul M. Coen, Katherine A. Collins-Bennett, Tiffany M. Cortes, Gary R. Cutter, Matthew Douglass, Daniel E. Forman, Will A. Fountain, Aaron H. Gouw, Kevin J. Gries, Fadia Haddad, Joseph A. Houmard, Kim M. Huffman, Ryan P. Hughes, John M. Jakicic, Catherine M. Jankowski, Neil M. Johannsen, Johanna L. Johnson, Erin E. Kershaw, Dillon J. Kuszmaul, Bridget Lester, Colleen E. Lynch, Edward L. Melanson, Cristhian Montenegro, Kerrie L. Moreau, Masatoshi Naruse, Bradley C Nindl, Tuomo Rankinen, Ulrika Raue, Ethan Robbins, Kaitlyn R. Rogers, Renee J. Rogers, Irene E. Schauer, Robert S. Schwartz, Chad M. Skiles, Lauren M. Sparks, Maja Stefanovic-Racic, Andrew M. Stroh, Kristen J. Sutton, Anna Thalacker-Mercer, Todd A. Trappe, Caroline S. Vincenty, Elena Volpi, Katie L. Whytock, Gilhyeon Yoon, Thomas W. Buford, Dan M. Cooper, Sara E. Espinoza, Bret H. Goodpaster, Wendy M. Kohrt, William E. Kraus, Nicolas Musi, Shlomit Radom-Aizik, Blake B. Rasmussen, Eric Ravussin, Scott Trappe

MoTrPAC Acknowledgements

Nicole Adams, Abdalla Ahmed, Andrea Anderson, Carter Asef, Arianne Aslamy, Marcas M. Bamman, Jerry Barnes, Susan Barr, Kelsey Belski, Will Bennett, Kevin Bonanno, Amanda Boyce, Brandon Bukas, Emily Carifi, Chih-Yu Chen, Haiying Chen, Shyh-Huei Chen, Maria Chikina, Samuel Cohen, Audrey Collins, Gavin Connolly, Elaine Cornell, Julia Dauberger, Carola Ekelund, Shannon S. Emilson, Karyn A. Esser, Jerome Fleg, Nicole Gagne, Mary-Catherine George, Ellie Gibbons, Jillian Gillespie, Laurie Goodyear, Aditi Goyal, Bruce Graham, Xueyun Gulbin, Jere Hamilton, Leora Henkin, Andrew Hepler, Andrea Hevener, Olga Ilkayeva, Lidija Ivic, Ronald Jackson, Andrew Jones, Lyndon Joseph, Leslie Kelly, Ian Lanza, Gary Lee, Jun Li, Adrian Loubriel, Kristal M. Maner-Smith, Ryan Martin, Padma Maruvada, Alyssa Mathews, Curtis McGinity, Lucas Medsker, Kiril Minchev, Samuel G. Moore, Michael Muehlbauer, K Sreekumaran Nair, Anne Newman, John Nichols, Concepcion R. Nierras, George Papanicolaou, Lorrie Penry, Vladislav A. Petyuk, June Pierce, David Popoli, Megan Reaves, Eric W. Reynolds, Jeremy Rogers, Scott Rushing, Santiago Saldana, Rohan Shah, Samiya M. Shimly, Cris Slentz, Deanna Spaw, Debbie Steinberg, Suchitra Sudarshan, Alyssa Sudnick, Jennifer W. Talton, Christy Tebsherani, Nevyana Todorova, Mark Viggars, Jennifer Walker, Michael P. Walkup, Anthony Weakland, Gary Weaver, Christopher Webb, Sawyer Welden, John P. Williams, Marilyn Williams, Leslie Willis, Yi Zhang

Disclosures

Euan A. Ashley is Founder: Personalis, Deepcell, Svexa, Saturnus Bio, Swift Bio. Founder Advisor: Candela, Parameter Health. Advisor: Pacific Biosciences. Non-executive director: AstraZeneca, Dexcom. Publicly traded stock: Personalis, Pacific Biosciences, AstraZeneca. Collaborative support in kind: Illumina, Pacific Biosciences, Oxford Nanopore, Cache, Cellsonics. Stephen A. Carr is on the scientific advisory boards of PrognomIQ, MOBILion Systems, Kymera, and Stand Up2 Cancer. Pierre Jean Beltran is currently an employee at Pfizer, Inc. Bret H. Goodpaster has served as a member of scientific advisory boards. Byron Jaeger receives consulting fees from Perisphere Real World Evidence, LLC, unrelated to this project. Stephen B. Montgomery is a member of the scientific advisory board for PhiTech, MyOme and Valinor Therapeutics. Gary R. Cutter is a part of: Data and Safety Monitoring Boards: Applied Therapeutics, AI therapeutics, Amgen-NMO peds, AMO Pharma, Argenx, Astra-Zeneca, Bristol Meyers Squibb, CSL Behring, DiamedicaTherapeutics, Horizon Pharmaceuticals, Immunic, Inhrbx-sanfofi, Karuna Therapeutics, Kezar Life Sciences, Medtronic, Merck, Meiji Seika Pharma, Mitsubishi Tanabe Pharma Holdings, Prothena Biosciences, Novartis, Pipeline Therapeutics (Contineum), Regeneron, Sanofi-Aventis, Teva Pharmaceuticals, United BioSource LLC, University of Texas Southwestern, Zenas Biopharmaceuticals. Consulting or Advisory Boards: Alexion, Antisense Therapeutics/Percheron, Avotres, Biogen, Clene Nanomedicine, Clinical Trial Solutions LLC, Endra Life Sciences, Genzyme, Genentech, Immunic, Klein-Buendel Incorporated, Kyverna Therapeutics, Inc. , Linical, Merck/Serono, Noema, Neurogenesis, Perception Neurosciences, Protalix Biotherapeutics, Regeneron, Revelstone Consulting, Roche, Sapience Therapeutics, Tenmile. Dr. Cutter is employed by the University of Alabama at Birmingham and President of Pythagoras, Inc. a private consulting company located in Birmingham AL. John M. Jakicic is on the Scientific Advisory Board for Wondr Health, Inc. Erin E. Kershaw is a consultant for

NodThera and Sparrow Pharmaceuticals and a site PI for clinical trials for Arrowhead Pharmaceuticals. Bradly. C. Nindl is member of the Science Advisory Council, Institute of Human and Machine Cognition, Pensacola, FL. Jeremy M. Robbins is a consultant for Edwards Lifesciences; Abbott Laboratories; Janssen Pharmaceuticals. Renee Rogers is a scientific advisor to AstraZeneca, Neurocrine Biosciences, and the American Council on Exercise, and a consultant to Wonder Health, Inc. and Seca. Stuart C. Sealfon is a founder of GNOMX Corp, leads its scientific advisory board and serves as its temporary Chief Scientific Officer. Michael P. Snyder is a cofounder and shareholder of January AI. Alexandria Vornholt is a consultant for GNOMX Corp.

Disclaimer: The content of this manuscript is solely the responsibility of the authors and does not necessarily represent the views of the National Institutes of Health, or the United States Department of Health and Human Services.

Figure 1. Overview of clinical study design

(A) Overview of the study design showing sedentary participants randomized to endurance exercise (EE), resistance exercise (RE), or control (CON). Blood biospecimens collections are indicated by blood tube icons. Samples are collected before, during (EE & CON only), or after the exercise bouts.

(B) Overview of the analysis plan.

(C) Histogram showing the number of analyte changes by exercise mode and -ome according to the main differential abundance (DA) model (p-adj <0.05). Analytes which increase and decrease are shown above and below the zero-line, respectively.

(D) Upset plots showing the overlap of DA features (relative to control) between exercise modes within blood transcripts, plasma proteins and metabolites. Bars represent the number of gene features within a group. Black dots show the measured group, and a connected line between black dots represents shared gene features between EE and RE at any time point. The UpSet plot is ordered by the greatest number of features.

Figure S1. Blood biochemical changes in response to acute endurance and resistance exercise according to blood biochemical profiling platform and in non-exercise controls.

(A) UpSet plots showing differentially abundant (DA) features for each blood or plasma biochemical profiling method across all EE and RE time points. Black dots indicate the plotted

group. A connected line between black dots indicates that the plotted bar represents features shared between those groups. The UpSet plot is ordered by the greatest number of features.

(B) Histogram showing molecular changes in the non-exercise controls at each time point in each ome (p-adj <0.05).

(C) Volcano plot showing all metabolite features changing in the control group at each time point. Features are plotted according to their log fold-change (X-axis) and -log10(p-value) Y-axis. Selected features are labeled.

Figure 2. Plasma metabolomic changes in response to EE and RE

(A-B) Volcano plots for plasma metabolite changes (p-adj <0.05 in the main DA analysis) at each time point for (A) EE and (B) RE with corresponding UpSet plots depicting overlap between DA analytes at each time point for each exercise mode. Features in volcano plots are plotted according to their log fold-change (X-axis) and -log10(p-value) (Y-axis). Selected features are labeled. For UpSet plots, black dots indicate number of significant features per plotted group. A connected line between black dots indicates that the plotted bar represents features shared between those groups. The UpSet plot is ordered by the greatest number of features per timepoint(s).

(C-D) Fuzzy c-means clustering of plasma metabolite trajectories following (C) EE and RE. (D) Adjacent heatmap shows enrichment of metabolite classes within each cluster according to RefMet classes from Correlation Adjusted MEan RAnk gene set test-PreRanked (CAMERA-PR) analyses.

Figure S2. Metabolite class enrichment by exercise mode and time point

(A-C) Metabolite class enrichment analysis using CAMERA-PR applied to metabolites features at each mode-time point pair. Panels show enrichment results for (A) all annotated metabolite classes that display an exercise effect, (B) C24 bile acids, and (C) xanthines. The plotted bubbles indicate the z-score (color/intensity) and significance (grey/white background) of the enrichment term; an * denotes p-adj <0.05. The key for post-exercise timepoint sampling and modalities is presented in panel A.

Figure 3. Temporal Patterns of Divergent Metabolite and Gene Expression Responses Across Plasma and Muscle

(A-B) Heatmaps of exercise mode-divergent changes in acylcarnitines (Car) and fatty acids in the (A) plasma and skeletal muscle, and (B) transcriptomic responses of key fatty acid oxidation genes in skeletal muscle following EE (orange) and RE (green) in the main DA model; an * denotes an p-adj <0.05 and a black field in (A) indicates a given Car species was not detected in a given tissue. Plasma metabolites shown correspond to those highlighted in S4 and S5B. The key for post-exercise timepoint sampling and modalities is presented in panel A.

Figure S3. Differential plasma metabolomic responses to EE and RE

(A) Metabolite changes at post 10 min between EE vs CON (log fold-change on X-axis) and RE vs CON (log fold-change on y-axis). (B) Exercise mode-divergent metabolites (circled metabolites in (A) that are FDR significant for EE and RE) highlighting plasma medium- and long-chain acylcarnitine and fatty acid responses (orange lines reflect EE response, green lines reflect RE responses).

Figure 4. Canonical Correlation Analysis Linking Plasma Metabolites to Clinical and Exercise Traits

(A) Network plot showing associations between the top three metabolite-derived canonical variates (CV1–CV3) and clinical or exercise-related traits. Canonical variates are weighted combinations of variables (metabolites) that are maximally correlated with corresponding combinations of traits (clinical and exercise-related phenotypes). Nodes on the left represent traits and nodes on the right represent CVs; edges connect each trait-CV pair, with edge color indicating the CCA score (red = positive, blue = negative) and edge width proportional to its absolute value. CV1 is associated with key endurance and strength traits such as VO_2peak, O_2pulse and peak torque; CV2 is associated with exercise and recovery blood pressure; CV3 is associated with body composition and heart rate recovery.

(B–D) Loadings for metabolites and phenotypes contributing to canonical variate 1 (B), canonical variate 2 (C), and canonical variate 3 (D). Bar height reflects the magnitude of contribution to the respective variate. Red bars denote positive loadings; blue bars denote negative loadings.

CV1 = metabolite canonical variate 1; CV2 = metabolite canonical variate 2; CV3 = metabolite canonical variate 3; end Watts = end Watts at termination; handgrip strength = average handgrip strength; peak torque = average peak torque from isokinetic test; avg VCO2 = average

VCO2 during CPET; avg VE = average ventilation during CPET; DBP end = end diastolic blood pressure; SBP end = end systolic blood pressure; DBP 1 min = diastolic blood pressure at 1 minute recovery; SBP 1 min = systolic blood pressure at 1 minute recovery; HR end = end heart rate; HR 1 min = heart rate at 1 minute recovery; avg RER = average respiratory exchange ratio during CPET; O2 pulse= oxygen pulse (VO_2/heart rate)

Figure 5. Plasma proteomic changes in response to acute endurance and resistance exercise

(A-B) Volcano plots for plasma protein changes (p-adj <0.05 in the main DA analysis) at each time point for (A) EE and (B) RE with corresponding UpSet plots depicting overlap between DA analytes at each time point for each exercise mode. Features in volcano plots are plotted according to their log fold-change (X-axis) and -log10(p-value) (Y-axis). Selected features are labeled. For UpSet plots, black dots indicate the number of significant features per the plotted group. A connected line between black dots indicates that the plotted bar represents features shared between those groups. The UpSet plot is ordered by the greatest number of features per timepoint(s).

(C) Number and percentage of secreted plasma proteins which are DA at each time point in each exercise mode.

(D) Log2 fold-change in protein abundance during each acute bout, relative to control. Shown are fibroblast growth factor 21 (FGF21), adrenomedullin (ADM), galanin (GAL), and corticotropin releasing hormone binding protein (CRHBP). Points with black dots indicate significance (p-adj< 0.05) by linear mixed effects model. Error bars indicate 95% confidence intervals.

Figure S5. Comparison of resistance versus endurance exercise on plasma proteins

(A) Distribution of baseline (resting) eGFR correlations for 95 proteins that are DA at 40 minutes during exercise in EE.

(B-D) Four-quadrant plots displaying log fold-change of DA proteins in EE (x-axis) and RE (y-axis) at (B) post 10 min, (C) post 30 min, and (D) post 3.5 h time points. Corresponding bar charts with DA features in each group (RE, green arrows; EE, orange arrows) that compare the magnitude of exercise effect between modes.

Figure 6. Putative tissue sources of exercise-responsive plasma proteins

(A) Tissue and cell type sources for all exercise-responsive (DA) plasma proteins in MoTrPAC (N=189) according to published human plasma protein atlases.[71]

(B) Distribution of global longitudinal scores (GLS) for exercise-responsive protein tissue annotations. GLS is a measure of confidence for a putative protein-tissue relationship created in the HATLAS resource[71]; GLS is scored 1-4, with higher scores reflecting higher confidence for a given assignment.

(C-D) Acute exercise-responsive plasma proteins annotated to (C) adipose (N=17) and/or (D) skeletal muscle (N=8) in HATLAS[71] with corresponding heatmaps demonstrating DA changes in the plasma protein, mRNA expression, and global proteomic levels at each time point in MoTrPAC. *: p-adj <0.05. Light grey boxes reflect time points not sampled. Dark grey boxes reflect features not detected.

Figure S6. Tissue-sources of plasma proteins that change in late exercise recovery

(A-B) (A) Heatmap of all DA plasma proteins at the 3.5 h timepoint show plasma protein changes, and skeletal muscle and adipose mRNA and global proteomic changes in EE and RE in MoTrPAC: *p-adj <0.05. Light grey boxes reflect time points not sampled. Dark grey boxes reflect features not detected. Red arrow highlighting that TNFRSF8 (CD30), a protein annotated to adipose tissue, shows no change in adipose mRNA expression during exercise but (B) decreased skeletal muscle mRNA expression after RE and EE with a subsequent decrease and trend towards decrease in plasma protein levels after RE and EE, respectively. Points with black dots indicate significance (p-adj <0.05) by linear mixed effects model. Error bars indicate 95% confidence intervals.

Figure 7. Whole-blood transcriptomic changes in response to acute endurance and resistance exercise

(A-B) Volcano plots for plasma transcriptional changes (p-adj <0.05 in the main DA analysis) at each time point for (A) EE and (B) RE with corresponding UpSet plots depicting overlap between DA analytes at each time point for each exercise mode. Features in volcano plots are plotted according to their log fold-change (X-axis) and -log10(p-value) Y-axis. Selected features are labeled. For UpSet plots, black dots indicate the plotted group. A connected line between black dots indicates that the plotted bar represents features shared between those groups. The UpSet plot is ordered by the greatest number of features.

(C) Pathway enrichment analysis using CAMERA-PR applied to transcriptomic features at each mode-time point pair. Features were curated to top non-redundant and biologically diverse pathway enrichments per contrast. The plotted bubbles indicate the z-score (color/intensity) and significance (grey/white background) of the enrichment term; a grey background denotes p-adj <0.05.

(D) Heatmap depicting z-scores of differential abundance of features in the Reactome HSP90 chaperone cycle for steroid hormone receptors (SHR) in the presence of ligand pathway according to exercise mode and time point for blood and muscle. Here, pathway transcripts undetected in a given tissue are shaded out in black; an * denotes p-adj <0.05 in linear mixed effects model. The intermediate post exercise timepoint was sampled at 30 min in the blood and 15 min in the skeletal muscle.

(E) Log2 fold-change in transcriptional abundance from pre-exercise, relative to control are shown for EE (orange lines) and RE (green lines) over time. Points with black dots indicate significance (p-adj <0.05) by linear mixed effects model. Error bars indicate 95% confidence intervals.

Figure S7. Differences in blood transcriptional responses to acute endurance and resistance exercise.

(A) Log2 fold-change in transcriptional abundance from pre-exercise, relative to control are shown for EE (orange lines) and RE (green lines) over time in adipose, blood, and skeletal muscle. Points with black dots indicate significance (p-adj <0.05) by linear mixed effects model. Error bars indicate 95% confidence intervals.

(B) Heatmap depicting z-scores of differential abundance of features in the Reactome HSF1 activation pathway according to exercise mode and time point for blood; an * denotes significance at p-adj <0.05 by linear mixed effects model.

Figure 8. Shifts in immune cell mobilization and activation following acute EE and RE

(A) Gene set enrichment analysis of whole blood transcriptomics using CAMERA-PR referenced to the CellMarker 2.0 database using human immune cell type curations. Terms were curated for reference cell populations from the blood, peripheral blood, spleen, lymph node and undefined tissue populations. The plotted bubbles indicate the z-score (color/intensity) and significance (grey/white background) of the enrichment term.

(B) Heatmap displaying Z-scores of select plasma proteomic lymphocyte markers reflects concordance in cytotoxic cell markers at the whole blood transcriptomic and plasma proteomic levels; an * denotes significance at p-adj <0.05 by linear mixed effects model.

(C-D) Trajectories of cytotoxic immune cell transcripts in whole blood in response to acute exercise. Points with black dots indicate significance (p-adj <0.05) by linear mixed effects model. Error bars indicate 95% confidence intervals.

(E) Left square displays the estimated percentage (mean proportion) of each cell type in the blood across groups in the sedentary state, with neutrophils representing the largest cell type in the peripheral blood. Right side bubble heatmap displays log2 fold-change (color) of each estimated cell type in the blood in each of the post-exercise time points and in time-matched controls, as well as the adjusted p-value significance of that change (size of bubble).

(F) Temporal changes in select cell type proportions are plotted to display individual changes in average log2 fold-change trajectories through all pre-, during and post- exercise time points; here a line is used to connect individual subjects. Significance in difference in cell type proportion is measured through a t-test. *p-adj <0.05; ** p-adj <0.005; *** p-adj <5e-4; ****p-adj <5e-5; ns: non-significant.

Figure S8. Feature level immune cell enrichments displaying mode-specific regulation.

(A-F) Heatmaps depicting z-scores of differential abundance of features in CellMarker 2.0 (A) eosinophil, (B) granulocyte, and (C) platelet human blood transcriptomic pathway enrichments according to exercise mode and time point for blood. Manually curated heatmaps representing transcriptomic markers of: (D) monocytes (E) NK cells, and (F) T cells. In (D), FCGR3A and FCGR3B represent CD16A and CD16B, respectively. Select MHC Class II genes are by select HLA subclasses, with CD11B denoted as ITGAM. In all figures, an * denotes significance at p-adj <0.05 by linear mixed effects model.

Table 1. Clinical Characteristics of the MoTrPAC Pre-COVID Blood Cohort

Characteristic	Overall N = 175[1]	CON N = 37[1]	EE N = 65[1]	RE N = 73[1]
Sex				
Female	126 (72%)	31 (84%)	46 (71%)	49 (67%)
Male	49 (28%)	6 (16%)	19 (29%)	24 (33%)
Age (yrs)	41 (15)	42 (15)	42 (14)	40 (15)
Height (cm)	168 (9)	167 (8)	168 (9)	168 (10)
Weight (kg)	76 (14)	73 (13)	76 (13)	77 (14)
BMI (kg/m²)	26.9 (4.0)	26.2 (3.9)	27.0 (4.0)	27.2 (4.0)
Waist Circumference (cm)	92 (12)	89 (13)	93 (11)	93 (12)
Systolic BP (mmHg)	116 (12)	114 (11)	117 (11)	116 (12)
Diastolic BP (mmHg)	72 (8)	72 (8)	73 (9)	72 (8)
Hemoglobin A1c (%)	5.30 (0.30)	5.29 (0.21)	5.29 (0.32)	5.31 (0.32)
eGFR (mL/min/1.73 m²)	101 (20)	99 (19)	103 (18)	101 (22)
Cardiopulmonary Exercise Test (CPET)				
VO2peak (L/min)	1.86 (0.65)	1.73 (0.56)	1.90 (0.68)	1.89 (0.65)
VO2peak (ml/min/kg)	24 (7)	24 (6)	25 (7)	25 (7)
Workload (Watts)	152 (50)	142 (40)	155 (53)	153 (52)
O2 Pulse (ml/beat)	10.6 (3.3)	10.0 (2.8)	10.9 (3.5)	10.8 (3.4)
RER	1.16 (0.08)	1.16 (0.08)	1.17 (0.07)	1.15 (0.08)

Strength Tests				
Isometric Knee Extension Torque (Nm)	148 (57)	137 (53)	145 (54)	156 (60)
Hand Grip Strength (kg)	30 (11)	29 (8)	30 (11)	31 (12)

[1] n (%); Mean (SD)

Table S1. Clinical Characteristics of the MoTrPAC Pre-COVID Blood Cohort by Biochemical Profiling Platform

	Transcriptomics				Proteomics				Metabolomics			
Characteristic	**Overall** N=173	**CON** N=37	**EE** N=64	**RE** N=72	**Overall** N=44	**CON** N=12	**EE** N=14	**RE** N=18	**Overall** N=175	**CON** N=37	**EE** N=65	**RE** N=73
Sex												
Female	125 (72%)	31 (84%)	46 (72%)	48 (67%)	33 (75%)	9 (75%)	11 (79%)	13 (72%)	126 (72%)	31 (84%)	46 (71%)	49 (67%)
Male	48 (28%)	6 (16%)	18 (28%)	24 (33%)	11 (25%)	3 (25%)	3 (21%)	5 (28%)	49 (28%)	6 (16%)	19 (29%)	24 (33%)
Age (yrs)	41 (15)	42 (15)	41 (14)	40 (15)	43 (16)	52 (13)	40 (18)	39 (15)	41 (15)	42 (15)	42 (14)	40 (15)
Height (cm)	168 (9)	167 (8)	168 (9)	169 (10)	166 (10)	166 (9)	166 (11)	166 (10)	168 (9)	167 (8)	168 (9)	168 (10)
Weight (kg)	76 (14)	73 (13)	76 (13)	77 (14)	73 (12)	71 (11)	75 (15)	73 (10)	76 (14)	73 (13)	76 (13)	77 (14)
BMI (kg/m²)	26.9 (4.0)	26.2 (3.9)	27.0 (4.0)	27.1 (4.0)	26.6 (3.5)	25.8 (3.2)	27.4 (4.1)	26.6 (3.2)	26.9 (4.0)	26.2 (3.9)	27.0 (4.0)	27.2 (4.0)
Waist Circumference (cm)	92 (12)	89 (13)	92 (11)	93 (12)	91 (10)	88 (11)	92 (12)	92 (8)	92 (12)	89 (13)	93 (11)	93 (12)
Systolic BP (mmHg)	116 (12)	114 (11)	117 (11)	116 (12)	117 (11)	119 (13)	120 (10)	113 (11)	116 (12)	114 (11)	117 (11)	116 (12)
Diastolic BP (mmHg)	72 (8)	72 (8)	73 (9)	72 (8)	71 (8)	73 (9)	74 (7)	69 (8)	72 (8)	72 (8)	73 (9)	72 (8)

Hemoglobin A1c (%)	5.29 (0.30)	5.29 (0.21)	5.28 (0.31)	5.31 (0.32)	5.33 (0.29)	5.33 (0.18)	5.31 (0.37)	5.35 (0.28)	5.30 (0.30)	5.29 (0.21)	5.29 (0.32)	5.31 (0.32)
eGFR (mL/min/1.73 m²)	101 (20)	99 (19)	103 (18)	101 (22)	101 (18)	94 (18)	107 (19)	100 (17)	101 (20)	99 (19)	103 (18)	101 (22)
Cardiopulmonary Exercise Test (CPET)												
VO2peak (L/min)	1.86 (0.65)	1.73 (0.56)	1.90 (0.69)	1.90 (0.66)	1.82 (0.73)	1.64 (0.53)	1.92 (0.79)	1.86 (0.80)	1.86 (0.65)	1.73 (0.56)	1.90 (0.68)	1.89 (0.65)
VO2peak (ml/min/kg)	25 (7)	24 (6)	25 (7)	25 (7)	25 (8)	23 (6)	25 (9)	25 (9)	24 (7)	24 (6)	25 (7)	25 (7)
Workload (Watts)	152 (51)	142 (40)	156 (54)	154 (53)	148 (59)	136 (42)	157 (63)	149 (68)	152 (50)	142 (40)	155 (53)	153 (52)
O2 Pulse (ml/beat)	10.7 (3.3)	10.0 (2.8)	10.9 (3.5)	10.8 (3.4)	10.4 (3.6)	9.9 (3.1)	10.8 (3.8)	10.5 (3.9)	10.6 (3.3)	10.0 (2.8)	10.9 (3.5)	10.8 (3.4)
RER	1.16 (0.08)	1.16 (0.08)	1.17 (0.07)	1.15 (0.08)	1.15 (0.07)	1.18 (0.09)	1.15 (0.05)	1.12 (0.07)	1.16 (0.08)	1.16 (0.08)	1.17 (0.07)	1.15 (0.08)
Strength Tests												
Isometric Knee Extension Torque (Nm)	147 (57)	137 (53)	143 (53)	156 (60)	145 (44)	148 (39)	145 (53)	141 (42)	148 (57)	137 (53)	145 (54)	156 (60)
Hand Grip Strength (kg)	30 (11)	29 (8)	30 (11)	31 (12)	28 (12)	29 (11)	28 (12)	27 (13)	30 (11)	29 (8)	30 (11)	31 (12)

[1] n (%); Mean (SD)

Table S2. Clinical Characteristics of the MoTrPAC Pre-COVID Blood Cohort by Sex

Characteristic	Female N = 126[1]	Male N = 49[1]
Group		
CON	31 (25%)	6 (12%)
EE	46 (37%)	19 (39%)
RE	49 (39%)	24 (49%)
Age (yrs)	41 (14)	42 (16)
Height (cm)	164 (6)	178 (7)
Weight (kg)	73 (12)	85 (13)
BMI (kg/m²)	26.9 (4.1)	26.9 (3.7)
Waist Circumference (cm)	90 (11)	96 (11)
Systolic BP (mmHg)	114 (11)	121 (11)
Diastolic BP (mmHg)	71 (8)	75 (9)
Hemoglobin A1c (%)	5.30 (0.31)	5.28 (0.28)
eGFR (mL/min/1.73 m²)	102 (19)	100 (21)
Cardiopulmonary Exercise Test (CPET)		
VO2peak (L/min)	1.58 (0.38)	2.59 (0.63)
VO2peak (ml/min/kg)	22 (5)	31 (7)
Workload (Watts)	130 (31)	208 (47)
O2 Pulse (ml/beat)	9.2 (1.9)	14.4 (3.2)
RER	1.15 (0.08)	1.17 (0.07)

Strength Tests		
Isometric Knee Extension Torque (Nm)	129 (43)	196 (58)
Hand Grip Strength (kg)	26 (7)	42 (10)

[1] n (%); Mean (SD)

Table S3. Metabolites by c-means clustering analyses

Table S4. Plasma protein associations with baseline estimated glomerular filtration rate

References

1. Booth FW, Roberts CK, Laye MJ. Lack of exercise is a major cause of chronic diseases. Compr Physiol. 2012;2(2):1143–211. Epub 2012/04/01. doi: 10.1002/cphy.c110025. PubMed PMID: 23798298; PMCID: PMC4241367.
2. Ruegsegger GN, Booth FW. Health Benefits of Exercise. Cold Spring Harb Perspect Med. 2018;8(7). Epub 2018/07/02. doi: 10.1101/cshperspect.a029694. PubMed PMID: 28507196.
3. Kanaley JA, Colberg SR, Corcoran MH, Malin SK, Rodriguez NR, Crespo CJ, Kirwan JP, Zierath JR. Exercise/Physical Activity in Individuals with Type 2 Diabetes: A Consensus Statement from the American College of Sports Medicine. Med Sci Sports Exerc. 2022;54(2):353–68. doi: 10.1249/MSS.0000000000002800. PubMed PMID: 35029593; PMCID: PMC8802999.
4. Tucker WJ, Fegers-Wustrow I, Halle M, Haykowsky MJ, Chung EH, Kovacic JC. Exercise for Primary and Secondary Prevention of Cardiovascular Disease: JACC Focus Seminar 1/4. J Am Coll Cardiol. 2022;80(11):1091–106. doi: 10.1016/j.jacc.2022.07.004. PubMed PMID: 36075680.
5. Courneya KS, Vardy JL, O'Callaghan CJ, Gill S, Friedenreich CM, Wong RKS, Dhillon HM, Coyle V, Chua NS, Jonker DJ, Beale PJ, Haider K, Tang PA, Bonaventura T, Wong R, Lim HJ, Burge ME, Hubay S, Sanatani M, Campbell KL, Arthuso FZ, Turner J, Meyer RM, Brundage M, O'Brien P, Tu D, Booth CM, Investigators C. Structured Exercise after Adjuvant Chemotherapy for Colon Cancer. N Engl J Med. 2025. Epub 20250601. doi: 10.1056/NEJMoa2502760. PubMed PMID: 40450658.
6. Pedersen BK. The Physiology of Optimizing Health with a Focus on Exercise as Medicine. Annu Rev Physiol. 2019;81:607–27. Epub 20181210. doi: 10.1146/annurev-physiol-020518-114339. PubMed PMID: 30526319.
7. Eckstrom E, Neukam S, Kalin L, Wright J. Physical Activity and Healthy Aging. Clin Geriatr Med. 2020;36(4):671–83. Epub 20200819. doi: 10.1016/j.cger.2020.06.009. PubMed PMID: 33010902.
8. Hawley JA, Hargreaves M, Joyner MJ, Zierath JR. Integrative biology of exercise. Cell. 2014;159(4):738–49. doi: 10.1016/j.cell.2014.10.029.
9. Amar D, Gay NR, Jean Beltran PM, Adkins JN, Almagro Armenteros JJ, Ashley E, Avila-Pacheco J, Bae D, Bararpour N, Burant C, Clish C, Cutter G, Dasari S, Dennis C, Evans CR, Fernández FM, Gaul D, Ge Y, Gerszten R, Goodyear LJ, Hou Z, Ilkayeva O, Ivanova AA, Jimenez-Morales D, Kachman MT, Keshishian H, Kraus WE, Lanza IR, Li J, Lindholm ME, Lira

AC, Many GM, Marwaha S, Miller ME, Muehlbauer MJ, Nair KS, Nair VD, Natarajan Raja A, Newgard C, Ortlund EA, Piehowski PD, Presby DM, Qian W-J, Rooney JL, Sanford JA, Savage E, Sealfon SC, Smith GR, Smith KS, Steep A, Stowe CL, Sun Y, Tracy R, Vetr NG, Walsh MJ, Wu S, Zhang T, Zhao B, Zhen J, Albertson BG, Amper MAS, Balci AT, Bamman M, Barton ER, Bergman B, Bessesen D, Booth F, Bouverat B, Buford TW, Caputo T, Chambers TL, Chavez C, Chikina M, Chiu R, Cicha M, Coen PM, Cooper D, Cornell E, Dalton KP, De Sousa LO, Farrar R, Gadde K, Gagne N, Goodpaster BH, Gritsenko MA, Guevara K, Haddad F, Hansen JR, Harris M, Hastie T, Hennig KM, Hershman SG, Hevener A, Hirshman MF, Hsu F-C, Huffman KM, Hung C-J, Hutchinson-Bunch C, Jackson BE, Jankowski C, Jin CA, Johannsen NM, Ke BG, Kohrt WM, Kramer KS, Leeuwenburgh C, Lessard SJ, Lester B, Liu X, Lu C-j, Makarewicz NS, Maner-Smith KM, Mani DR, Marjanovic N, Marshall A, May S, Melanson E, Monroe ME, Moore RJ, Moore S, Moreau KL, Mundorff CC, Musi N, Nachun D, Nestor MD, Newton RL, Nicklas B, Nigro P, Nudelman G, Pahor M, Pearce C, Petyuk VA, Pincas H, Powers S, Radom-Aizik S, Ramachandran K, Ramaker ME, Ramos I, Rankinen T, Raskind A, Rasmussen BB, Ravussin E, Rector RS, Rejeski WJ, Richards C, Rirak S, Robbins JM, Rubenstein AB, Ruf-Zamojski F, Rushing S, Sagendorf TJ, Samdarshi M, Schauer IE, Schwartz R, Seenarine N, Soni T, Sparks LM, Teng C, Thalacker-Mercer A, Thyfault J, Tibshirani R, Trappe S, Trappe TA, Uppal K, Vangeti S, Vasoya M, Volpi E, Vornholt A, Walkup MP, Williams J, Xia A, Yan Z, Yu X, Zang C, Zaslavsky E, Zebarjadi N, Bodine SC, Carr S, Esser K, Montgomery SB, Schenk S, Snyder MP, Wheeler MT. Temporal dynamics of the multi-omic response to endurance exercise training across tissues. bioRxiv. 2022:2022.09.21.508770. doi: 10.1101/2022.09.21.508770.

10. Ross R, Goodpaster BH, Koch LG, Sarzynski MA, Kohrt WM, Johannsen NM, Skinner JS, Castro A, Irving BA, Noland RC, Sparks LM, Spielmann G, Day AG, Pitsch W, Hopkins WG, Bouchard C. Precision exercise medicine: understanding exercise response variability. Br J Sports Med. 2019;53(18):1141–53. Epub 20190312. doi: 10.1136/bjsports-2018-100328. PubMed PMID: 30862704; PMCID: PMC6818669.

11. Bouchard C, Rankinen T. Individual differences in response to regular physical activity. Med Sci Sports Exerc. 2001;33(6 Suppl):S446–51; discussion S52–3. PubMed PMID: 11427769.

12. Sanford JA, Nogiec CD, Lindholm ME, Adkins JN, Amar D, Dasari S, Drugan JK, Fernández FM, Radom-Aizik S, Schenk S, Snyder MP, Tracy RP, Vanderboom P, Trappe S, Walsh MJ. Molecular Transducers of Physical Activity Consortium (MoTrPAC): Mapping the Dynamic Responses to Exercise. Cell. 2020;181(7):1464–74. doi: 10.1016/j.cell.2020.06.004. PubMed PMID: 32589957; PMCID: PMC8800485.

13. Chow LS, Gerszten RE, Taylor JM, Pedersen BK, van Praag H, Trappe S, Febbraio MA, Galis ZS, Gao Y, Haus JM, Lanza IR, Lavie CJ, Lee CH, Lucia A, Moro C, Pandey A, Robbins JM, Stanford KI, Thackray AE, Villeda S, Watt MJ, Xia A, Zierath JR, Goodpaster BH, Snyder MP. Exerkines in health, resilience and disease. Nat Rev Endocrinol. 2022;18(5):273–89. Epub 20220318. doi: 10.1038/s41574-022-00641-2. PubMed PMID: 35304603; PMCID: PMC9554896.

14. Robbins JM, Gerszten RE. Exercise, exerkines, and cardiometabolic health: from individual players to a team sport. J Clin Invest. 2023;133(13). Epub 20230703. doi: 10.1172/JCI172916. PubMed PMID: 37395284; PMCID: PMC10313356.

15. McPherron AC, Lawler AM, Lee SJ. Regulation of skeletal muscle mass in mice by a new TGF-beta superfamily member. Nature. 1997;387(6628):83–90. doi: 10.1038/387083a0. PubMed PMID: 9139826.

16. Nalbandian M, Takeda M. Lactate as a Signaling Molecule That Regulates Exercise-Induced Adaptations. Biology (Basel). 2016;5(4). Epub 20161008. doi: 10.3390/biology5040038. PubMed PMID: 27740597; PMCID: PMC5192418.

17. Febbraio MA, Ott P, Nielsen HB, Steensberg A, Keller C, Krustrup P, Secher NH, Pedersen BK. Exercise induces hepatosplanchnic release of heat shock protein 72 in humans. J

Physiol. 2002;544(3):957–62. doi: 10.1113/jphysiol.2002.025148. PubMed PMID: 12411538; PMCID: PMC2290618.
18. Takahashi H, Alves CRR, Stanford KI, Middelbeek RJW, Pasquale N, Ryan RE, Xue R, Sakaguchi M, Lynes MD, So K, Mul JD, Lee MY, Balan E, Pan H, Dreyfuss JM, Hirshman MF, Azhar M, Hannukainen JC, Nuutila P, Kalliokoski KK, Nielsen S, Pedersen BK, Kahn CR, Tseng YH, Goodyear LJ. TGF-β2 is an exercise-induced adipokine that regulates glucose and fatty acid metabolism. Nat Metab. 2019;1(2):291–303. Epub 2019/04/30. doi: 10.1038/s42255-018-0030-7. PubMed PMID: 31032475; PMCID: PMC6481955.
19. Subbotina E, Sierra A, Zhu Z, Gao Z, Koganti SR, Reyes S, Stepniak E, Walsh SA, Acevedo MR, Perez-Terzic CM, Hodgson-Zingman DM, Zingman LV. Musclin is an activity-stimulated myokine that enhances physical endurance. Proc Natl Acad Sci U S A. 2015;112(52):16042–7. Epub 20151214. doi: 10.1073/pnas.1514250112. PubMed PMID: 26668395; PMCID: PMC4702977.
20. Roberts LD, Boström P, O'Sullivan JF, Schinzel RT, Lewis GD, Dejam A, Lee Y-K, Palma MJ, Calhoun S, Georgiadi A, Chen M-H, Ramachandran VS, Larson MG, Bouchard C, Rankinen T, Souza AL, Clish CB, Wang TJ, Estall JL, Soukas AA, Cowan CA, Spiegelman BM, Gerszten RE. β-Aminoisobutyric acid induces browning of white fat and hepatic β-oxidation and is inversely correlated with cardiometabolic risk factors. Cell metabolism. 2014;19(1):96–108. doi: 10.1016/j.cmet.2013.12.003.
21. Stanford KI, Lynes MD, Takahashi H, Baer LA, Arts PJ, May FJ, Lehnig AC, Middelbeek RJW, Richard JJ, So K, Chen EY, Gao F, Narain NR, Distefano G, Shettigar VK, Hirshman MF, Ziolo MT, Kiebish MA, Tseng Y-H, Coen PM, Goodyear LJ. 12,13-diHOME: An Exercise-Induced Lipokine that Increases Skeletal Muscle Fatty Acid Uptake. Cell metabolism. 2018;27(5):1111–20.e3. doi: 10.1016/j.cmet.2018.03.020.
22. Steensberg A, van Hall G, Osada T, Sacchetti M, Saltin B, Klarlund Pedersen B. Production of interleukin-6 in contracting human skeletal muscles can account for the exercise-induced increase in plasma interleukin-6. J Physiol. 2000;529 Pt 1:237–42. doi: 10.1111/j.1469-7793.2000.00237.x. PubMed PMID: 11080265; PMCID: PMC2270169.
23. Strömberg A, Olsson K, Dijksterhuis JP, Rullman E, Schulte G, Gustafsson T. CX3CL1--a macrophage chemoattractant induced by a single bout of exercise in human skeletal muscle. Am J Physiol Regul Integr Comp Physiol. 2016;310(3):R297–304. Epub 20151202. doi: 10.1152/ajpregu.00236.2015. PubMed PMID: 26632602.
24. Robbins JM, Benson M, Verkerke ARP, Tiwari G, Deng S, Rao P, Tahir UA, Avila-Pacheco J, Shi X, Guan Y, Tendoh FG, Barber JL, Miller PE, Perry AS, Hall ME, Wood AC, Taylor KD, Post WS, Rich SS, Nayor M, Wilson JG, Lewis GD, Shah RV, Rotter JI, Summers SA, Raffield LM, Kajimura S, Bouchard C, Clish CB, Sarzynski MA, Gerszten RE. N-Palmitoyl Glutamine Is a Candidate Mediator of Cardiorespiratory Fitness. Circulation. 2025. Epub 20251112. doi: 10.1161/CIRCULATIONAHA.125.074187. PubMed PMID: 41221589.
25. Pedersen BK. Anti-inflammatory effects of exercise: role in diabetes and cardiovascular disease. Eur J Clin Invest. 2017;47(8):600–11. Epub 2017/07/20. doi: 10.1111/eci.12781. PubMed PMID: 28722106.
26. Robbins JM, Herzig M, Morningstar J, Sarzynski MA, Cruz DE, Wang TJ, Gao Y, Wilson JG, Bouchard C, Rankinen T, Gerszten RE. Association of Dimethylguanidino Valeric Acid With Partial Resistance to Metabolic Health Benefits of Regular Exercise. JAMA Cardiol. 2019;4(7):636–43. doi: 10.1001/jamacardio.2019.1573. PubMed PMID: 31166569; PMCID: PMC6551586.
27. Robbins JM, Peterson B, Schranner D, Tahir UA, Rienmuller T, Deng S, Keyes MJ, Katz DH, Beltran PMJ, Barber JL, Baumgartner C, Carr SA, Ghosh S, Shen C, Jennings LL, Ross R, Sarzynski MA, Bouchard C, Gerszten RE. Human plasma proteomic profiles indicative of cardiorespiratory fitness. Nat Metab. 2021;3(6):786–97. Epub 20210527. doi: 10.1038/s42255-021-00400-z. PubMed PMID: 34045743; PMCID: PMC9216203.

28. Robbins JM, Rao P, Deng S, Keyes MJ, Tahir UA, Katz DH, Beltran PMJ, Marchildon F, Barber JL, Peterson B, Gao Y, Correa A, Wilson JG, Smith JG, Cohen P, Ross R, Bouchard C, Sarzynski MA, Gerszten RE. Plasma proteomic changes in response to exercise training are associated with cardiorespiratory fitness adaptations. JCI Insight. 2023;8(7). Epub 20230410. doi: 10.1172/jci.insight.165867. PubMed PMID: 37036009; PMCID: PMC10132160.
29. Perry AS, Farber-Eger E, Gonzales T, Tanaka T, Robbins JM, Murthy VL, Stolze LK, Zhao S, Huang S, Colangelo LA, Deng S, Hou L, Lloyd-Jones DM, Walker KA, Ferrucci L, Watts EL, Barber JL, Rao P, Mi MY, Gabriel KP, Hornikel B, Sidney S, Houstis N, Lewis GD, Liu GY, Thyagarajan B, Khan SS, Choi B, Washko G, Kalhan R, Wareham N, Bouchard C, Sarzynski MA, Gerszten RE, Brage S, Wells QS, Nayor M, Shah RV. Proteomic analysis of cardiorespiratory fitness for prediction of mortality and multisystem disease risks. Nat Med. 2024;30(6):1711–21. Epub 20240604. doi: 10.1038/s41591-024-03039-x. PubMed PMID: 38834850; PMCID: PMC11186767.
30. Lewis GD, Farrell L, Wood MJ, Martinovic M, Arany Z, Rowe GC, Souza A, Cheng S, McCabe EL, Yang E, Shi X, Deo R, Roth FP, Asnani A, Rhee EP, Systrom DM, Semigran MJ, Vasan RS, Carr SA, Wang TJ, Sabatine MS, Clish CB, Gerszten RE. Metabolic signatures of exercise in human plasma. Sci Transl Med. 2010;2(33):33ra7. doi: 10.1126/scitranslmed.3001006. PubMed PMID: 20505214; PMCID: PMC3010398.
31. Nayor M, Shah RV, Miller PE, Blodgett JB, Tanguay M, Pico AR, Murthy VL, Malhotra R, Houstis NE, Deik A, Pierce KA, Bullock K, Dailey L, Velagaleti RS, Moore SA, Ho JE, Baggish AL, Clish CB, Larson MG, Vasan RS, Lewis GD. Metabolic Architecture of Acute Exercise Response in Middle-Aged Adults in the Community. Circulation. 2020;142(20):1905–24. doi: 10.1161/CIRCULATIONAHA.120.050281.
32. Mi MY, Barber JL, Rao P, Farrell LA, Sarzynski MA, Bouchard C, Robbins JM, Gerszten RE. Plasma Proteomic Kinetics in Response to Acute Exercise. Mol Cell Proteomics. 2023;22(8):100601. Epub 20230619. doi: 10.1016/j.mcpro.2023.100601. PubMed PMID: 37343698; PMCID: PMC10460691.
33. Guseh JS, Churchill TW, Yeri A, Lo C, Brown M, Houstis NE, Aragam KG, Lieberman DE, Rosenzweig A, Baggish AL. An expanded repertoire of intensity-dependent exercise-responsive plasma proteins tied to loci of human disease risk. Sci Rep. 2020;10(1):10831. Epub 2020/07/02. doi: 10.1038/s41598-020-67669-0. PubMed PMID: 32616758; PMCID: PMC7331669.
34. Morville T, Sahl RE, Moritz T, Helge JW, Clemmensen C. Plasma Metabolome Profiling of Resistance Exercise and Endurance Exercise in Humans. Cell Rep. 2020;33(13):108554. doi: 10.1016/j.celrep.2020.108554. PubMed PMID: 33378671.
35. MoTr PACSG, Jakicic JM, Kohrt WM, Houmard JA, Miller ME, Radom-Aizik S, Rasmussen BB, Ravussin E, Serra M, Stowe CL, Trappe S, Abouassi H, Adkins JN, Alekel DL, Ashley E, Bamman MM, Bergman BC, Bessesen DH, Broskey NT, Buford TW, Burant CF, Chen H, Christle JW, Clish CB, Coen PM, Collier D, Collins KA, Cooper DM, Cortes T, Cutter GR, Dubis G, Fernandez FM, Firnhaber J, Forman DE, Gaul DA, Gay N, Gerszten RE, Goodpaster BH, Gritsenko MA, Haddad F, Huffman KM, Ilkayeva O, Jankowski CM, Jin C, Johannsen NM, Johnson J, Kelly L, Kershaw E, Kraus WE, Laughlin M, Lester B, Lindholm ME, Lowe A, Lu CJ, McGowan J, Melanson EL, Montgomery S, Moore SG, Moreau KL, Muehlbauer M, Musi N, Nair VD, Newgard CB, Newman AB, Nicklas B, Nindl BC, Ormond K, Piehowski PD, Qian WJ, Rankinen T, Rejeski WJ, Robbins J, Rogers RJ, Rooney JL, Rushing S, Sanford JA, Schauer IE, Schwartz RS, Sealfon SC, Slentz C, Sloan R, Smith KS, Snyder M, Spahn J, Sparks LM, Stefanovic-Racic M, Tanner CJ, Thalacker-Mercer A, Tracy R, Trappe TA, Volpi E, Walsh MJ, Wheeler MT, Willis L. Molecular Transducers of Physical Activity Consortium (MoTrPAC): human studies design and protocol. J Appl Physiol (1985). 2024;137(3):473–93. Epub 20240418. doi: 10.1152/japplphysiol.00102.2024. PubMed PMID: 38634503; PMCID: PMC11427038.

36. Wueest S, Item F, Boyle CN, Jirkof P, Cesarovic N, Ellingsgaard H, Boni-Schnetzler M, Timper K, Arras M, Donath MY, Lutz TA, Schoenle EJ, Konrad D. Interleukin-6 contributes to early fasting-induced free fatty acid mobilization in mice. Am J Physiol Regul Integr Comp Physiol. 2014;306(11):R861–7. Epub 20140402. doi: 10.1152/ajpregu.00533.2013. PubMed PMID: 24694381.
37. Ahmad TR, Haeusler RA. Bile acids in glucose metabolism and insulin signalling - mechanisms and research needs. Nat Rev Endocrinol. 2019;15(12):701–12. Epub 20191015. doi: 10.1038/s41574-019-0266-7. PubMed PMID: 31616073; PMCID: PMC6918475.
38. Boudou P, De Kerviler E, Vexiau P, Fiet J, Cathelineau G, Gautier J. Effects of a single bout of exercise and exercise training on steroid levels in middle-aged type 2 diabetic men: relationship to abdominal adipose tissue distribution and metabolic status. Diabetes Metab. 2000;26(6):450–7. PubMed PMID: 11173715.
39. Tsai YM, Chou SW, Lin YC, Hou CW, Hung KC, Kung HW, Lin TW, Chen SM, Lin CY, Kuo CH. Effect of resistance exercise on dehydroepiandrosterone sulfate concentrations during a 72-h recovery: relation to glucose tolerance and insulin response. Life Sci. 2006;79(13):1281–6. Epub 20060522. doi: 10.1016/j.lfs.2006.04.001. PubMed PMID: 16716364.
40. Kumar L, M EF. Mfuzz: a software package for soft clustering of microarray data. Bioinformation. 2007;2(1):5–7. Epub 20070520. doi: 10.6026/97320630002005. PubMed PMID: 18084642; PMCID: PMC2139991.
41. Romijn JA, Coyle EF, Sidossis LS, Gastaldelli A, Horowitz JF, Endert E, Wolfe RR. Regulation of endogenous fat and carbohydrate metabolism in relation to exercise intensity and duration. Am J Physiol. 1993;265(3 Pt 1):E380–91. Epub 1993/09/01. doi: 10.1152/ajpendo.1993.265.3.E380. PubMed PMID: 8214047.
42. van Loon LJ, Greenhaff PL, Constantin-Teodosiu D, Saris WH, Wagenmakers AJ. The effects of increasing exercise intensity on muscle fuel utilisation in humans. J Physiol. 2001;536(Pt 1):295–304. doi: 10.1111/j.1469-7793.2001.00295.x. PubMed PMID: 11579177; PMCID: PMC2278845.
43. Contrepois K, Wu S, Moneghetti KJ, Hornburg D, Ahadi S, Tsai M-S, Metwally AA, Wei E, Lee-McMullen B, Quijada JV, Chen S, Christle JW, Ellenberger M, Balliu B, Taylor S, Durrant MG, Knowles DA, Choudhry H, Ashland M, Bahmani A, Enslen B, Amsallem M, Kobayashi Y, Avina M, Perelman D, Schüssler-Fiorenza Rose SM, Zhou W, Ashley EA, Montgomery SB, Chaib H, Haddad F, Snyder MP. Molecular Choreography of Acute Exercise. Cell. 2020;181(5):1112–30.e16. doi: 10.1016/j.cell.2020.04.043.
44. Hoene M, Li J, Li Y, Runge H, Zhao X, Haring HU, Lehmann R, Xu G, Weigert C. Muscle and liver-specific alterations in lipid and acylcarnitine metabolism after a single bout of exercise in mice. Sci Rep. 2016;6:22218. Epub 20160226. doi: 10.1038/srep22218. PubMed PMID: 26916151; PMCID: PMC4768182.
45. Hargreaves M, Spriet LL. Skeletal muscle energy metabolism during exercise. Nat Metab. 2020;2(9):817–28. Epub 20200803. doi: 10.1038/s42255-020-0251-4. PubMed PMID: 32747792.
46. Tesch PA, Colliander EB, Kaiser P. Muscle metabolism during intense, heavy-resistance exercise. Eur J Appl Physiol Occup Physiol. 1986;55(4):362–6. doi: 10.1007/BF00422734. PubMed PMID: 3758035.
47. Kuang J, McGinley C, Lee MJ, Saner NJ, Garnham A, Bishop DJ. Interpretation of exercise-induced changes in human skeletal muscle mRNA expression depends on the timing of the post-exercise biopsies. PeerJ. 2022;10:e12856. Epub 20220204. doi: 10.7717/peerj.12856. PubMed PMID: 35186464; PMCID: PMC8820226.
48. Leick L, Plomgaard P, Gronlokke L, Al-Abaiji F, Wojtaszewski JF, Pilegaard H. Endurance exercise induces mRNA expression of oxidative enzymes in human skeletal muscle late in recovery. Scand J Med Sci Sports. 2010;20(4):593–9. Epub 20090823. doi: 10.1111/j.1600-0838.2009.00988.x. PubMed PMID: 19705999.

49. Pillon NJ, Gabriel BM, Dollet L, Smith JAB, Sardón Puig L, Botella J, Bishop DJ, Krook A, Zierath JR. Transcriptomic profiling of skeletal muscle adaptations to exercise and inactivity. Nat Commun. 2020;11(1):470. Epub 2020/01/24. doi: 10.1038/s41467-019-13869-w. PubMed PMID: 31980607; PMCID: PMC6981202.
50. Witten DM, Tibshirani R, Hastie T. A penalized matrix decomposition, with applications to sparse principal components and canonical correlation analysis. Biostatistics. 2009;10(3):515–34. Epub 20090417. doi: 10.1093/biostatistics/kxp008. PubMed PMID: 19377034; PMCID: PMC2697346.
51. Haus JM, Kashyap SR, Kasumov T, Zhang R, Kelly KR, Defronzo RA, Kirwan JP. Plasma ceramides are elevated in obese subjects with type 2 diabetes and correlate with the severity of insulin resistance. Diabetes. 2009;58(2):337–43. Epub 20081113. doi: 10.2337/db08-1228. PubMed PMID: 19008343; PMCID: PMC2628606.
52. Cheng JM, Suoniemi M, Kardys I, Vihervaara T, de Boer SP, Akkerhuis KM, Sysi-Aho M, Ekroos K, Garcia-Garcia HM, Oemrawsingh RM, Regar E, Koenig W, Serruys PW, van Geuns RJ, Boersma E, Laaksonen R. Plasma concentrations of molecular lipid species in relation to coronary plaque characteristics and cardiovascular outcome: Results of the ATHEROREMO-IVUS study. Atherosclerosis. 2015;243(2):560–6. Epub 20151023. doi: 10.1016/j.atherosclerosis.2015.10.022. PubMed PMID: 26523994.
53. Laaksonen R, Ekroos K, Sysi-Aho M, Hilvo M, Vihervaara T, Kauhanen D, Suoniemi M, Hurme R, Marz W, Scharnagl H, Stojakovic T, Vlachopoulou E, Lokki ML, Nieminen MS, Klingenberg R, Matter CM, Hornemann T, Juni P, Rodondi N, Raber L, Windecker S, Gencer B, Pedersen ER, Tell GS, Nygard O, Mach F, Sinisalo J, Luscher TF. Plasma ceramides predict cardiovascular death in patients with stable coronary artery disease and acute coronary syndromes beyond LDL-cholesterol. Eur Heart J. 2016;37(25):1967–76. Epub 20160428. doi: 10.1093/eurheartj/ehw148. PubMed PMID: 27125947; PMCID: PMC4929378.
54. Tarasov K, Ekroos K, Suoniemi M, Kauhanen D, Sylvanne T, Hurme R, Gouni-Berthold I, Berthold HK, Kleber ME, Laaksonen R, Marz W. Molecular lipids identify cardiovascular risk and are efficiently lowered by simvastatin and PCSK9 deficiency. J Clin Endocrinol Metab. 2014;99(1):E45–52. Epub 20131220. doi: 10.1210/jc.2013-2559. PubMed PMID: 24243630; PMCID: PMC3928964.
55. Lee S. The association of genetically controlled CpG methylation (cg158269415) of protein tyrosine phosphatase, receptor type N2 (PTPRN2) with childhood obesity. Sci Rep. 2019;9(1):4855. Epub 20190319. doi: 10.1038/s41598-019-40486-w. PubMed PMID: 30890718; PMCID: PMC6425015.
56. Catoire M, Mensink M, Kalkhoven E, Schrauwen P, Kersten S. Identification of human exercise-induced myokines using secretome analysis. Physiol Genomics. 2014;46(7):256–67. Epub 20140211. doi: 10.1152/physiolgenomics.00174.2013. PubMed PMID: 24520153.
57. Wahl P, Jansen F, Achtzehn S, Schmitz T, Bloch W, Mester J, Werner N. Effects of high intensity training and high volume training on endothelial microparticles and angiogenic growth factors. PLoS One. 2014;9(4):e96024. Epub 20140425. doi: 10.1371/journal.pone.0096024. PubMed PMID: 24770423; PMCID: PMC4000202.
58. Trusolino L, Bertotti A, Comoglio PM. MET signalling: principles and functions in development, organ regeneration and cancer. Nat Rev Mol Cell Biol. 2010;11(12):834–48. doi: 10.1038/nrm3012. PubMed PMID: 21102609.
59. McMurray JJ, Packer M, Desai AS, Gong J, Lefkowitz MP, Rizkala AR, Rouleau JL, Shi VC, Solomon SD, Swedberg K, Zile MR, Investigators P-H, Committees. Angiotensin-neprilysin inhibition versus enalapril in heart failure. N Engl J Med. 2014;371(11):993–1004. Epub 20140830. doi: 10.1056/NEJMoa1409077. PubMed PMID: 25176015.
60. Middlekauff HR, Nitzsche EU, Nguyen AH, Hoh CK, Gibbs GG. Modulation of renal cortical blood flow during static exercise in humans. Circ Res. 1997;80(1):62–8. doi: 10.1161/01.res.80.1.62. PubMed PMID: 8978323.

61. Rocha MP, Gliemann L. Exercise and the kidneys: How does renal blood flow behave when measured during exercise? Physiol Rep. 2022;10(19):e15485. doi: 10.14814/phy2.15485. PubMed PMID: 36200293; PMCID: PMC9535345.
62. Kawakami S, Yasuno T, Kawakami S, Ito A, Fujimi K, Matsuda T, Nakashima S, Masutani K, Uehara Y, Higaki Y, Michishita R. The moderate-intensity continuous exercise maintains renal blood flow and does not impair the renal function. Physiol Rep. 2022;10(15):e15420. doi: 10.14814/phy2.15420. PubMed PMID: 35924347; PMCID: PMC9350468.
63. Wideman L, Weltman JY, Hartman ML, Veldhuis JD, Weltman A. Growth hormone release during acute and chronic aerobic and resistance exercise: recent findings. Sports Med. 2002;32(15):987–1004. doi: 10.2165/00007256-200232150-00003. PubMed PMID: 12457419.
64. Pilli VS, Datta A, Afreen S, Catalano D, Szabo G, Majumder R. Hypoxia downregulates protein S expression. Blood. 2018;132(4):452–5. Epub 20180521. doi: 10.1182/blood-2018-04-841585. PubMed PMID: 29784640; PMCID: PMC6071559.
65. Henke RM, Dastidar RG, Shah A, Cadinu D, Yao X, Hooda J, Zhang L. Hypoxia elicits broad and systematic changes in protein subcellular localization. Am J Physiol Cell Physiol. 2011;301(4):C913–28. Epub 20110713. doi: 10.1152/ajpcell.00481.2010. PubMed PMID: 21753182; PMCID: PMC3191569.
66. Revuelta-Lopez E, Castellano J, Roura S, Galvez-Monton C, Nasarre L, Benitez S, Bayes-Genis A, Badimon L, Llorente-Cortes V. Hypoxia induces metalloproteinase-9 activation and human vascular smooth muscle cell migration through low-density lipoprotein receptor-related protein 1-mediated Pyk2 phosphorylation. Arterioscler Thromb Vasc Biol. 2013;33(12):2877–87. Epub 20130926. doi: 10.1161/ATVBAHA.113.302323. PubMed PMID: 24072693.
67. Uhlen M, Fagerberg L, Hallstrom BM, Lindskog C, Oksvold P, Mardinoglu A, Sivertsson A, Kampf C, Sjostedt E, Asplund A, Olsson I, Edlund K, Lundberg E, Navani S, Szigyarto CA, Odeberg J, Djureinovic D, Takanen JO, Hober S, Alm T, Edqvist PH, Berling H, Tegel H, Mulder J, Rockberg J, Nilsson P, Schwenk JM, Hamsten M, von Feilitzen K, Forsberg M, Persson L, Johansson F, Zwahlen M, von Heijne G, Nielsen J, Ponten F. Proteomics. Tissue-based map of the human proteome. Science. 2015;347(6220):1260419. doi: 10.1126/science.1260419. PubMed PMID: 25613900.
68. Uhlen M, Karlsson MJ, Hober A, Svensson AS, Scheffel J, Kotol D, Zhong W, Tebani A, Strandberg L, Edfors F, Sjostedt E, Mulder J, Mardinoglu A, Berling A, Ekblad S, Dannemeyer M, Kanje S, Rockberg J, Lundqvist M, Malm M, Volk AL, Nilsson P, Manberg A, Dodig-Crnkovic T, Pin E, Zwahlen M, Oksvold P, von Feilitzen K, Haussler RS, Hong MG, Lindskog C, Ponten F, Katona B, Vuu J, Lindstrom E, Nielsen J, Robinson J, Ayoglu B, Mahdessian D, Sullivan D, Thul P, Danielsson F, Stadler C, Lundberg E, Bergstrom G, Gummesson A, Voldborg BG, Tegel H, Hober S, Forsstrom B, Schwenk JM, Fagerberg L, Sivertsson A. The human secretome. Science signaling. 2019;12(609). Epub 20191126. doi: 10.1126/scisignal.aaz0274. PubMed PMID: 31772123.
69. Knox C, Wilson M, Klinger CM, Franklin M, Oler E, Wilson A, Pon A, Cox J, Chin NEL, Strawbridge SA, Garcia-Patino M, Kruger R, Sivakumaran A, Sanford S, Doshi R, Khetarpal N, Fatokun O, Doucet D, Zubkowski A, Rayat DY, Jackson H, Harford K, Anjum A, Zakir M, Wang F, Tian S, Lee B, Liigand J, Peters H, Wang RQR, Nguyen T, So D, Sharp M, da Silva R, Gabriel C, Scantlebury J, Jasinski M, Ackerman D, Jewison T, Sajed T, Gautam V, Wishart DS. DrugBank 6.0: the DrugBank Knowledgebase for 2024. Nucleic Acids Res. 2024;52(D1):D1265–D75. doi: 10.1093/nar/gkad976. PubMed PMID: 37953279; PMCID: PMC10767804.
70. Beutgen VM, Shinkevich V, Porschke J, Meena C, Steitz AM, Pogge von Strandmann E, Graumann J, Gomez-Serrano M. Secretome Analysis Using Affinity Proteomics and Immunoassays: A Focus on Tumor Biology. Mol Cell Proteomics. 2024;23(9):100830. Epub

20240813. doi: 10.1016/j.mcpro.2024.100830. PubMed PMID: 39147028; PMCID: PMC11417252.
71. Malmstrom E, Malmstrom L, Hauri S, Mohanty T, Scott A, Karlsson C, Gueto-Tettay C, Ahrman E, Nozohoor S, Tingstedt B, Regner S, Elfving P, Bjermer L, Forsvall A, Doyle A, Magnusson M, Hedenfalk I, Kannisto P, Brandt C, Nilsson E, Dahlin LB, Malm J, Linder A, Nimeus E, Malmstrom J. Human proteome distribution atlas for tissue-specific plasma proteome dynamics. Cell. 2025. Epub 20250404. doi: 10.1016/j.cell.2025.03.013. PubMed PMID: 40203824.
72. Jiang L, Wang M, Lin S, Jian R, Li X, Chan J, Dong G, Fang H, Robinson AE, Consortium GT, Snyder MP. A Quantitative Proteome Map of the Human Body. Cell. 2020;183(1):269–83 e19. Epub 20200910. doi: 10.1016/j.cell.2020.08.036. PubMed PMID: 32916130; PMCID: PMC7575058.
73. Moreno P, Fexova S, George N, Manning JR, Miao Z, Mohammed S, Munoz-Pomer A, Fullgrabe A, Bi Y, Bush N, Iqbal H, Kumbham U, Solovyev A, Zhao L, Prakash A, Garcia-Seisdedos D, Kundu DJ, Wang S, Walzer M, Clarke L, Osumi-Sutherland D, Tello-Ruiz MK, Kumari S, Ware D, Eliasova J, Arends MJ, Nawijn MC, Meyer K, Burdett T, Marioni J, Teichmann S, Vizcaino JA, Brazma A, Papatheodorou I. Expression Atlas update: gene and protein expression in multiple species. Nucleic Acids Res. 2022;50(D1):D129–D40. doi: 10.1093/nar/gkab1030. PubMed PMID: 34850121; PMCID: PMC8728300.
74. Egan B, Zierath JR. Exercise metabolism and the molecular regulation of skeletal muscle adaptation. Cell Metab. 2013;17(2):162–84. doi: 10.1016/j.cmet.2012.12.012. PubMed PMID: 23395166.
75. Basu M, Wang K, Ruppin E, Hannenhalli S. Predicting tissue-specific gene expression from whole blood transcriptome. Sci Adv. 2021;7(14). Epub 20210402. doi: 10.1126/sciadv.abd6991. PubMed PMID: 33811070; PMCID: PMC11057699.
76. Kruger K, Reichel T, Zeilinger C. Role of heat shock proteins 70/90 in exercise physiology and exercise immunology and their diagnostic potential in sports. J Appl Physiol (1985). 2019;126(4):916–27. Epub 20190207. doi: 10.1152/japplphysiol.01052.2018. PubMed PMID: 30730806.
77. Hooshmand N, El-Sayed MA. Collective multipole oscillations direct the plasmonic coupling at the nanojunction interfaces. Proc Natl Acad Sci U S A. 2019;116(39):19299–304. Epub 20190905. doi: 10.1073/pnas.1909416116. PubMed PMID: 31488713; PMCID: PMC6765250.
78. Genest O, Wickner S, Doyle SM. Hsp90 and Hsp70 chaperones: Collaborators in protein remodeling. J Biol Chem. 2019;294(6):2109–20. Epub 20181106. doi: 10.1074/jbc.REV118.002806. PubMed PMID: 30401745; PMCID: PMC6369297.
79. Henstridge DC, Febbraio MA, Hargreaves M. Heat shock proteins and exercise adaptations. Our knowledge thus far and the road still ahead. J Appl Physiol (1985). 2016;120(6):683–91. Epub 20151217. doi: 10.1152/japplphysiol.00811.2015. PubMed PMID: 26679615.
80. Sakamoto M, Minamino T, Toko H, Kayama Y, Zou Y, Sano M, Takaki E, Aoyagi T, Tojo K, Tajima N, Nakai A, Aburatani H, Komuro I. Upregulation of heat shock transcription factor 1 plays a critical role in adaptive cardiac hypertrophy. Circ Res. 2006;99(12):1411–8. Epub 20061109. doi: 10.1161/01.RES.0000252345.80198.97. PubMed PMID: 17095722.
81. Tian X, Zhou N, Yuan J, Lu L, Zhang Q, Wei M, Zou Y, Yuan L. Heat shock transcription factor 1 regulates exercise-induced myocardial angiogenesis after pressure overload via HIF-1alpha/VEGF pathway. J Cell Mol Med. 2020;24(3):2178–88. Epub 20200112. doi: 10.1111/jcmm.14872. PubMed PMID: 31930683; PMCID: PMC7011135.
82. Hu C, Li T, Xu Y, Zhang X, Li F, Bai J, Chen J, Jiang W, Yang K, Ou Q, Li X, Wang P, Zhang Y. CellMarker 2.0: an updated database of manually curated cell markers in human/mouse and web tools based on scRNA-seq data. Nucleic Acids Res.

2023;51(D1):D870–D6. doi: 10.1093/nar/gkac947. PubMed PMID: 36300619; PMCID: PMC9825416.
83. Vallejo MC, Sarkar S, Elliott EC, Henry HR, Powell SM, Diaz Ludovico I, You Y, Huang F, Payne SH, Ramanadham S, Sims EK, Metz TO, Mirmira RG, Nakayasu ES. A proteomic meta-analysis refinement of plasma extracellular vesicles. Sci Data. 2023;10(1):837. Epub 20231128. doi: 10.1038/s41597-023-02748-1. PubMed PMID: 38017024; PMCID: PMC10684639.
84. Ziegler-Heitbrock L. The CD14+ CD16+ blood monocytes: their role in infection and inflammation. J Leukoc Biol. 2007;81(3):584–92. Epub 20061129. doi: 10.1189/jlb.0806510. PubMed PMID: 17135573.
85. Steppich B, Dayyani F, Gruber R, Lorenz R, Mack M, Ziegler-Heitbrock HW. Selective mobilization of CD14(+)CD16(+) monocytes by exercise. Am J Physiol Cell Physiol. 2000;279(3):C578–86. doi: 10.1152/ajpcell.2000.279.3.C578. PubMed PMID: 10942707.
86. Ponta H, Sherman L, Herrlich PA. CD44: from adhesion molecules to signalling regulators. Nat Rev Mol Cell Biol. 2003;4(1):33–45. doi: 10.1038/nrm1004. PubMed PMID: 12511867.
87. Israels SJ, McMillan-Ward EM, Easton J, Robertson C, McNicol A. CD63 associates with the alphaIIb beta3 integrin-CD9 complex on the surface of activated platelets. Thromb Haemost. 2001;85(1):134–41. PubMed PMID: 11204565.
88. Graca FA, Minden-Birkenmaier BA, Stephan A, Demontis F, Labelle M. Signaling roles of platelets in skeletal muscle regeneration. Bioessays. 2023;45(12):e2300134. Epub 20230915. doi: 10.1002/bies.202300134. PubMed PMID: 37712935; PMCID: PMC10840841.
89. Newman AM, Steen CB, Liu CL, Gentles AJ, Chaudhuri AA, Scherer F, Khodadoust MS, Esfahani MS, Luca BA, Steiner D, Diehn M, Alizadeh AA. Determining cell type abundance and expression from bulk tissues with digital cytometry. Nat Biotechnol. 2019;37(7):773–82. Epub 20190506. doi: 10.1038/s41587-019-0114-2. PubMed PMID: 31061481; PMCID: PMC6610714.
90. Huang J, Zhu Z, Ji D, Sun R, Yang Y, Liu L, Shao Y, Chen Y, Li L, Sun B. Single-Cell Transcriptome Profiling Reveals Neutrophil Heterogeneity and Functional Multiplicity in the Early Stage of Severe Burn Patients. Front Immunol. 2021;12:792122. Epub 20220118. doi: 10.3389/fimmu.2021.792122. PubMed PMID: 35116026; PMCID: PMC8803731.
91. Bigley AB, Lowder TW, Spielmann G, Rector JL, Pircher H, Woods JA, Simpson RJ. NK-cells have an impaired response to acute exercise and a lower expression of the inhibitory receptors KLRG1 and CD158a in humans with latent cytomegalovirus infection. Brain Behav Immun. 2012;26(1):177–86. Epub 20110910. doi: 10.1016/j.bbi.2011.09.004. PubMed PMID: 21933704.
92. Amar D, Lindholm ME, Norrbom J, Wheeler MT, Rivas MA, Ashley EA. Time trajectories in the transcriptomic response to exercise - a meta-analysis. Nat Commun. 2021;12(1):3471. Epub 20210609. doi: 10.1038/s41467-021-23579-x. PubMed PMID: 34108459; PMCID: PMC8190306.
93. American College of Sports M. American College of Sports Medicine position stand. Progression models in resistance training for healthy adults. Med Sci Sports Exerc. 2009;41(3):687–708. doi: 10.1249/MSS.0b013e3181915670. PubMed PMID: 19204579.
94. Garber CE, Blissmer B, Deschenes MR, Franklin BA, Lamonte MJ, Lee IM, Nieman DC, Swain DP, American College of Sports M. American College of Sports Medicine position stand. Quantity and quality of exercise for developing and maintaining cardiorespiratory, musculoskeletal, and neuromotor fitness in apparently healthy adults: guidance for prescribing exercise. Med Sci Sports Exerc. 2011;43(7):1334–59. doi: 10.1249/MSS.0b013e318213fefb. PubMed PMID: 21694556.
95. Maisonpierre PC, Suri C, Jones PF, Bartunkova S, Wiegand SJ, Radziejewski C, Compton D, McClain J, Aldrich TH, Papadopoulos N, Daly TJ, Davis S, Sato TN, Yancopoulos

GD. Angiopoietin-2, a natural antagonist for Tie2 that disrupts in vivo angiogenesis. Science. 1997;277(5322):55–60. doi: 10.1126/science.277.5322.55. PubMed PMID: 9204896.
96. Lobov IB, Brooks PC, Lang RA. Angiopoietin-2 displays VEGF-dependent modulation of capillary structure and endothelial cell survival in vivo. Proc Natl Acad Sci U S A. 2002;99(17):11205–10. Epub 20020805. doi: 10.1073/pnas.172161899. PubMed PMID: 12163646; PMCID: PMC123234.
97. Felcht M, Luck R, Schering A, Seidel P, Srivastava K, Hu J, Bartol A, Kienast Y, Vettel C, Loos EK, Kutschera S, Bartels S, Appak S, Besemfelder E, Terhardt D, Chavakis E, Wieland T, Klein C, Thomas M, Uemura A, Goerdt S, Augustin HG. Angiopoietin-2 differentially regulates angiogenesis through TIE2 and integrin signaling. J Clin Invest. 2012;122(6):1991–2005. Epub 2012/05/15. doi: 10.1172/JCI58832. PubMed PMID: 22585576; PMCID: PMC3366398.
98. Campbell DJ. Long-term neprilysin inhibition - implications for ARNIs. Nat Rev Cardiol. 2017;14(3):171–86. Epub 20161215. doi: 10.1038/nrcardio.2016.200. PubMed PMID: 27974807.
99. Brutsaert TD, Kiyamu M, Elias Revollendo G, Isherwood JL, Lee FS, Rivera-Ch M, Leon-Velarde F, Ghosh S, Bigham AW. Association of EGLN1 gene with high aerobic capacity of Peruvian Quechua at high altitude. Proc Natl Acad Sci U S A. 2019;116(48):24006–11. Epub 20191111. doi: 10.1073/pnas.1906171116. PubMed PMID: 31712437; PMCID: PMC6883775.
100. Kistner TM, Pedersen BK, Lieberman DE. Interleukin 6 as an energy allocator in muscle tissue. Nat Metab. 2022;4(2):170–9. Epub 20220224. doi: 10.1038/s42255-022-00538-4. PubMed PMID: 35210610.
101. Orange ST, Leslie J, Ross M, Mann DA, Wackerhage H. The exercise IL-6 enigma in cancer. Trends Endocrinol Metab. 2023;34(11):749–63. Epub 20230824. doi: 10.1016/j.tem.2023.08.001. PubMed PMID: 37633799.
102. Bigley AB, Rezvani K, Chew C, Sekine T, Pistillo M, Crucian B, Bollard CM, Simpson RJ. Acute exercise preferentially redeploys NK-cells with a highly-differentiated phenotype and augments cytotoxicity against lymphoma and multiple myeloma target cells. Brain Behav Immun. 2014;39:160–71. Epub 20131105. doi: 10.1016/j.bbi.2013.10.030. PubMed PMID: 24200514.
103. Cho E, Stampley J, Wall R, Matthews R, Zunica E, Brown JC, Johannsen NM, Irving BA, Spielmann G. Acute Exercise Increases NK Cell Mitochondrial Respiration and Cytotoxicity against Triple-Negative Breast Cancer Cells under Hypoxic Conditions. Med Sci Sports Exerc. 2023;55(12):2132–42. Epub 20230705. doi: 10.1249/MSS.0000000000003250. PubMed PMID: 37436930; PMCID: PMC10662621.
104. Schauer T, Djurhuus SS, Simonsen C, Brasso K, Christensen JF. The effects of acute exercise and inflammation on immune function in early-stage prostate cancer. Brain Behav Immun Health. 2022;25:100508. Epub 20220907. doi: 10.1016/j.bbih.2022.100508. PubMed PMID: 36133956; PMCID: PMC9483738.
105. Heredia JE, Mukundan L, Chen FM, Mueller AA, Deo RC, Locksley RM, Rando TA, Chawla A. Type 2 innate signals stimulate fibro/adipogenic progenitors to facilitate muscle regeneration. Cell. 2013;153(2):376–88. doi: 10.1016/j.cell.2013.02.053. PubMed PMID: 23582327; PMCID: PMC3663598.
106. Tidball JG, Villalta SA. Regulatory interactions between muscle and the immune system during muscle regeneration. Am J Physiol Regul Integr Comp Physiol. 2010;298(5):R1173–87. Epub 20100310. doi: 10.1152/ajpregu.00735.2009. PubMed PMID: 20219869; PMCID: PMC2867520.
107. Graca FA, Stephan A, Minden-Birkenmaier BA, Shirinifard A, Wang YD, Demontis F, Labelle M. Platelet-derived chemokines promote skeletal muscle regeneration by guiding neutrophil recruitment to injured muscles. Nat Commun. 2023;14(1):2900. Epub 20230522. doi: 10.1038/s41467-023-38624-0. PubMed PMID: 37217480; PMCID: PMC10203137.

108. Maden SK, Kwon SH, Huuki-Myers LA, Collado-Torres L, Hicks SC, Maynard KR. Challenges and opportunities to computationally deconvolve heterogeneous tissue with varying cell sizes using single cell RNA-sequencing datasets. ArXiv. 2023. Epub 20230510. PubMed PMID: 37214135; PMCID: PMC10197733.
109. Morville T, Sahl RE, Trammell SA, Svenningsen JS, Gillum MP, Helge JW, Clemmensen C. Divergent effects of resistance and endurance exercise on plasma bile acids, FGF19, and FGF21 in humans. JCI Insight. 2018;3(15). Epub 20180809. doi: 10.1172/jci.insight.122737. PubMed PMID: 30089729; PMCID: PMC6129127.
110. Muñoz-Cánoves P, Scheele C, Pedersen BK, Serrano AL. Interleukin-6 myokine signaling in skeletal muscle: a double-edged sword? FEBS J. 2013;280(17):4131–48. Epub 20130618. doi: 10.1111/febs.12338. PubMed PMID: 23663276; PMCID: PMC4163639.
111. Wei W, Riley NM, Lyu X, Shen X, Guo J, Raun SH, Zhao M, Moya-Garzon MD, Basu H, Sheng-Hwa Tung A, Li VL, Huang W, Wiggenhorn AL, Svensson KJ, Snyder MP, Bertozzi CR, Long JZ. Organism-wide, cell-type-specific secretome mapping of exercise training in mice. Cell Metab. 2023;35(7):1261–79 e11. Epub 20230503. doi: 10.1016/j.cmet.2023.04.011. PubMed PMID: 37141889; PMCID: PMC10524249.
112. Cho KF, Branon TC, Udeshi ND, Myers SA, Carr SA, Ting AY. Proximity labeling in mammalian cells with TurboID and split-TurboID. Nat Protoc. 2020;15(12):3971–99. Epub 20201102. doi: 10.1038/s41596-020-0399-0. PubMed PMID: 33139955.
113. Newman AM, Liu CL, Green MR, Gentles AJ, Feng W, Xu Y, Hoang CD, Diehn M, Alizadeh AA. Robust enumeration of cell subsets from tissue expression profiles. Nat Methods. 2015;12(5):453–7. Epub 20150330. doi: 10.1038/nmeth.3337. PubMed PMID: 25822800; PMCID: PMC4739640.
114. Zhao K, Rhee SY. Interpreting omics data with pathway enrichment analysis. Trends Genet. 2023;39(4):308–19. Epub 20230206. doi: 10.1016/j.tig.2023.01.003. PubMed PMID: 36750393.
115. Martin M. Cutadapt removes adapter sequences from high-throughput sequencing reads. 2011. 2011;17(1):3. Epub 2011-08-02. doi: 10.14806/ej.17.1.200.
116. Dobin A, Davis CA, Schlesinger F, Drenkow J, Zaleski C, Jha S, Batut P, Chaisson M, Gingeras TR. STAR: ultrafast universal RNA-seq aligner. Bioinformatics. 2012;29(1):15–21. doi: 10.1093/bioinformatics/bts635.
117. Li B, Dewey CN. RSEM: accurate transcript quantification from RNA-Seq data with or without a reference genome. BMC Bioinformatics. 2011;12:323. Epub 20110804. doi: 10.1186/1471-2105-12-323. PubMed PMID: 21816040; PMCID: PMC3163565.
118. Langmead B, Salzberg SL. Fast gapped-read alignment with Bowtie 2. Nat Methods. 2012;9(4):357–9. Epub 20120304. doi: 10.1038/nmeth.1923. PubMed PMID: 22388286; PMCID: PMC3322381.
119. Hoffman GE. variancePartition. Bioconductor; 2017.
120. Ritchie ME, Phipson B, Wu D, Hu Y, Law CW, Shi W, Smyth GK. limma powers differential expression analyses for RNA-sequencing and microarray studies. Nucleic Acids Res. 2015;43(7):e47. Epub 20150120. doi: 10.1093/nar/gkv007. PubMed PMID: 25605792; PMCID: PMC4402510.
121. Assarsson E, Lundberg M, Holmquist G, Bjorkesten J, Thorsen SB, Ekman D, Eriksson A, Rennel Dickens E, Ohlsson S, Edfeldt G, Andersson AC, Lindstedt P, Stenvang J, Gullberg M, Fredriksson S. Homogenous 96-plex PEA immunoassay exhibiting high sensitivity, specificity, and excellent scalability. PLoS One. 2014;9(4):e95192. Epub 20140422. doi: 10.1371/journal.pone.0095192. PubMed PMID: 24755770; PMCID: PMC3995906.
122. Mertins P, Tang LC, Krug K, Clark DJ, Gritsenko MA, Chen L, Clauser KR, Clauss TR, Shah P, Gillette MA, Petyuk VA, Thomas SN, Mani DR, Mundt F, Moore RJ, Hu Y, Zhao R, Schnaubelt M, Keshishian H, Monroe ME, Zhang Z, Udeshi ND, Mani D, Davies SR, Townsend RR, Chan DW, Smith RD, Zhang H, Liu T, Carr SA. Reproducible workflow for multiplexed

deep-scale proteome and phosphoproteome analysis of tumor tissues by liquid chromatography-mass spectrometry. Nat Protoc. 2018;13(7):1632–61. doi: 10.1038/s41596-018-0006-9. PubMed PMID: 29988108; PMCID: PMC6211289.
123. Zecha J, Satpathy S, Kanashova T, Avanessian SC, Kane MH, Clauser KR, Mertins P, Carr SA, Kuster B. TMT Labeling for the Masses: A Robust and Cost-efficient, In-solution Labeling Approach. Mol Cell Proteomics. 2019;18(7):1468–78. Epub 20190409. doi: 10.1074/mcp.TIR119.001385. PubMed PMID: 30967486; PMCID: PMC6601210.
124. Jimenez D, Samdarshi M, Hershman S. MoTrPAC/motrpac-proteomics-pipeline: MoTrPAC Proteomics Pipeline v1.3.0. v1.3.0 ed: Zenodo; 2024.
125. Kwee LC, Ilkayeva O, Muehlbauer MJ, Bihlmeyer N, Wolfe B, Purnell JQ, Xavier Pi-Sunyer F, Chen H, Bahnson J, Newgard CB, Shah SH, Laferrère B. Metabolites and diabetes remission after weight loss. Nutr Diabetes. 2021;11(1):10. doi: 10.1038/s41387-021-00151-6; PMCID: PMC7904757.
126. Olson KC, Chen G, Lynch CJ. Quantification of branched-chain keto acids in tissue by ultra fast liquid chromatography-mass spectrometry. Anal Biochem. 2013;439(2):116–22. doi: 10.1016/j.ab.2013.05.002; PMCID: PMC3887392.
127. Deutsch J, Grange E, Rapoport SI, Purdon AD. Isolation and quantitation of long-chain acyl-coenzyme A esters in brain tissue by solid-phase extraction. Anal Biochem. 1994;220(2):321–3. doi: 10.1006/abio.1994.1344.
128. Magnes C, Sinner FM, Regittnig W, Pieber TR. LC/MS/MS method for quantitative determination of long-chain fatty acyl-CoAs. Anal Chem. 2005;77(9):2889–94. doi: 10.1021/ac048314i.
129. Minkler PE, Stoll MSK, Ingalls ST, Yang S, Kerner J, Hoppel CL. Quantification of carnitine and acylcarnitines in biological matrices by HPLC electrospray ionization-mass spectrometry. Clin Chem. 2008;54(9):1451–62. doi: 10.1373/clinchem.2007.099226.
130. Cordell RL, Hill SJ, Ortori CA, Barrett DA. Quantitative profiling of nucleotides and related phosphate-containing metabolites in cultured mammalian cells by liquid chromatography tandem electrospray mass spectrometry. J Chromatogr B Analyt Technol Biomed Life Sci. 2008;871(1):115–24. doi: 10.1016/j.jchromb.2008.07.005.
131. Gooding JR, Jensen MV, Dai X, Wenner BR, Lu D, Arumugam R, Ferdaoussi M, MacDonald PE, Newgard CB. Adenylosuccinate is an insulin secretagogue derived from glucose-induced purine metabolism. Cell Rep. 2015;13(1):157–67. doi: 10.1016/j.celrep.2015.08.072; PMCID: PMC4598307.
132. Lanza IR, Zhang S, Ward LE, Karakelides H, Raftery D, Nair KS. Quantitative metabolomics by H-NMR and LC-MS/MS confirms altered metabolic pathways in diabetes. PLoS One. 2010;5(5):e10538. doi: 10.1371/journal.pone.0010538; PMCID: PMC2866659.
133. Gonsalves WI, Broniowska K, Jessen E, Petterson X-M, Bush AG, Gransee J, Lacy MQ, Hitosugi T, Kumar SK. Metabolomic and lipidomic profiling of bone marrow plasma differentiates patients with monoclonal gammopathy of undetermined significance from multiple myeloma. Sci Rep. 2020;10(1):10250. doi: 10.1038/s41598-020-67105-3; PMCID: PMC7314797.
134. Wilkins J, Sakrikar D, Petterson X-M, Lanza IR, Trushina E. A comprehensive protocol for multiplatform metabolomics analysis in patient-derived skin fibroblasts. Metabolomics. 2019;15(6):83. doi: 10.1007/s11306-019-1544-z; PMCID: PMC7928486.
135. Dutta T, Kudva YC, Persson X-MT, Schenck LA, Ford GC, Singh RJ, Carter R, Nair KS. Impact of long-term poor and good glycemic control on metabolomics alterations in type 1 diabetic people. J Clin Endocrinol Metab. 2016;101(3):1023–33. doi: 10.1210/jc.2015-2640; PMCID: PMC4803168.
136. Collins JM, Jones DP, Sharma A, Khadka M, Liu KH, Kempker RR, Prideaux B, Maner-Smith K, Tukvadze N, Shah NS, Brust JCM, Sékaly R-P, Gandhi NR, Blumberg HM, Ortlund EA, Ziegler TR. TCA cycle remodeling drives proinflammatory signaling in humans with

pulmonary tuberculosis. PLoS Pathog. 2021;17(9):e1009941. doi: 10.1371/journal.ppat.1009941; PMCID: PMC8494353.
137. Maner-Smith KM, Goll JB, Khadka M, Jensen TL, Colucci JK, Gelber CE, Albert CJ, Bosinger SE, Franke JD, Natrajan M, Rouphael N, Johnson RA, Sanz P, Anderson EJ, Hoft DF, Mulligan MJ, Ford DA, Ortlund EA. Alterations in the human plasma lipidome in response to tularemia vaccination. Vaccines (Basel). 2020;8(3):414. doi: 10.3390/vaccines8030414; PMCID: PMC7564507.
138. Pino LK, Searle BC, Bollinger JG, Nunn B, MacLean B, MacCoss MJ. The Skyline ecosystem: Informatics for quantitative mass spectrometry proteomics. Mass Spectrom Rev. 2020;39(3):229–44. doi: 10.1002/mas.21540; PMCID: PMC5799042.
139. Harrell FE, Jr. Hmisc: Harrell Miscellaneous. The R Foundation; 2003.
140. Wei T, Simko V. Corrplot: Visualization of a correlation matrix. The R Foundation; 2010.
141. Foldnes N, Olsson UH. A simple simulation technique for nonnormal data with prespecified skewness, kurtosis, and covariance matrix. Multivariate Behav Res. 2016;51(2-3):207–19. doi: 10.1080/00273171.2015.1133274.
142. Tahir UA, Katz DH, Avila-Pachecho J, Bick AG, Pampana A, Robbins JM, Yu Z, Chen Z-Z, Benson MD, Cruz DE, Ngo D, Deng S, Shi X, Zheng S, Eisman AS, Farrell L, Hall ME, Correa A, Tracy RP, Durda P, Taylor KD, Liu Y, Johnson WC, Guo X, Yao J, Chen Y-DI, Manichaikul AW, Ruberg FL, Blaner WS, Jain D, Bouchard C, Sarzynski MA, Rich SS, Rotter JI, Wang TJ, Wilson JG, Clish CB, Natarajan P, Gerszten RE. Whole Genome Association Study of the Plasma Metabolome Identifies Metabolites Linked to Cardiometabolic Disease in Black Individuals. Nat Commun. 2022;13(1):4923. doi: 10.1038/s41467-022-32275-3.
143. Katz DH, Tahir UA, Bick AG, Pampana A, Ngo D, Benson MD, Yu Z, Robbins JM, Chen Z-Z, Cruz DE, Deng S, Farrell L, Sinha S, Schmaier AA, Shen D, Gao Y, Hall ME, Correa A, Tracy RP, Durda P, Taylor KD, Liu Y, Johnson WC, Guo X, Yao J, Ida Chen Y-D, Manichaikul AW, Jain D, Bouchard C, Sarzynski MA, Rich SS, Rotter JI, Wang TJ, Wilson JG, Natarajan P, Gerszten RE, National Heart L, Blood Institute TC. Whole Genome Sequence Analysis of the Plasma Proteome in Black Adults Provides Novel Insights Into Cardiovascular Disease. Circulation. 2022;145(5):357–70. doi: 10.1161/CIRCULATIONAHA.121.055117.
144. Benjamini Y, Hochberg Y. Controlling the false discovery rate: a practical and powerful approach to multiple testing. Journal of the royal statistical society series b-methodological. 1995;57(1):289–300. doi: 10.1111/J.2517-6161.1995.TB02031.X.
145. Dyer SC, Austine-Orimoloye O, Azov AG, Barba M, Barnes I, Barrera-Enriquez VP, Becker A, Bennett R, Beracochea M, Berry A, Bhai J, Bhurji SK, Boddu S, Branco Lins PR, Brooks L, Ramaraju SB, Campbell LI, Martinez MC, Charkhchi M, Cortes LA, Davidson C, Denni S, Dodiya K, Donaldson S, El Houdaigui B, El Naboulsi T, Falola O, Fatima R, Genez T, Martinez JG, Gurbich T, Hardy M, Hollis Z, Hunt T, Kay M, Kaykala V, Lemos D, Lodha D, Mathlouthi N, Merino GA, Merritt R, Mirabueno LP, Mushtaq A, Hossain SN, Pérez-Silva JG, Perry M, Piližota I, Poppleton D, Prosovetskaia I, Raj S, Salam AIA, Saraf S, Saraiva-Agostinho N, Sinha S, Sipos B, Sitnik V, Steed E, Suner M-M, Surapaneni L, Sutinen K, Tricomi FF, Tsang I, Urbina-Gómez D, Veidenberg A, Walsh TA, Willhoft NL, Allen J, Alvarez-Jarreta J, Chakiachvili M, Cheema J, da Rocha JB, De Silva NH, Giorgetti S, Haggerty L, Ilsley GR, Keatley J, Loveland JE, Moore B, Mudge JM, Naamati G, Tate J, Trevanion SJ, Winterbottom A, Flint B, Frankish A, Hunt SE, Finn RD, Freeberg MA, Harrison PW, Martin FJ, Yates AD. Ensembl 2025. Nucleic Acids Res. 2025;53(D1):D948–D57. doi: 10.1093/nar/gkae1071; PMCID: PMC11701638.
146. UniProt C. UniProt: The universal protein knowledgebase in 2025. Nucleic Acids Res. 2025;53(D1):D609–D17. doi: 10.1093/nar/gkae1010; PMCID: PMC11701636.
147. Durinck S, Spellman PT, Birney E, Huber W. Mapping identifiers for the integration of genomic datasets with the R/Bioconductor package biomaRt. Nat Protoc. 2009;4(8):1184–91. doi: 10.1038/nprot.2009.97; PMCID: PMC3159387.

148. Yu G, Wang L-G, He Q-Y. ChIPseeker: an R/Bioconductor package for ChIP peak annotation, comparison and visualization. Bioinformatics. 2015;31(14):2382–3. doi: 10.1093/bioinformatics/btv145.
149. Workbench M. PR0000012016. doi: 10.21228/M8159B.
150. Tenenbaum D, Maintainer BP. KEGGREST: Client-side REST access to the Kyoto Encyclopedia of Genes and Genomes (KEGG)2025.
151. Rath S, Sharma R, Gupta R, Ast T, Chan C, Durham TJ, Goodman RP, Grabarek Z, Haas ME, Hung WHW, Joshi PR, Jourdain AA, Kim SH, Kotrys AV, Lam SS, McCoy JG, Meisel JD, Miranda M, Panda A, Patgiri A, Rogers R, Sadre S, Shah H, Skinner OS, To T-L, Walker MA, Wang H, Ward PS, Wengrod J, Yuan C-C, Calvo SE, Mootha VK. MitoCarta3.0: an updated mitochondrial proteome now with sub-organelle localization and pathway annotations. Nucleic Acids Res. 2021;49(D1):D1541–D7. doi: 10.1093/nar/gkaa1011; PMCID: PMC7778944.
152. Liberzon A, Birger C, Thorvaldsdóttir H, Ghandi M, Mesirov JP, Tamayo P. The Molecular Signatures Database (MSigDB) hallmark gene set collection. Cell Syst. 2015;1(6):417–25. doi: 10.1016/j.cels.2015.12.004; PMCID: PMC4707969.
153. Fahy E, Subramaniam S. RefMet: a reference nomenclature for metabolomics. Nat Methods. 2020;17(12):1173–4. doi: 10.1038/s41592-020-01009-y.
154. Wu D, Smyth GK. Camera: a competitive gene set test accounting for inter-gene correlation. Nucleic Acids Res. 2012;40(17):e133. doi: 10.1093/nar/gks461; PMCID: PMC3458527.
155. Sagendorf T. TMSig: Tools for Molecular Signatures. R package version 1.5.0 ed: Bioconductor; 2025.
156. Team RC. R: A Language and Environment for Statistical Computing2025.
157. Ioannidis JPA. Why most published research findings are false. PLoS Med. 2005;2(8):e124. doi: 10.1371/journal.pmed.0020124; PMCID: PMC1182327.
158. Kang M, Ragan BG, Park J-H. Issues in outcomes research: an overview of randomization techniques for clinical trials. J Athl Train. 2008;43(2):215–21. doi: 10.4085/1062-6050-43.2.215; PMCID: PMC2267325.
159. Lachin JM, Matts JP, Wei LJ. Randomization in clinical trials: conclusions and recommendations. Control Clin Trials. 1988;9(4):365–74. doi: 10.1016/0197-2456(88)90049-9.
160. Collins FS, Tabak LA. Policy: NIH plans to enhance reproducibility. Nature. 2014;505(7485):612–3. doi: 10.1038/505612a; PMCID: PMC4058759.
161. Brookes ST, Whitely E, Egger M, Smith GD, Mulheran PA, Peters TJ. Subgroup analyses in randomized trials: risks of subgroup-specific analyses; power and sample size for the interaction test. J Clin Epidemiol. 2004;57(3):229–36. doi: 10.1016/j.jclinepi.2003.08.009.
162. Lachenbruch PA, Cohen J. Statistical Power Analysis for the Behavioral Sciences (2nd ed.). J Am Stat Assoc. 1989;84(408):1096. doi: 10.2307/2290095.

Temporal biochemical profiling in the blood in response to acute exercise

Baseline Testing

N = 175
Age =41 years
Female, 72%
BMI =26 kg/m²
VO_2max = 25 ml/kg/min

F31, M6
F46, M19
F49, M24

Multi-tissue, Multi-modality, Multi-time point sampling

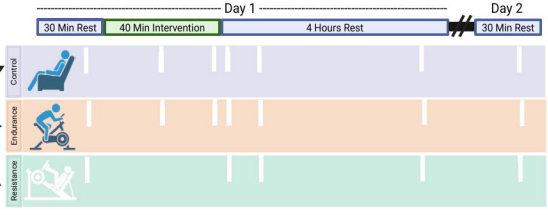

- *Plasma proteomics (Olink)*
- *LC-MS plasma metabolomics (10 methods)*
- *Whole blood transcriptomics (PAXgene)*

Single analyte temporal profile

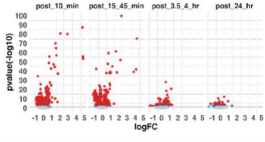

Ome-wide Changes

Early vs late changes after acute exercise

Early cytokine vs late hormonal responses

Immune cell responses

Differential innate immune cellular responses

Differential metabolic responses to EE and RE

Divergent carnitine & free fatty acid response

Integration with clinical phenotypes

Canonical correlation analysis: shared molecular features across traits

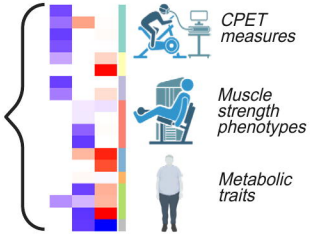

Figure 1

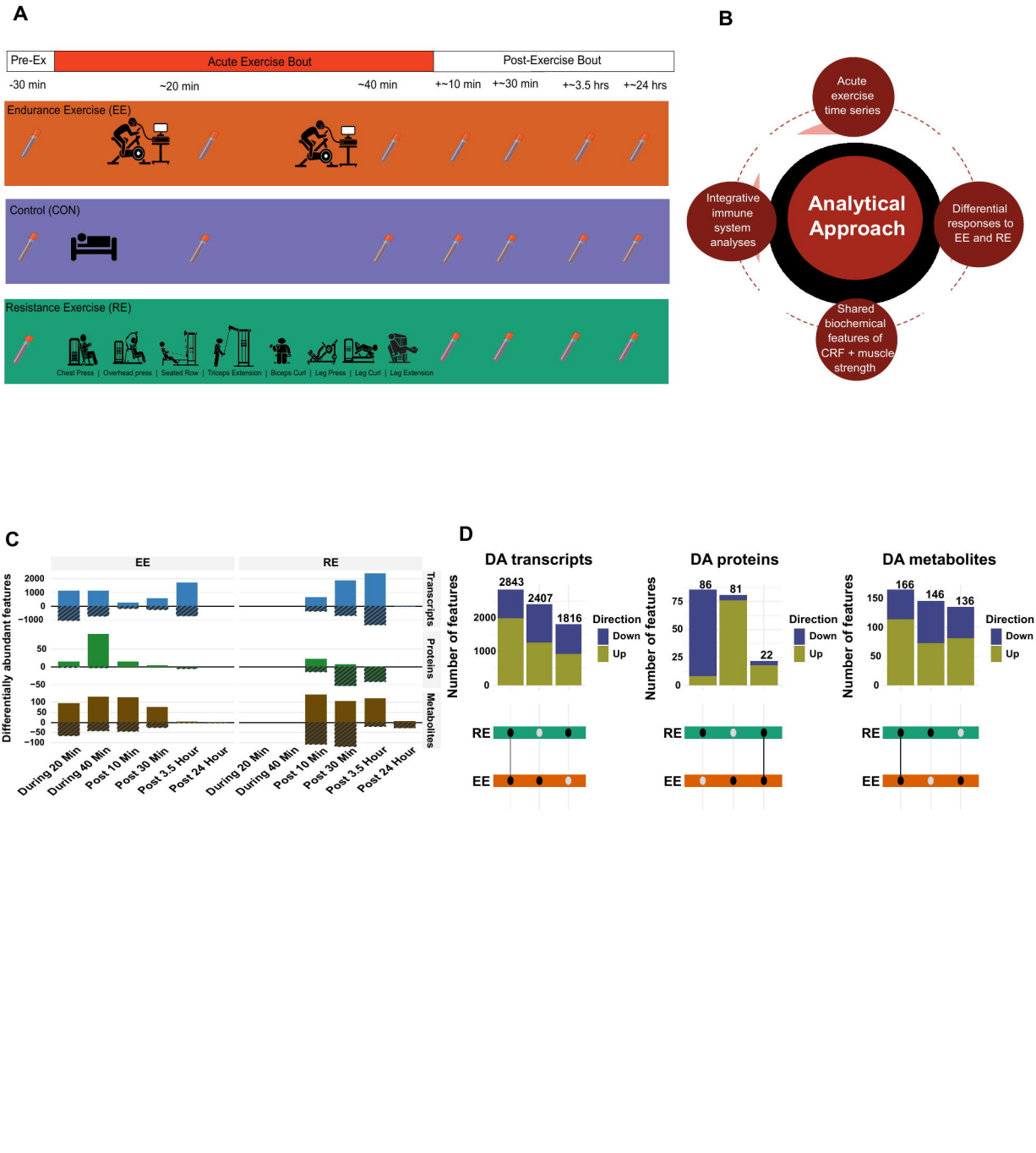
A
Pre-Ex
Acute Exercise Bout
Post-Exercise Bout
-30 min
~20 min
~40 min
+~10 min
+~30 min
+~3.5 hrs
+~24 hrs
Endurance Exercise (EE)
Control (CON)
Resistance Exercise (RE)
Chest Press | Overhead press | Seated Row | Triceps Extension | Biceps Curl | Leg Press | Leg Curl | Leg Extension
B
Acute exercise time series
Integrative immune system analyses
Analytical Approach
Differential responses to EE and RE
Shared biochemical features of CRF + muscle strength
C
EE
RE
Differentially abundant features
Transcripts
Proteins
Metabolites
During 20 Min
During 40 Min
Post 10 Min
Post 30 Min
Post 3.5 Hour
Post 24 Hour
D
DA transcripts
DA proteins
DA metabolites
Number of features
Direction
Down
Up
2843
2407
1816
86
81
22
166
146
136
RE
EE

Figure S1

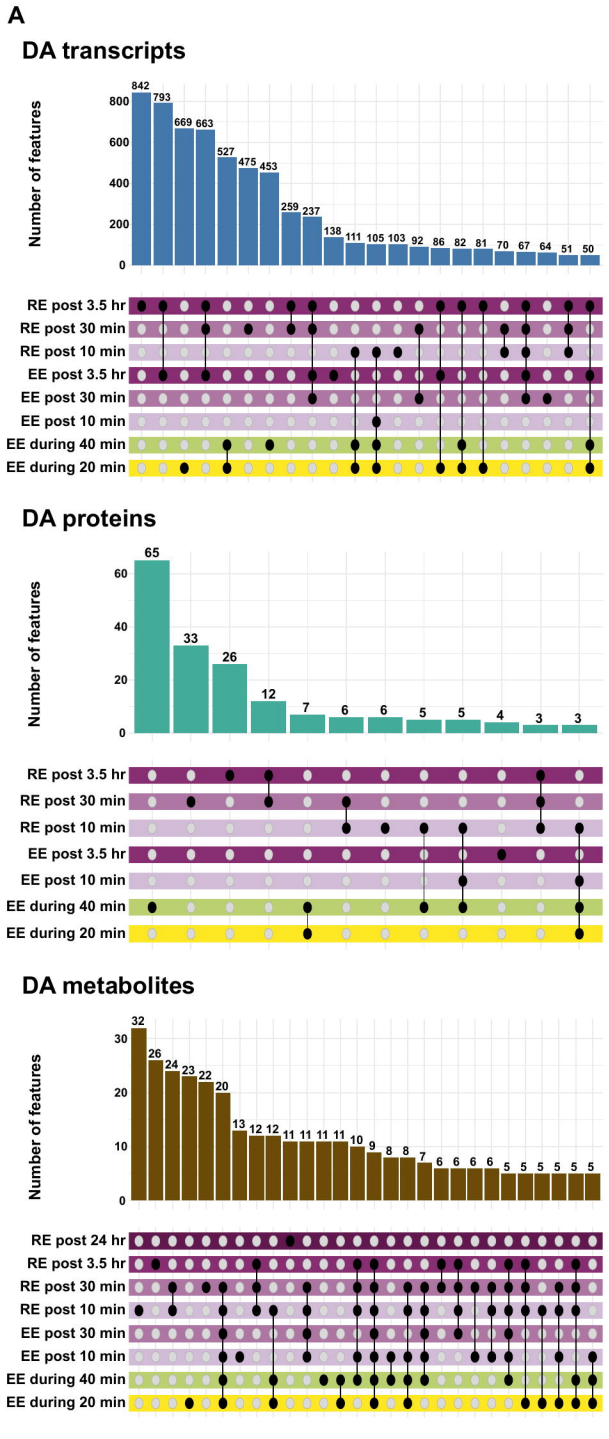
A
DA transcripts
Number of features
842 793 669 663 527 475 453 259 237 138 111 105 103 92 86 82 81 70 67 64 51 50
RE post 3.5 hr
RE post 30 min
RE post 10 min
EE post 3.5 hr
EE post 30 min
EE post 10 min
EE during 40 min
EE during 20 min
DA proteins
Number of features
65 33 26 12 7 6 6 5 5 4 3 3
RE post 3.5 hr
RE post 30 min
RE post 10 min
EE post 3.5 hr
EE post 10 min
EE during 40 min
EE during 20 min
DA metabolites
Number of features
32 26 24 23 22 20 13 12 12 11 11 11 11 10 9 8 8 7 6 6 6 6 5 5 5 5 5 5
RE post 24 hr
RE post 3.5 hr
RE post 30 min
RE post 10 min
EE post 30 min
EE post 10 min
EE during 40 min
EE during 20 min

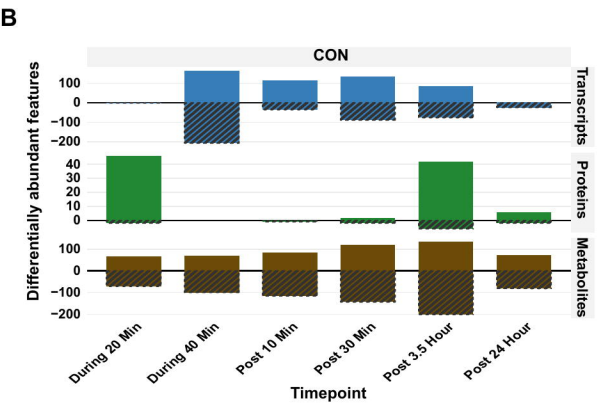
B
CON
Differentially abundant features
Transcripts
Proteins
Metabolites
During 20 Min
During 40 Min
Post 10 Min
Post 30 Min
Post 3.5 Hour
Post 24 Hour
Timepoint

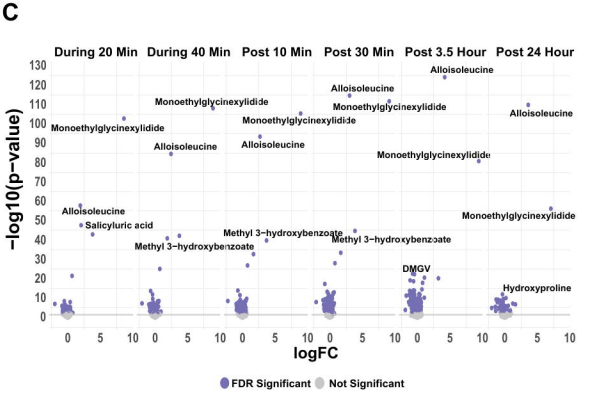
C
During 20 Min
During 40 Min
Post 10 Min
Post 30 Min
Post 3.5 Hour
Post 24 Hour
−log10(p−value)
logFC
Alloisoleucine
Monoethylglycinexylidide
Salicyluric acid
Methyl 3−hydroxybenzoate
DMGV
Hydroxyproline
FDR Significant
Not Significant

Figure 2

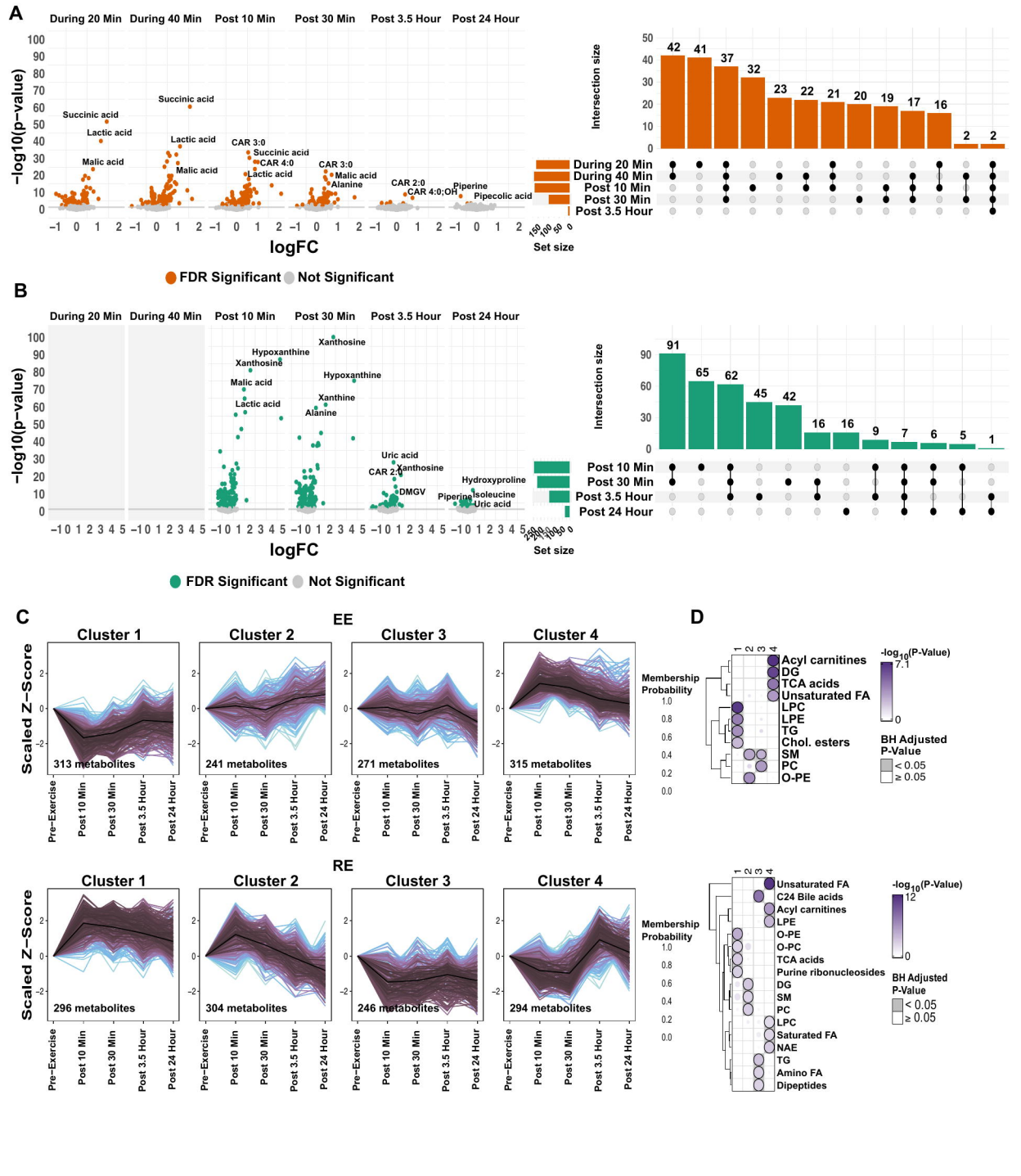
A
During 20 Min
During 40 Min
Post 10 Min
Post 30 Min
Post 3.5 Hour
Post 24 Hour
−log10(p−value)
logFC
Succinic acid
Lactic acid
Malic acid
CAR 3:0
CAR 4:0
Alanine
CAR 2:0
CAR 4:0;OH
Piperine
Pipecolic acid
Intersection size
42
41
37
32
23
22
21
20
19
17
16
2
2
Set size
FDR Significant
Not Significant
B
Hypoxanthine
Xanthosine
Xanthine
Uric acid
DMGV
Hydroxyproline
Isoleucine
91
65
62
45
42
16
16
9
7
6
5
1
C
EE
RE
Cluster 1
Cluster 2
Cluster 3
Cluster 4
Scaled Z−Score
313 metabolites
241 metabolites
271 metabolites
315 metabolites
296 metabolites
304 metabolites
246 metabolites
294 metabolites
Pre−Exercise
Post 10 Min
Post 30 Min
Post 3.5 Hour
Post 24 Hour
D
Membership Probability
Acyl carnitines
DG
TCA acids
Unsaturated FA
LPC
LPE
TG
Chol. esters
SM
PC
O-PE
C24 Bile acids
O-PC
Purine ribonucleosides
Saturated FA
NAE
Amino FA
Dipeptides
-log10(P-Value)
BH Adjusted P-Value
< 0.05
≥ 0.05

Figure S2

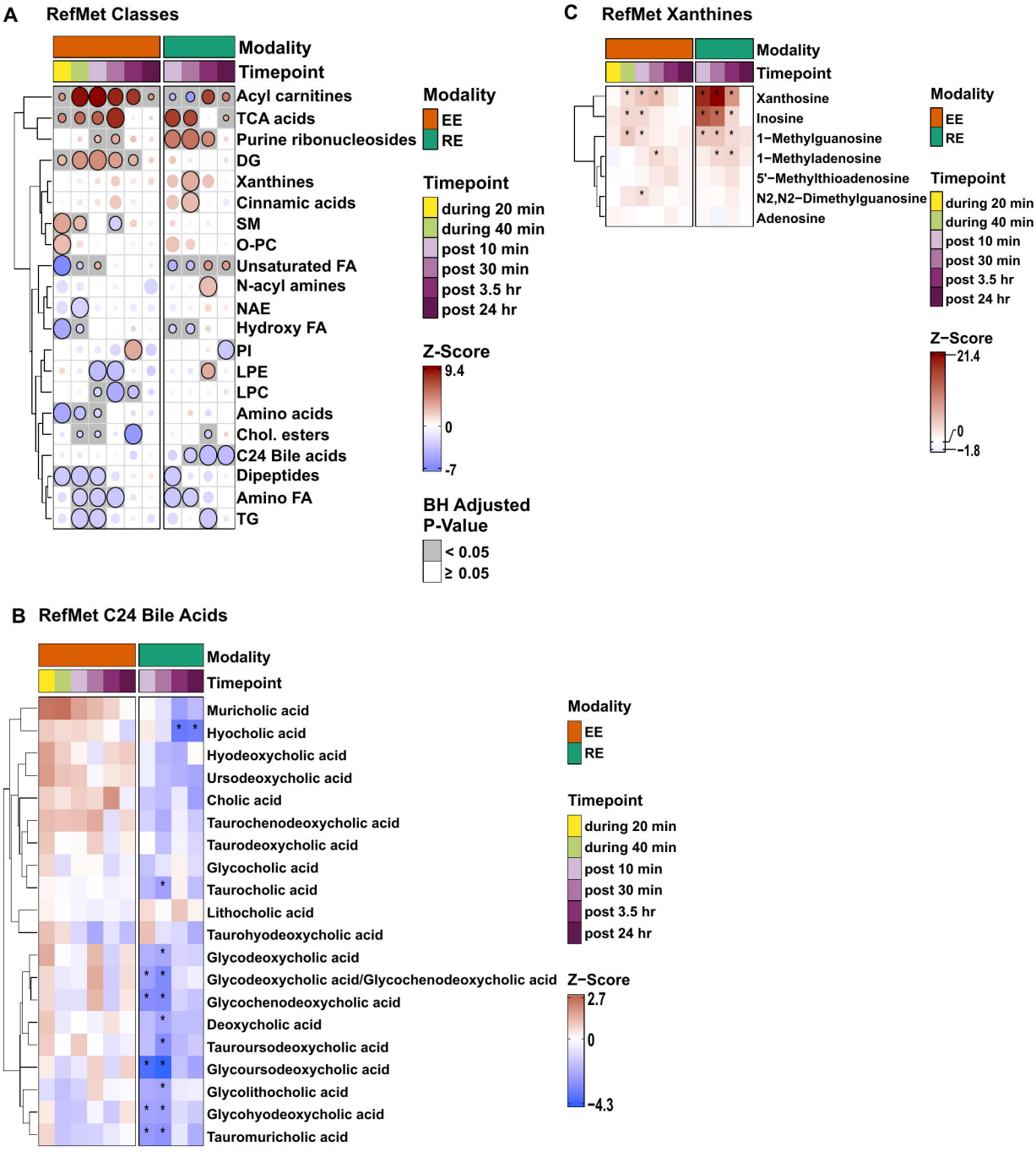
A
RefMet Classes
Modality
Timepoint
Acyl carnitines
TCA acids
Purine ribonucleosides
DG
Xanthines
Cinnamic acids
SM
O-PC
Unsaturated FA
N-acyl amines
NAE
Hydroxy FA
PI
LPE
LPC
Amino acids
Chol. esters
C24 Bile acids
Dipeptides
Amino FA
TG
Modality
EE
RE
Timepoint
during 20 min
during 40 min
post 10 min
post 30 min
post 3.5 hr
post 24 hr
Z-Score
9.4
0
-7
BH Adjusted P-Value
< 0.05
≥ 0.05
C
RefMet Xanthines
Modality
Timepoint
Xanthosine
Inosine
1−Methylguanosine
1−Methyladenosine
5'−Methylthioadenosine
N2,N2−Dimethylguanosine
Adenosine
Modality
EE
RE
Timepoint
during 20 min
during 40 min
post 10 min
post 30 min
post 3.5 hr
post 24 hr
Z−Score
21.4
0
−1.8
B
RefMet C24 Bile Acids
Modality
Timepoint
Muricholic acid
Hyocholic acid
Hyodeoxycholic acid
Ursodeoxycholic acid
Cholic acid
Taurochenodeoxycholic acid
Taurodeoxycholic acid
Glycocholic acid
Taurocholic acid
Lithocholic acid
Taurohyodeoxycholic acid
Glycodeoxycholic acid
Glycodeoxycholic acid/Glycochenodeoxycholic acid
Glycochenodeoxycholic acid
Deoxycholic acid
Tauroursodeoxycholic acid
Glycoursodeoxycholic acid
Glycolithocholic acid
Glycohyodeoxycholic acid
Tauromuricholic acid
Modality
EE
RE
Timepoint
during 20 min
during 40 min
post 10 min
post 30 min
post 3.5 hr
post 24 hr
Z−Score
2.7
0
−4.3

Figure 3

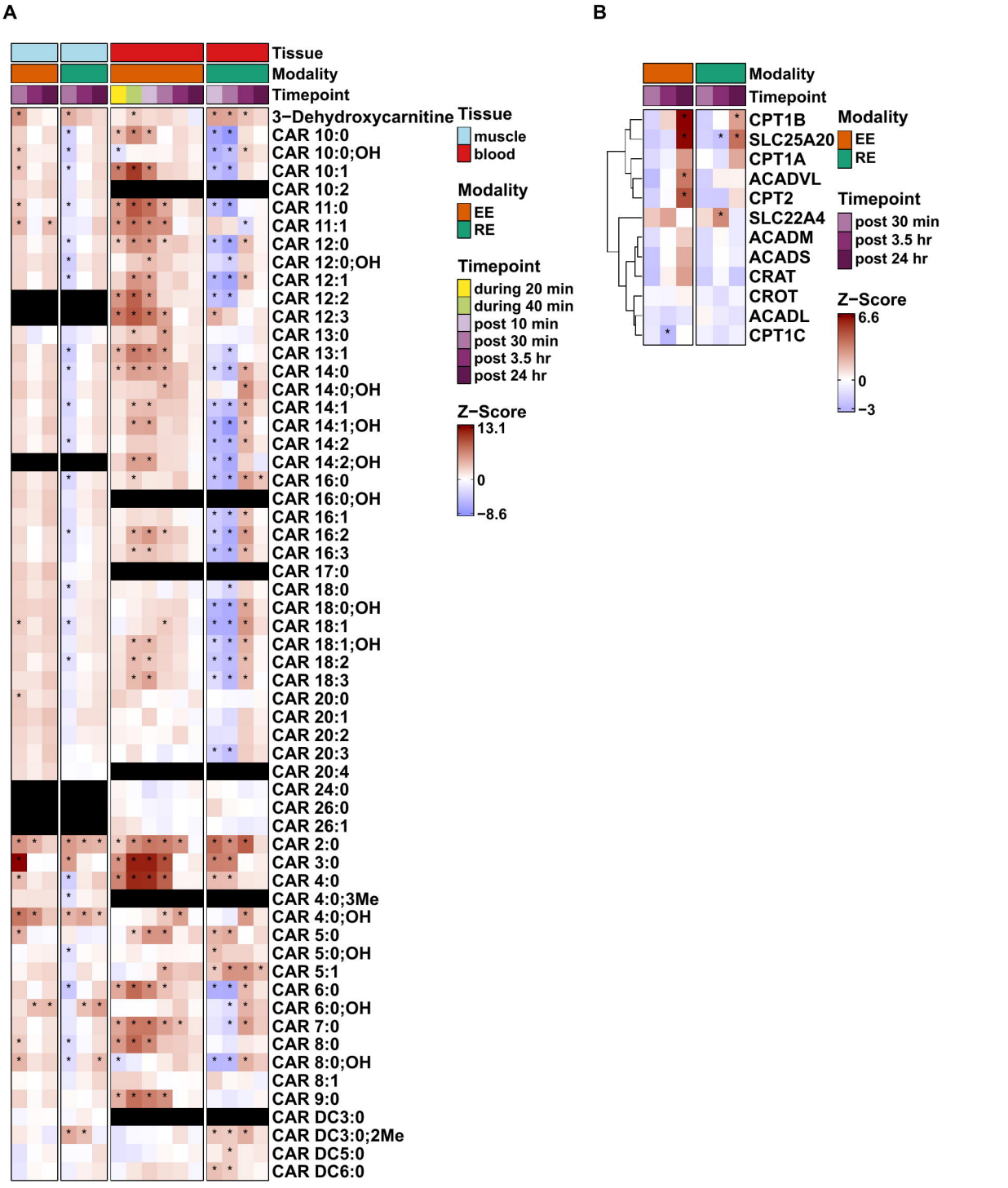
A
Tissue
Modality
Timepoint
3−Dehydroxycarnitine
CAR 10:0
CAR 10:0;OH
CAR 10:1
CAR 10:2
CAR 11:0
CAR 11:1
CAR 12:0
CAR 12:0;OH
CAR 12:1
CAR 12:2
CAR 12:3
CAR 13:0
CAR 13:1
CAR 14:0
CAR 14:0;OH
CAR 14:1
CAR 14:1;OH
CAR 14:2
CAR 14:2;OH
CAR 16:0
CAR 16:0;OH
CAR 16:1
CAR 16:2
CAR 16:3
CAR 17:0
CAR 18:0
CAR 18:0;OH
CAR 18:1
CAR 18:1;OH
CAR 18:2
CAR 18:3
CAR 20:0
CAR 20:1
CAR 20:2
CAR 20:3
CAR 20:4
CAR 24:0
CAR 26:0
CAR 26:1
CAR 2:0
CAR 3:0
CAR 4:0
CAR 4:0;3Me
CAR 4:0;OH
CAR 5:0
CAR 5:0;OH
CAR 5:1
CAR 6:0
CAR 6:0;OH
CAR 7:0
CAR 8:0
CAR 8:0;OH
CAR 8:1
CAR 9:0
CAR DC3:0
CAR DC3:0;2Me
CAR DC5:0
CAR DC6:0
Tissue
muscle
blood
Modality
EE
RE
Timepoint
during 20 min
during 40 min
post 10 min
post 30 min
post 3.5 hr
post 24 hr
Z−Score
13.1
0
−8.6
B
Modality
Timepoint
CPT1B
SLC25A20
CPT1A
ACADVL
CPT2
SLC22A4
ACADM
ACADS
CRAT
CROT
ACADL
CPT1C
Modality
EE
RE
Timepoint
post 30 min
post 3.5 hr
post 24 hr
Z−Score
6.6
0
−3

Figure S3

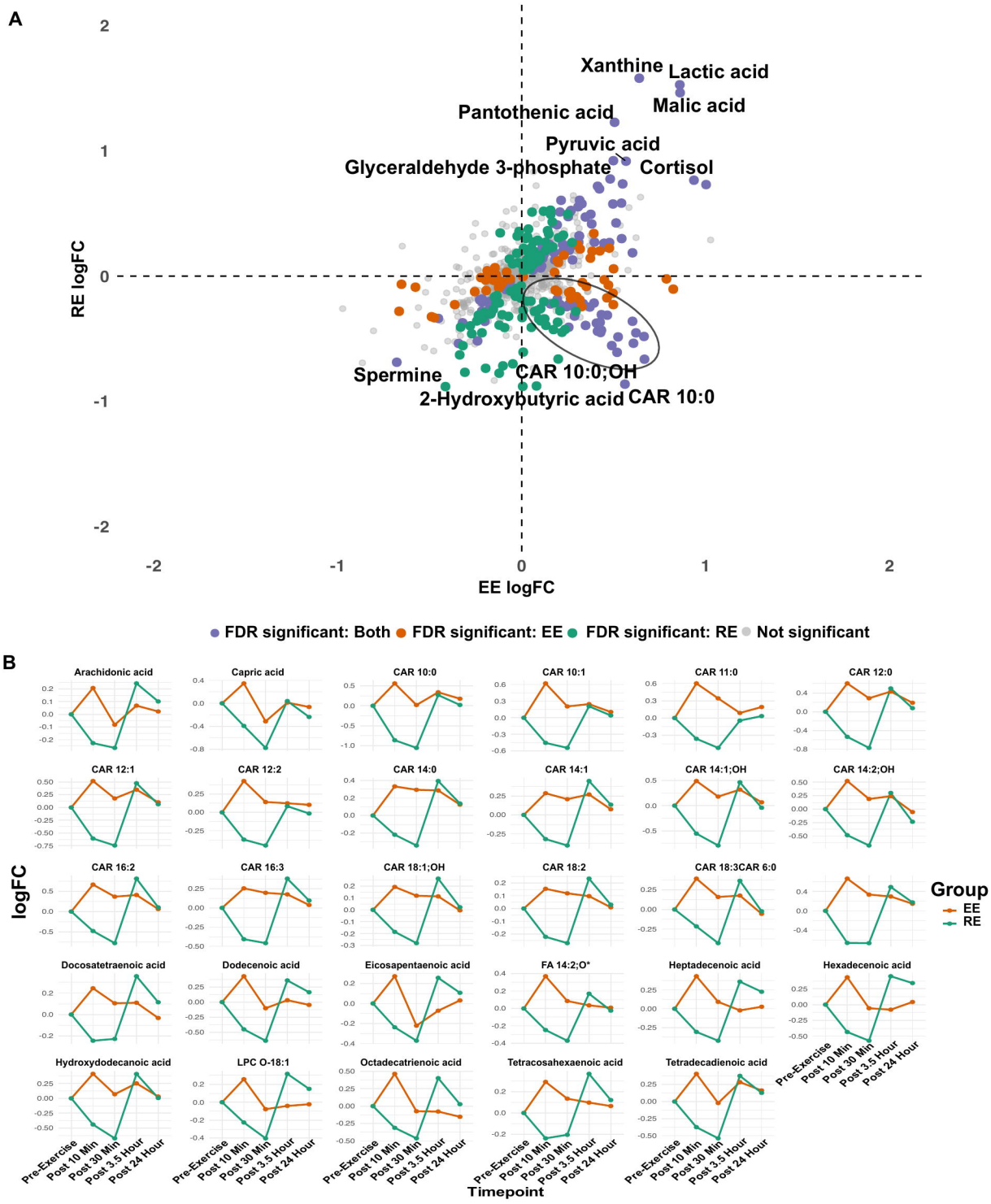
A
Xanthine
Lactic acid
Malic acid
Pantothenic acid
Pyruvic acid
Glyceraldehyde 3-phosphate
Cortisol
Spermine
CAR 10:0;OH
2-Hydroxybutyric acid
CAR 10:0
RE logFC
EE logFC
FDR significant: Both
FDR significant: EE
FDR significant: RE
Not significant
B
Arachidonic acid
Capric acid
CAR 10:0
CAR 10:1
CAR 11:0
CAR 12:0
CAR 12:1
CAR 12:2
CAR 14:0
CAR 14:1
CAR 14:1;OH
CAR 14:2;OH
CAR 16:2
CAR 16:3
CAR 18:1;OH
CAR 18:2
CAR 18:3CAR 6:0
Docosatetraenoic acid
Dodecenoic acid
Eicosapentaenoic acid
FA 14:2;O*
Heptadecenoic acid
Hexadecenoic acid
Hydroxydodecanoic acid
LPC O-18:1
Octadecatrienoic acid
Tetracosahexaenoic acid
Tetradecadienoic acid
logFC
Pre-Exercise
Post 10 Min
Post 30 Min
Post 3.5 Hour
Post 24 Hour
Timepoint
Group
EE
RE

Figure 4

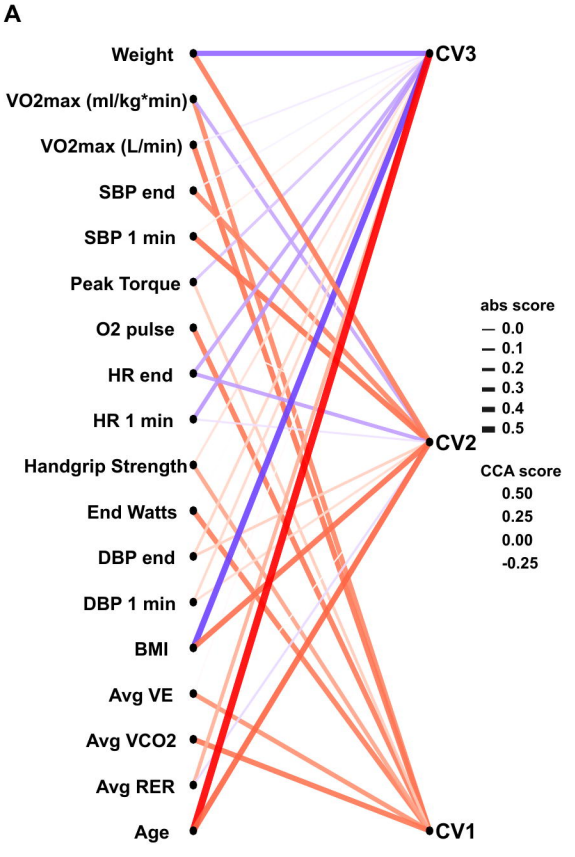
A
Weight
VO2max (ml/kg*min)
VO2max (L/min)
SBP end
SBP 1 min
Peak Torque
O2 pulse
HR end
HR 1 min
Handgrip Strength
End Watts
DBP end
DBP 1 min
BMI
Avg VE
Avg VCO2
Avg RER
Age
CV3
CV2
CV1
abs score
0.0
0.1
0.2
0.3
0.4
0.5
CCA score
0.50
0.25
0.00
-0.25

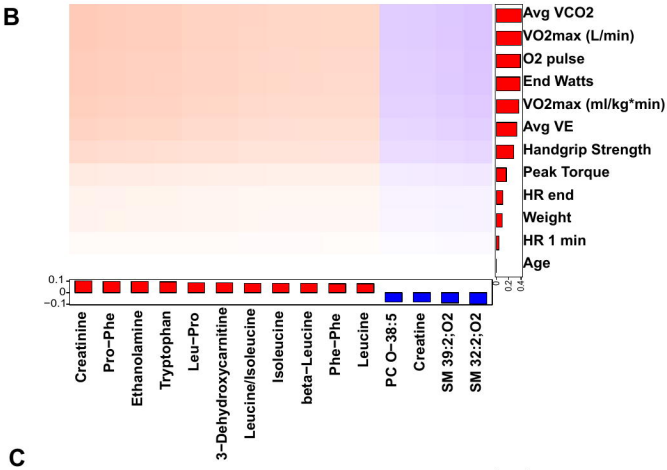
B
Avg VCO2
VO2max (L/min)
O2 pulse
End Watts
VO2max (ml/kg*min)
Avg VE
Handgrip Strength
Peak Torque
HR end
Weight
HR 1 min
Age
Creatinine
Pro−Phe
Ethanolamine
Tryptophan
Leu−Pro
3−Dehydroxycarnitine
Leucine/Isoleucine
Isoleucine
beta−Leucine
Phe−Phe
Leucine
PC O−38:5
Creatine
SM 39:2;O2
SM 32:2;O2

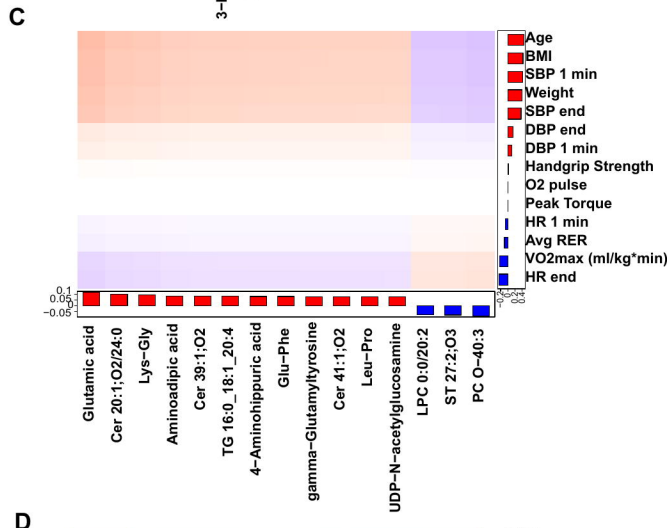
C
Age
BMI
SBP 1 min
Weight
SBP end
DBP end
DBP 1 min
Handgrip Strength
O2 pulse
Peak Torque
HR 1 min
Avg RER
VO2max (ml/kg*min)
HR end
Glutamic acid
Cer 20:1;O2/24:0
Lys−Gly
Aminoadipic acid
Cer 39:1;O2
TG 16:0_18:1_20:4
4−Aminohippuric acid
Glu−Phe
gamma−Glutamyltyrosine
Cer 41:1;O2
Leu−Pro
UDP−N−acetylglucosamine
LPC 0:0/20:2
ST 27:2;O3
PC O−40:3

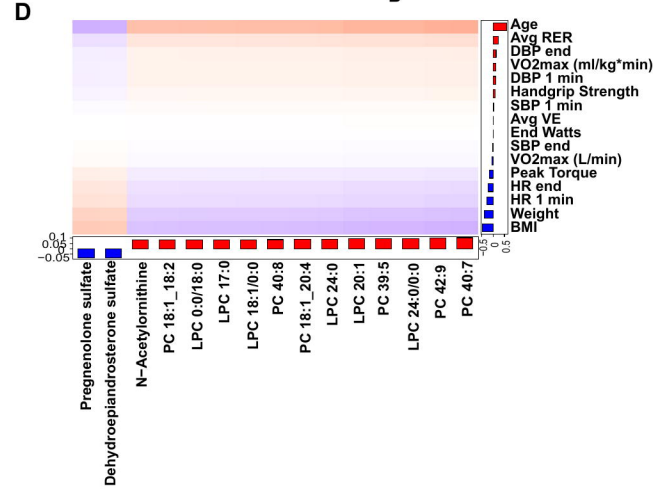
D
Age
Avg RER
DBP end
VO2max (ml/kg*min)
DBP 1 min
Handgrip Strength
SBP 1 min
Avg VE
End Watts
SBP end
VO2max (L/min)
Peak Torque
HR end
HR 1 min
Weight
BMI
Pregnenolone sulfate
Dehydroepiandrosterone sulfate
N−Acetylornithine
PC 18:1_18:2
LPC 0:0/18:0
LPC 17:0
LPC 18:1/0:0
PC 40:8
PC 18:1_20:4
LPC 24:0
LPC 20:1
PC 39:5
LPC 24:0/0:0
PC 42:9
PC 40:7

Figure 5

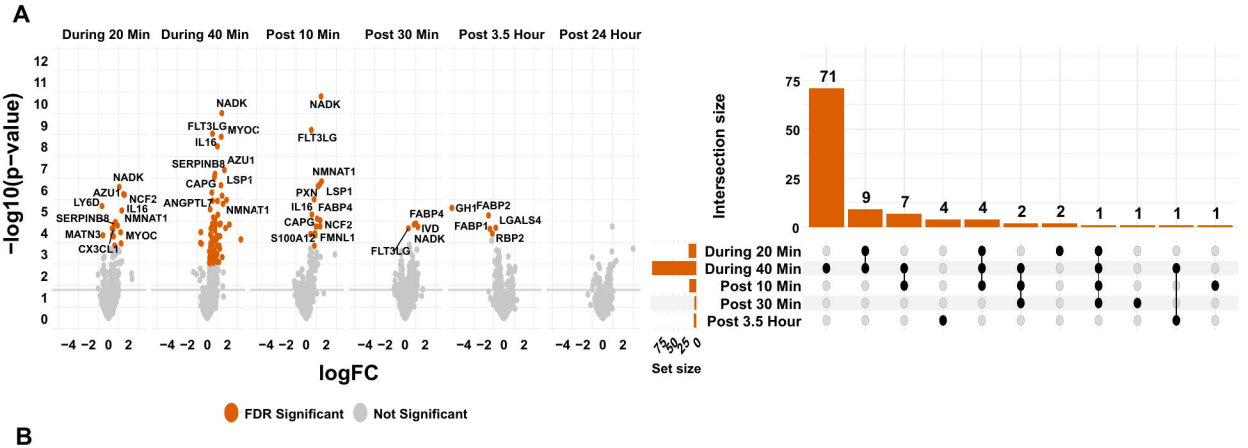
A
During 20 Min
During 40 Min
Post 10 Min
Post 30 Min
Post 3.5 Hour
Post 24 Hour
−log10(p−value)
logFC
FDR Significant
Not Significant
Intersection size
Set size
During 20 Min
During 40 Min
Post 10 Min
Post 30 Min
Post 3.5 Hour

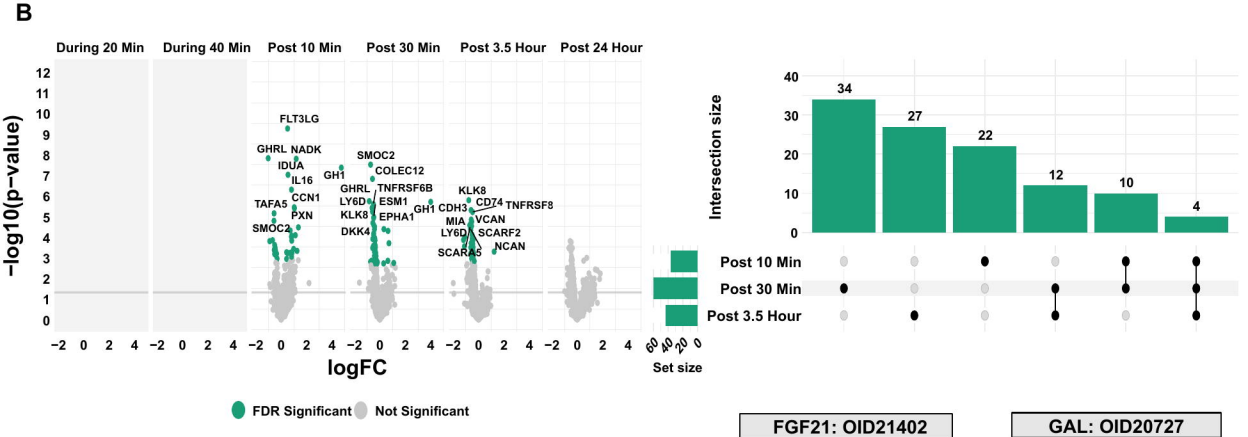
B
During 20 Min
During 40 Min
Post 10 Min
Post 30 Min
Post 3.5 Hour
Post 24 Hour
−log10(p−value)
logFC
FDR Significant
Not Significant
Intersection size
Set size
Post 10 Min
Post 30 Min
Post 3.5 Hour

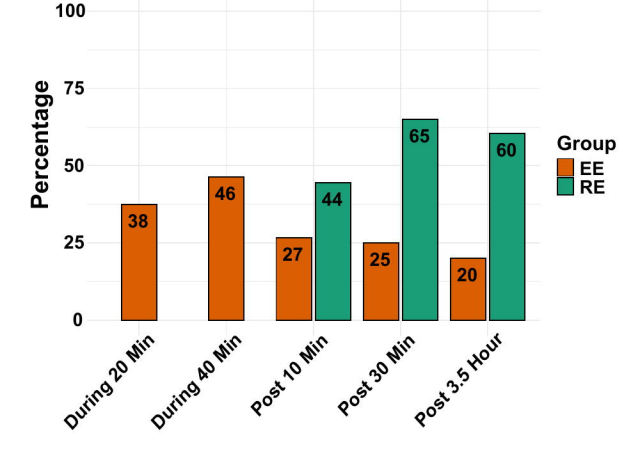
C
Percentage
Group
EE
RE
During 20 Min
During 40 Min
Post 10 Min
Post 30 Min
Post 3.5 Hour

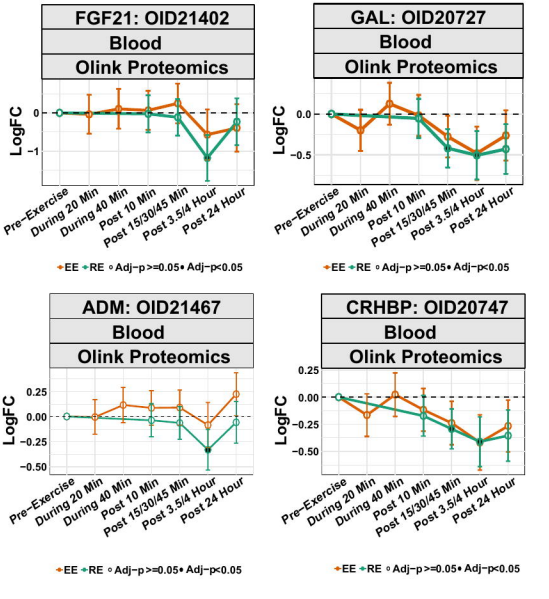
D
FGF21: OID21402
GAL: OID20727
ADM: OID21467
CRHBP: OID20747
Blood
Olink Proteomics
LogFC
Pre−Exercise
During 20 Min
During 40 Min
Post 10 Min
Post 15/30/45 Min
Post 3.5/4 Hour
Post 24 Hour
EE
RE
Adj−p>=0.05
Adj−p<0.05

Figure S5

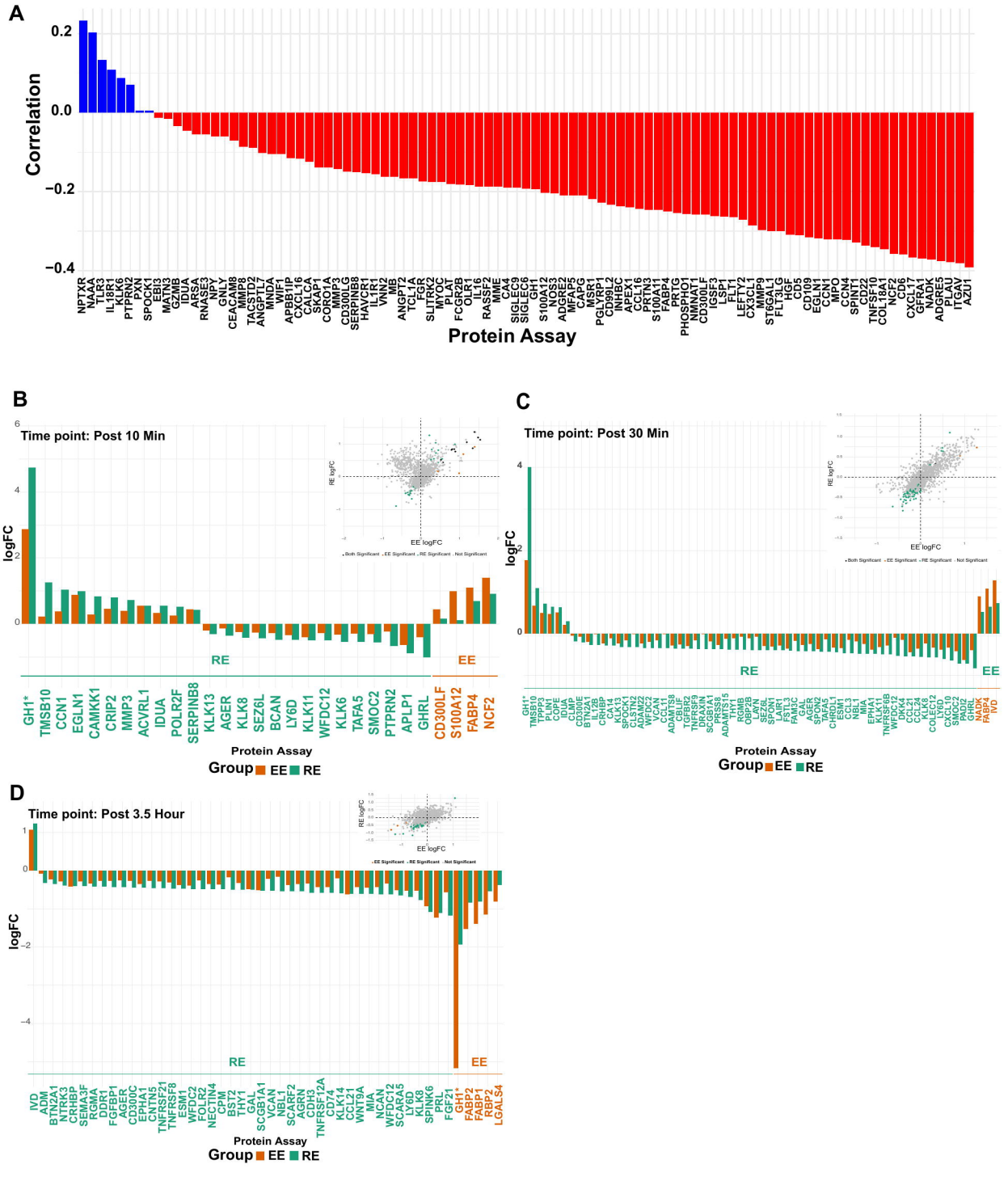
A
Correlation
0.2
0.0
−0.2
−0.4
NPTXR NAA TLR3 IL18R1 KLK6 PTPRN2 PXN SPOCK1 EBI3 MATN3 GZMB IDUA ARSA RNASE3 NPY GNLY CEACAM8 MMP8 TACSTD2 ANGPTL7 MNDA WIF1 APBB1IP CXCL16 CALCA KLK1 CORO1A MMP3 CD300LG SERPINB8 HAVCR1 UMOD VNN2 MB ANGPT2 TCL1A FGR SLITRK2 MYOC PLAT FCGR2B OLR1 IL16 RASSF2 MME CA4 SIGLEC9 SIGLEC6 GH1 S100A12 NOS3 ADGRE2 MFAP5 CAPG MSR1 PGLYRP1 CD99L2 INHBC APEX1 CCL16 PRTN3 S100A11 FABP4 PRTG PHOSPHO1 NMNAT1 CD300LF IGSF3 SPP1 FLT1 LEFTY2 CX3CL1 MMP9 STC1 FLT3LG HGF CD5 CD109 EGLN1 CHI3L1 MPO CCN4 SPINT1 CD22 TNFSF10 COL14A1 NCF2 CD6 CXCL17 GFRA1 NADK ADGRE5 PLAG1 ITGAV AZU1
Protein Assay
B
Time point: Post 10 Min
logFC
6
4
2
0
RE logFC
EE logFC
Both Significant EE Significant RE Significant Not Significant
RE
EE
GH1* TMSB10 CCN1 EGLN1 CAMKK1 CRIP2 MMP3 ACVRL1 IDUA POLR2F SERPINB8 KLK13 AGER KLK8 SEZ6L BCAN LY6D KLK11 WFDC12 KLK6 TAFA5 SMOC2 PTPRN2 APLP1 GHRL CD300LF S100A12 FABP4 NCF2
Protein Assay
Group EE RE
C
Time point: Post 30 Min
logFC
4
2
0
RE logFC
EE logFC
Both Significant EE Significant RE Significant Not Significant
RE
EE
GH1* TMSB10 CCN1 EGLN1 CAMKK1 CRIP2 MMP3 ACVRL1 IDUA POLR2F SERPINB8 KLK13 AGER KLK8 SEZ6L BCAN LY6D KLK11 WFDC12 KLK6 TAFA5 SMOC2 PTPRN2 APLP1 GHRL CD300LF S100A12 FABP4 NCF2
Protein Assay
Group EE RE
D
Time point: Post 3.5 Hour
logFC
1
0
−2
−4
RE logFC
EE logFC
EE Significant RE Significant Not Significant
RE
EE
IVD ADM BTN2A1 NTRK3 CRHBP SEMA3F RGMA DDR1 FGFBP1 AGER CD300C EPHA1 CNTN5 TNFRSF21 TNFRSF8 ESM1 WFDC2 FOLR2 NECTIN4 CPM BST2 THY1 GAL SCGB1A1 VCAN NBL1 SCARF2 AGRN CDH3 TNFRSF12A CD74 KLK14 CCL21 WNT9A MIA NCAN WFDC12 SCARA5 LY6D KLK6 SPINK6 PRL FGF21 GH1* FABP2 FABP1 RBP2 LGALS4
Protein Assay
Group EE RE

Figure 6

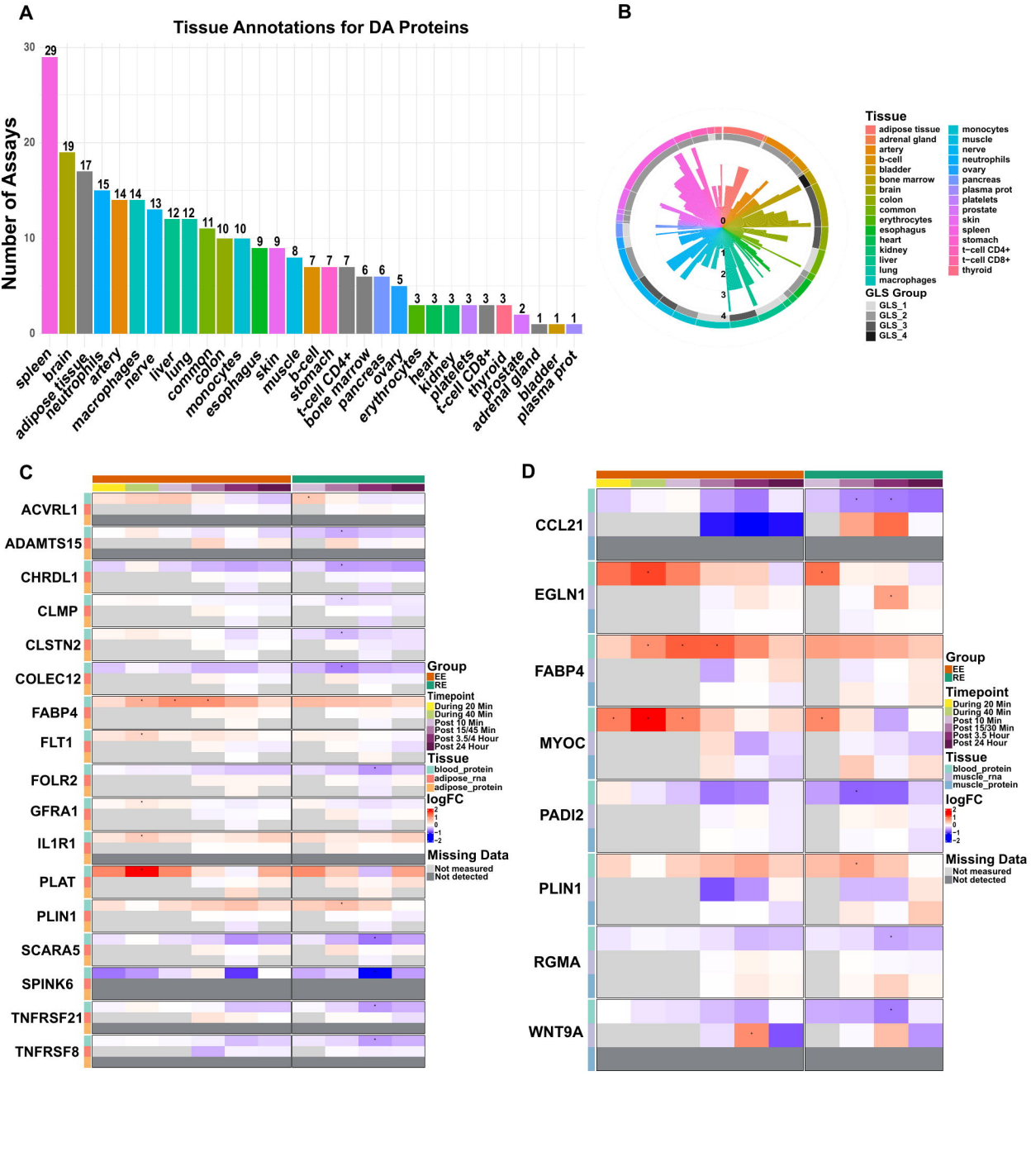
A
Tissue Annotations for DA Proteins
Number of Assays
30
20
10
0
29
19
17
15
14 14
13
12 12
11
10 10
9 9
8
7 7 7
6 6
5
3 3 3 3 3 3
2
1 1 1
spleen
brain
adipose tissue
neutrophils
artery
macrophages
nerve
liver
lung
common
colon
monocytes
esophagus
skin
muscle
b-cell
stomach
t-cell CD4+
bone marrow
pancreas
ovary
erythrocytes
heart
kidney
platelets
t-cell CD8+
thyroid
prostate
adrenal gland
bladder
plasma prot
B
Tissue
adipose tissue
adrenal gland
artery
b-cell
bladder
bone marrow
brain
colon
common
erythrocytes
esophagus
heart
kidney
liver
lung
macrophages
monocytes
muscle
nerve
neutrophils
ovary
pancreas
plasma prot
platelets
prostate
skin
spleen
stomach
t−cell CD4+
t−cell CD8+
thyroid
GLS Group
GLS_1
GLS_2
GLS_3
GLS_4
C
ACVRL1
ADAMTS15
CHRDL1
CLMP
CLSTN2
COLEC12
FABP4
FLT1
FOLR2
GFRA1
IL1R1
PLAT
PLIN1
SCARA5
SPINK6
TNFRSF21
TNFRSF8
Group
EE
RE
Timepoint
During 20 Min
During 40 Min
Post 10 Min
Post 15/45 Min
Post 3.5/4 Hour
Post 24 Hour
Tissue
blood_protein
adipose_rna
adipose_protein
logFC
Missing Data
Not measured
Not detected
D
CCL21
EGLN1
FABP4
MYOC
PADI2
PLIN1
RGMA
WNT9A
Group
EE
RE
Timepoint
During 20 Min
During 40 Min
Post 10 Min
Post 15/30 Min
Post 3.5 Hour
Post 24 Hour
Tissue
blood_protein
muscle_rna
muscle_protein
logFC
Missing Data
Not measured
Not detected

Figure S6

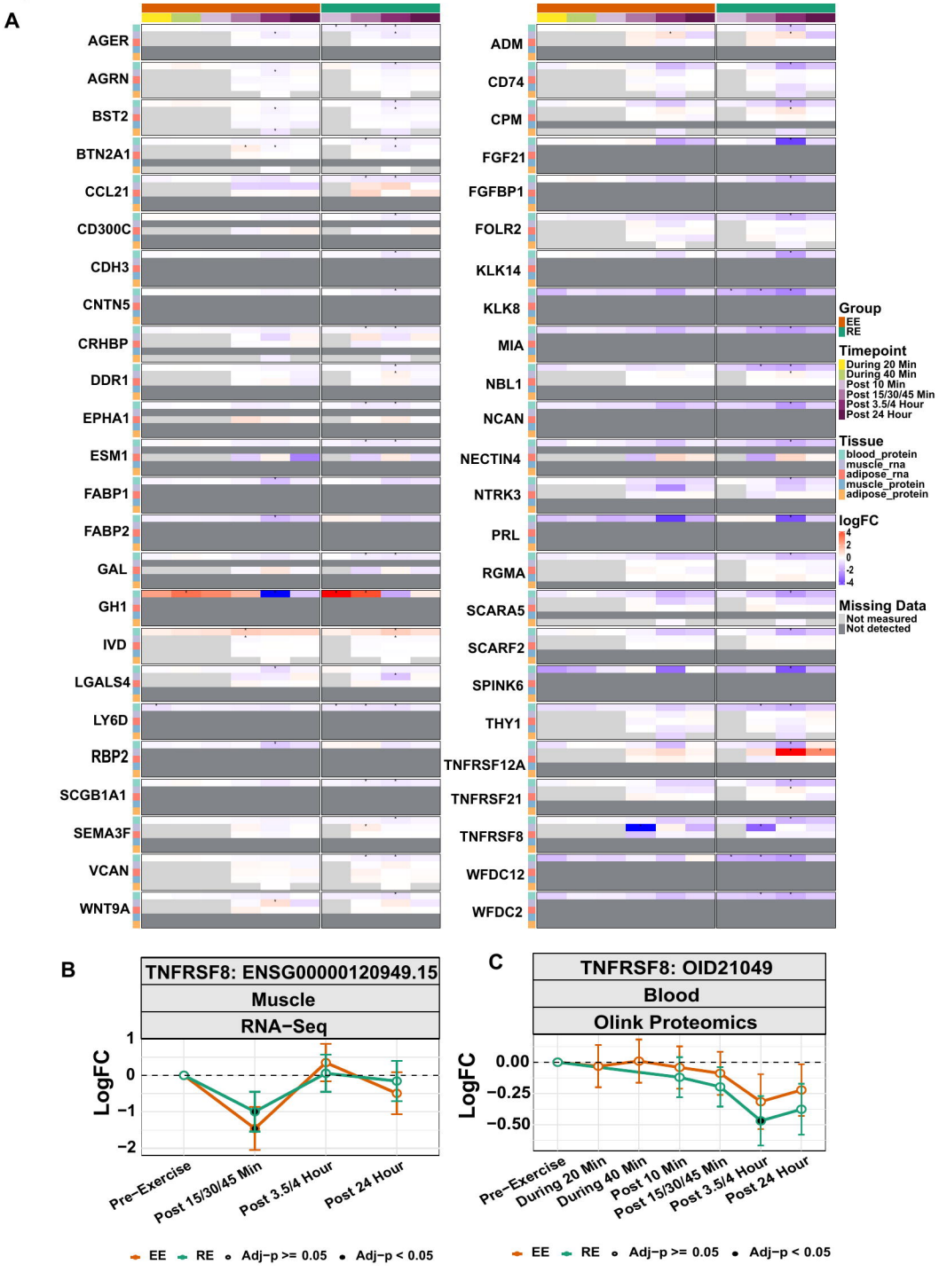
A
AGER
AGRN
BST2
BTN2A1
CCL21
CD300C
CDH3
CNTN5
CRHBP
DDR1
EPHA1
ESM1
FABP1
FABP2
GAL
GH1
IVD
LGALS4
LY6D
RBP2
SCGB1A1
SEMA3F
VCAN
WNT9A
ADM
CD74
CPM
FGF21
FGFBP1
FOLR2
KLK14
KLK8
MIA
NBL1
NCAN
NECTIN4
NTRK3
PRL
RGMA
SCARA5
SCARF2
SPINK6
THY1
TNFRSF12A
TNFRSF21
TNFRSF8
WFDC12
WFDC2
Group
EE
RE
Timepoint
During 20 Min
During 40 Min
Post 10 Min
Post 15/30/45 Min
Post 3.5/4 Hour
Post 24 Hour
Tissue
blood_protein
muscle_rna
adipose_rna
muscle_protein
adipose_protein
logFC
4
2
0
-2
-4
Missing Data
Not measured
Not detected
B
TNFRSF8: ENSG00000120949.15
Muscle
RNA−Seq
LogFC
1
0
−1
−2
Pre−Exercise
Post 15/30/45 Min
Post 3.5/4 Hour
Post 24 Hour
EE
RE
Adj−p >= 0.05
Adj−p < 0.05
C
TNFRSF8: OID21049
Blood
Olink Proteomics
LogFC
0.00
−0.25
−0.50
Pre−Exercise
During 20 Min
During 40 Min
Post 10 Min
Post 15/30/45 Min
Post 3.5/4 Hour
Post 24 Hour
EE
RE
Adj−p >= 0.05
Adj−p < 0.05

Figure 7

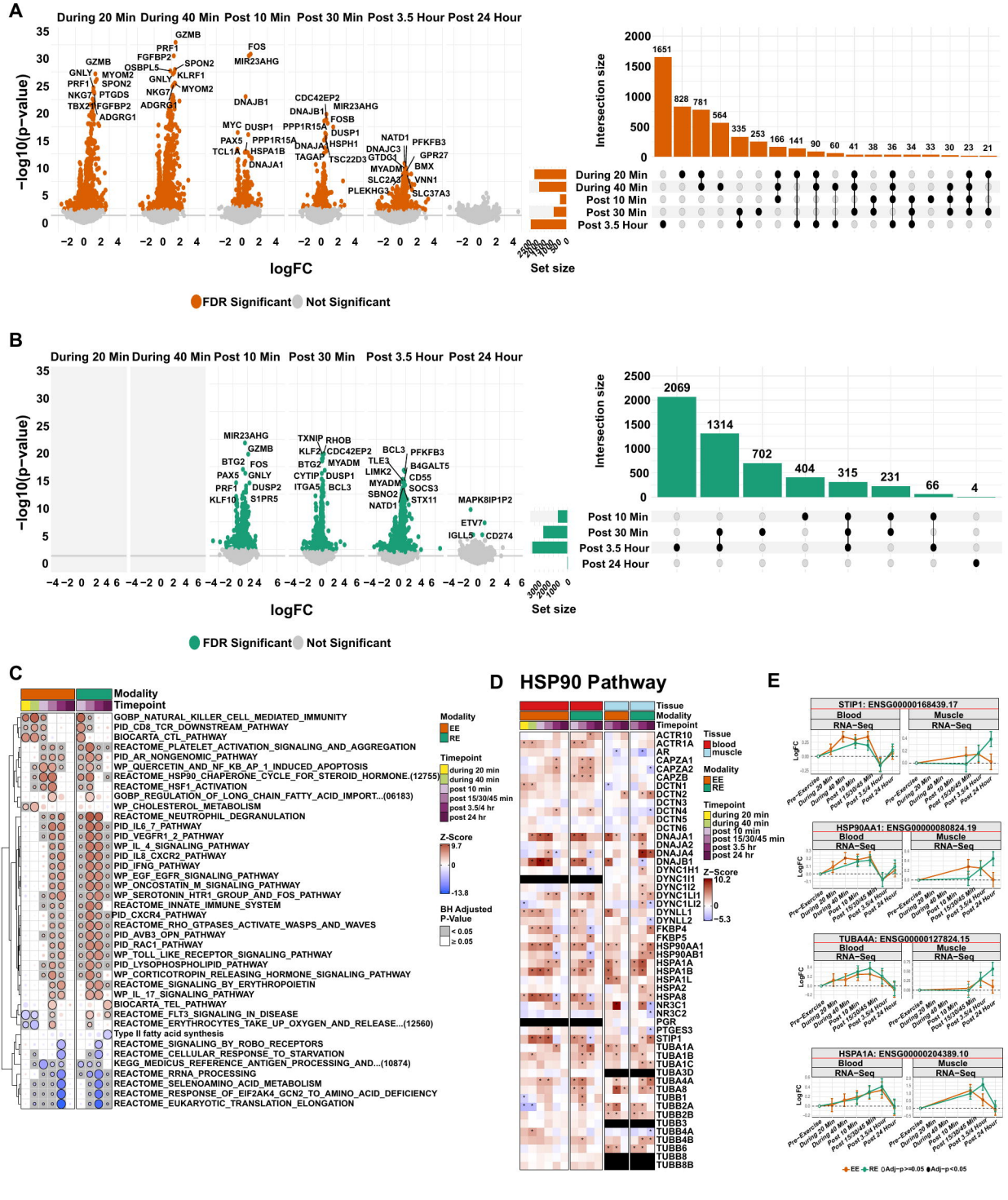
A
During 20 Min During 40 Min Post 10 Min Post 30 Min Post 3.5 Hour Post 24 Hour
−log10(p−value)
logFC
FDR Significant Not Significant
Intersection size
2000
1500
1000
500
0
1651
828
781
564
335
253
166
141
90
60
41
38
36
34
33
30
23
21
During 20 Min
During 40 Min
Post 10 Min
Post 30 Min
Post 3.5 Hour
Set size
B
During 20 Min During 40 Min Post 10 Min Post 30 Min Post 3.5 Hour Post 24 Hour
−log10(p−value)
logFC
FDR Significant Not Significant
Intersection size
2500
2000
1500
1000
500
0
2069
1314
702
404
315
231
66
4
Post 10 Min
Post 30 Min
Post 3.5 Hour
Post 24 Hour
Set size
C
Modality
Timepoint
GOBP_NATURAL_KILLER_CELL_MEDIATED_IMMUNITY
PID_CD8_TCR_DOWNSTREAM_PATHWAY
BIOCARTA_CTL_PATHWAY
REACTOME_PLATELET_ACTIVATION_SIGNALING_AND_AGGREGATION
PID_AR_NONGENOMIC_PATHWAY
PID_QUERCETIN_AND_NF_KB_AP_1_INDUCED_APOPTOSIS
REACTOME_HSP90_CHAPERONE_CYCLE_FOR_STEROID_HORMONE...(12755)
REACTOME_HSF1_ACTIVATION
GOBP_REGULATION_OF_LONG_CHAIN_FATTY_ACID_IMPORT...(06183)
WP_CHOLESTEROL_METABOLISM
REACTOME_NEUTROPHIL_DEGRANULATION
PID_IL6_7_PATHWAY
PID_VEGFR1_2_PATHWAY
WP_IL_4_SIGNALING_PATHWAY
PID_IL8_CXCR2_PATHWAY
PID_IFNG_PATHWAY
WP_EGF_EGFR_SIGNALING_PATHWAY
WP_ONCOSTATIN_M_SIGNALING_PATHWAY
WP_SEROTONIN_HTR1_GROUP_AND_FOS_PATHWAY
REACTOME_INNATE_IMMUNE_SYSTEM
PID_CXCR4_PATHWAY
REACTOME_RHO_GTPASES_ACTIVATE_WASPS_AND_WAVES
PID_AVB3_OPN_PATHWAY
PID_RAC1_PATHWAY
WP_TOLL_LIKE_RECEPTOR_SIGNALING_PATHWAY
PID_LYSOPHOSPHOLIPID_PATHWAY
WP_CORTICOTROPIN_RELEASING_HORMONE_SIGNALING_PATHWAY
REACTOME_SIGNALING_BY_ERYTHROPOIETIN
WP_IL_17_SIGNALING_PATHWAY
BIOCARTA_TEL_PATHWAY
REACTOME_FLT3_SIGNALING_IN_DISEASE
REACTOME_ERYTHROCYTES_TAKE_UP_OXYGEN_AND_RELEASE...(12560)
Type II fatty acid synthesis
REACTOME_SIGNALING_BY_ROBO_RECEPTORS
REACTOME_CELLULAR_RESPONSE_TO_STARVATION
KEGG_MEDICUS_REFERENCE_ANTIGEN_PROCESSING_AND...(10874)
REACTOME_RRNA_PROCESSING
REACTOME_SELENOAMINO_ACID_METABOLISM
REACTOME_RESPONSE_OF_EIF2AK4_GCN2_TO_AMINO_ACID_DEFICIENCY
REACTOME_EUKARYOTIC_TRANSLATION_ELONGATION
Modality
EE
RE
Timepoint
during 20 min
during 40 min
post 10 min
post 15/30/45 min
post 3.5/4 hr
post 24 hr
Z-Score
9.7
0
-13.8
BH Adjusted P-Value
< 0.05
≥ 0.05
D HSP90 Pathway
Tissue
Modality
Timepoint
ACTR10
ACTR1A
AR
CAPZA1
CAPZA2
CAPZB
DCTN1
DCTN2
DCTN3
DCTN4
DCTN5
DCTN6
DNAJA1
DNAJA2
DNAJA4
DNAJB1
DYNC1H1
DYNC1I1
DYNC1I2
DYNC1LI1
DYNC1LI2
DYNLL1
DYNLL2
FKBP4
FKBP5
HSP90AA1
HSP90AB1
HSPA1A
HSPA1B
HSPA1L
HSPA2
HSPA8
NR3C1
NR3C2
PGR
PTGES3
STIP1
TUBA1A
TUBA1B
TUBA1C
TUBA3D
TUBA4A
TUBA8
TUBB1
TUBB2A
TUBB2B
TUBB3
TUBB4A
TUBB4B
TUBB6
TUBB8
TUBB8B
Tissue
blood
muscle
Modality
EE
RE
Timepoint
during 20 min
during 40 min
post 10 min
post 15/30/45 min
post 3.5 hr
post 24 hr
Z-Score
10.2
0
-5.3
E
STIP1: ENSG00000168439.17
HSP90AA1: ENSG00000080824.19
TUBA4A: ENSG00000127824.15
HSPA1A: ENSG00000204389.10
Blood
Muscle
RNA−Seq
LogFC
Pre−Exercise
During 20 Min
During 40 Min
Post 10 Min
Post 15/30/45 Min
Post 3.5/4 Hour
Post 24 Hour
EE
RE
Adj−p>=0.05
Adj−p<0.05

Figure S7

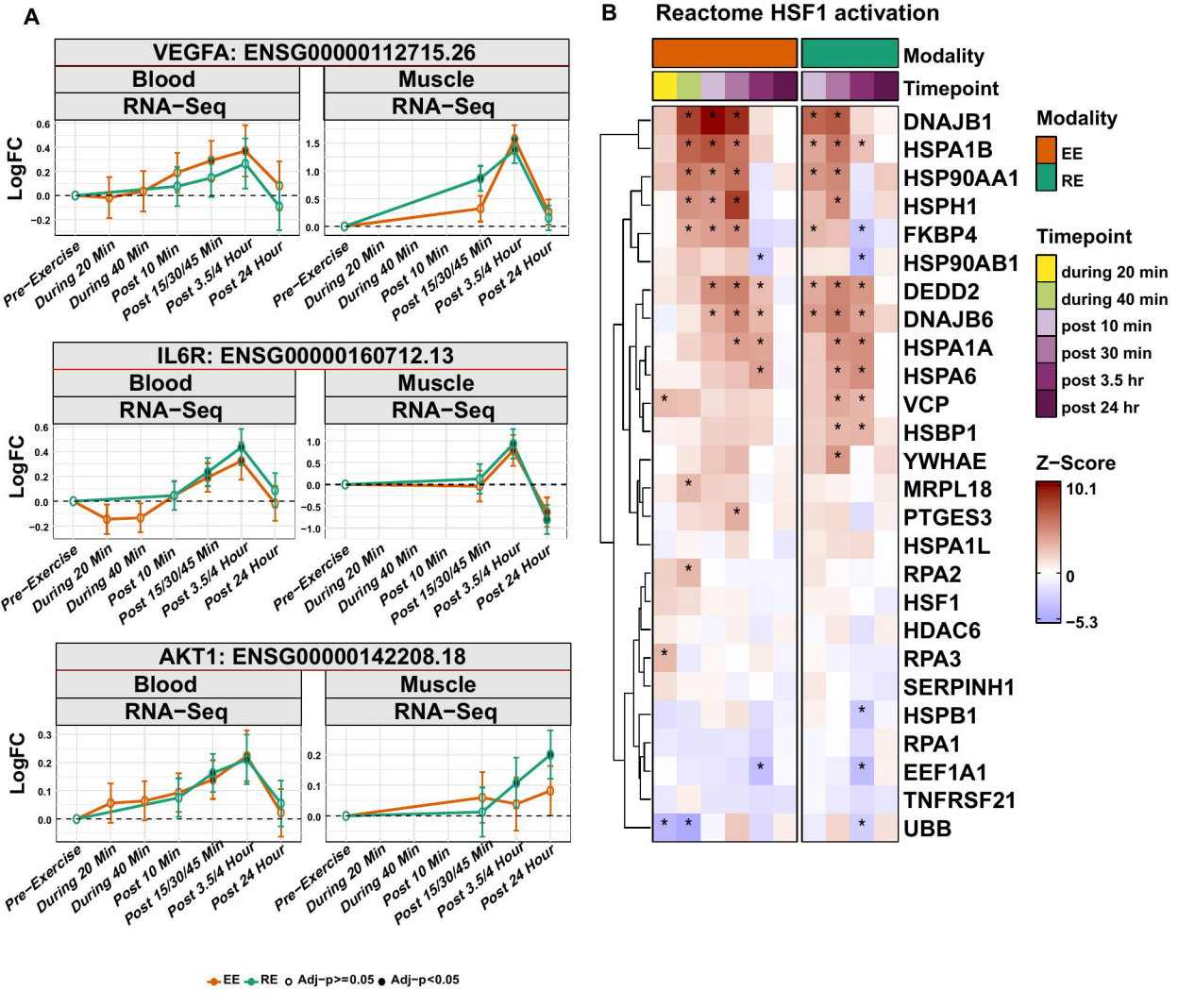
A
VEGFA: ENSG00000112715.26
Blood
Muscle
RNA−Seq
RNA−Seq
LogFC
IL6R: ENSG00000160712.13
AKT1: ENSG00000142208.18
Pre−Exercise
During 20 Min
During 40 Min
Post 10 Min
Post 15/30/45 Min
Post 3.5/4 Hour
Post 24 Hour
EE
RE
Adj−p>=0.05
Adj−p<0.05
B
Reactome HSF1 activation
Modality
Timepoint
DNAJB1
HSPA1B
HSP90AA1
HSPH1
FKBP4
HSP90AB1
DEDD2
DNAJB6
HSPA1A
HSPA6
VCP
HSBP1
YWHAE
MRPL18
PTGES3
HSPA1L
RPA2
HSF1
HDAC6
RPA3
SERPINH1
HSPB1
RPA1
EEF1A1
TNFRSF21
UBB
during 20 min
during 40 min
post 10 min
post 30 min
post 3.5 hr
post 24 hr
Z−Score
10.1
0
−5.3

Figure 8

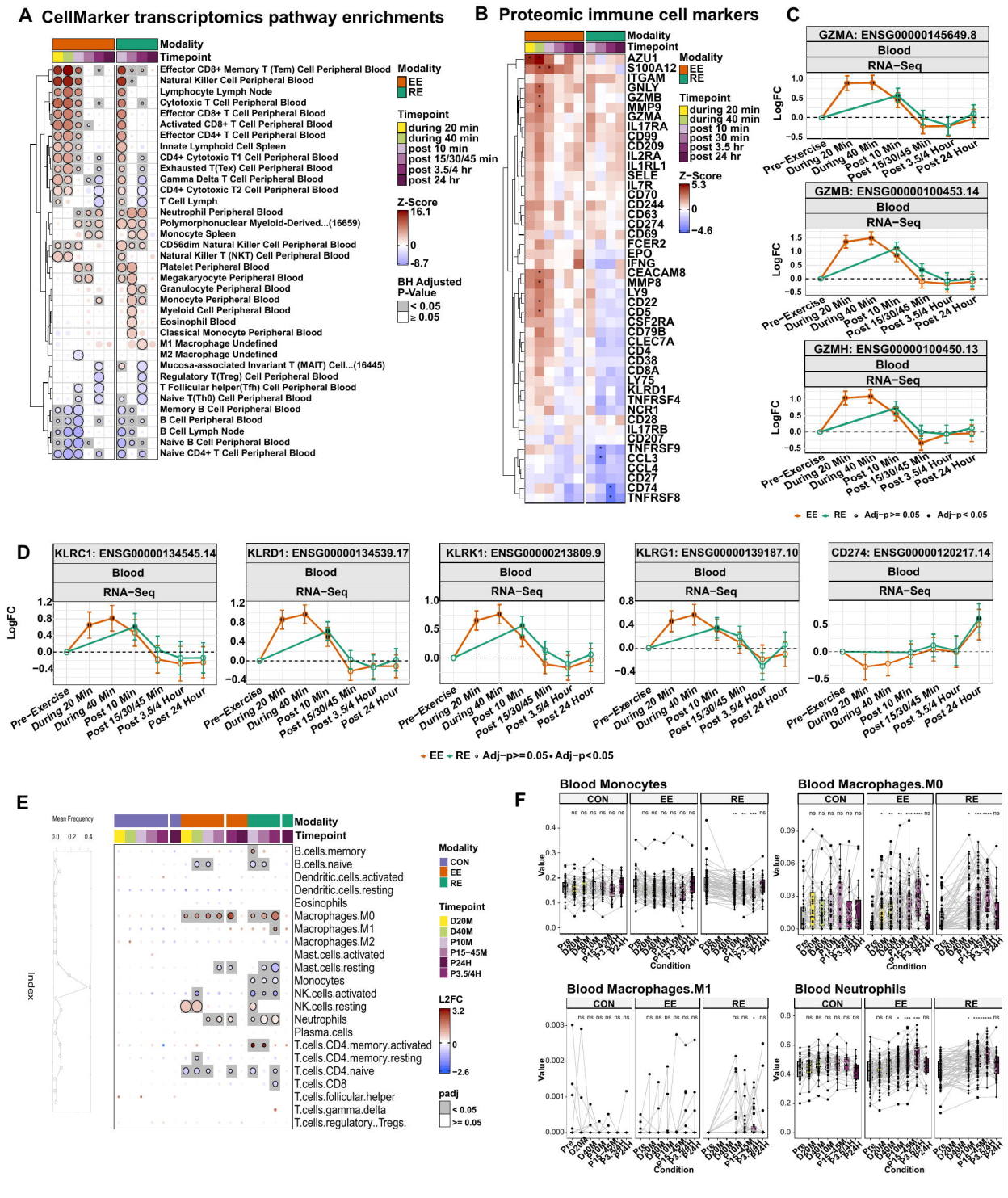
A CellMarker transcriptomics pathway enrichments
Modality
Timepoint
Effector CD8+ Memory T (Tem) Cell Peripheral Blood
Natural Killer Cell Peripheral Blood
Lymphocyte Lymph Node
Cytotoxic T Cell Peripheral Blood
Effector CD8+ T Cell Peripheral Blood
Activated CD8+ T Cell Peripheral Blood
Effector CD4+ T Cell Peripheral Blood
Innate Lymphoid Cell Spleen
CD4+ Cytotoxic T1 Cell Peripheral Blood
Exhausted T(Tex) Cell Peripheral Blood
Gamma Delta T Cell Peripheral Blood
CD4+ Cytotoxic T2 Cell Peripheral Blood
T Cell Lymph
Neutrophil Peripheral Blood
Polymorphonuclear Myeloid-Derived...(16659)
Monocyte Spleen
CD56dim Natural Killer Cell Peripheral Blood
Natural Killer T (NKT) Cell Peripheral Blood
Platelet Peripheral Blood
Megakaryocyte Peripheral Blood
Granulocyte Peripheral Blood
Monocyte Peripheral Blood
Myeloid Cell Peripheral Blood
Eosinophil Blood
Classical Monocyte Peripheral Blood
M1 Macrophage Undefined
M2 Macrophage Undefined
Mucosa-associated Invariant T (MAIT) Cell...(16445)
Regulatory T(Treg) Cell Peripheral Blood
T Follicular helper(Tfh) Cell Peripheral Blood
Naive T(Th0) Cell Peripheral Blood
Memory B Cell Peripheral Blood
B Cell Peripheral Blood
B Cell Lymph Node
Naive B Cell Peripheral Blood
Naive CD4+ T Cell Peripheral Blood
Modality
EE
RE
Timepoint
during 20 min
during 40 min
post 10 min
post 15/30/45 min
post 3.5/4 hr
post 24 hr
Z-Score
16.1
0
-8.7
BH Adjusted P-Value
< 0.05
≥ 0.05
B Proteomic immune cell markers
Modality
Timepoint
AZU1
S100A12
ITGAM
GNLY
GZMB
MMP9
GZMA
IL17RA
CD99
CD209
IL2RA
IL1RL1
SELE
IL7R
CD70
CD244
CD63
CD274
CD69
FCER2
EPO
IFNG
CEACAM8
MMP8
LY9
CD22
CD5
CSF2RA
CD79B
CLEC7A
CD4
CD38
CD8A
LY75
KLRD1
TNFRSF4
NCR1
CD28
IL17RB
CD207
TNFRSF9
CCL3
CCL4
CD27
CD74
TNFRSF8
Modality
EE
RE
Timepoint
during 20 min
during 40 min
post 10 min
post 30 min
post 3.5 hr
post 24 hr
Z-Score
5.3
0
-4.6
C
GZMA: ENSG00000145649.8
GZMB: ENSG00000100453.14
GZMH: ENSG00000100450.13
Blood
RNA-Seq
LogFC
Pre-Exercise
During 20 Min
During 40 Min
Post 10 Min
Post 15/30/45 Min
Post 3.5/4 Hour
Post 24 Hour
EE
RE
Adj-p>= 0.05
Adj-p< 0.05
D
KLRC1: ENSG00000134545.14
KLRD1: ENSG00000134539.17
KLRK1: ENSG00000213809.9
KLRG1: ENSG00000139187.10
CD274: ENSG00000120217.14
Blood
RNA-Seq
LogFC
Pre-Exercise
During 20 Min
During 40 Min
Post 10 Min
Post 15/30/45 Min
Post 3.5/4 Hour
Post 24 Hour
EE
RE
Adj-p>=0.05
Adj-p<0.05
E
Mean Frequency
0.0
0.2
0.4
Modality
Timepoint
B.cells.memory
B.cells.naive
Dendritic.cells.activated
Dendritic.cells.resting
Eosinophils
Macrophages.M0
Macrophages.M1
Macrophages.M2
Mast.cells.activated
Mast.cells.resting
Monocytes
NK.cells.activated
NK.cells.resting
Neutrophils
Plasma.cells
T.cells.CD4.memory.activated
T.cells.CD4.memory.resting
T.cells.CD4.naive
T.cells.CD8
T.cells.follicular.helper
T.cells.gamma.delta
T.cells.regulatory..Tregs.
Index
Modality
CON
EE
RE
Timepoint
D20M
D40M
P10M
P15-45M
P24H
P3.5/4H
L2FC
3.2
0
-2.6
padj
< 0.05
>= 0.05
F
Blood Monocytes
Blood Macrophages.M0
Blood Macrophages.M1
Blood Neutrophils
CON
EE
RE
Value
Condition
P0M
D20M
D40M
P10M
P15-45M
P3.5/4H
P24H

Figure S8

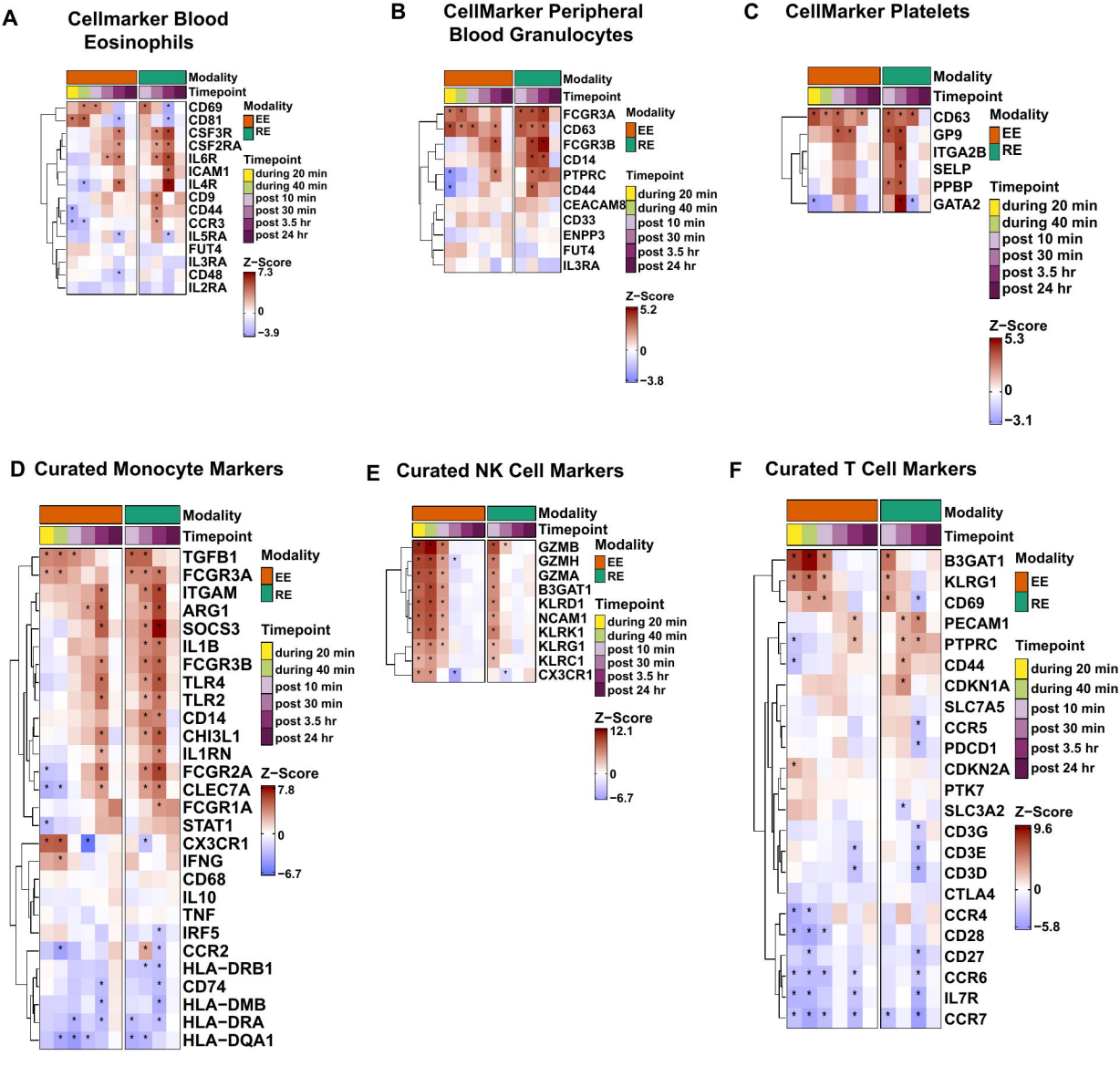
A
Cellmarker Blood Eosinophils
Modality
Timepoint
CD69
CD81
CSF3R
CSF2RA
IL6R
ICAM1
IL4R
CD9
CD44
CCR3
IL5RA
FUT4
IL3RA
CD48
IL2RA
Modality
EE
RE
Timepoint
during 20 min
during 40 min
post 10 min
post 30 min
post 3.5 hr
post 24 hr
Z−Score
7.3
0
−3.9
B
CellMarker Peripheral Blood Granulocytes
Modality
Timepoint
FCGR3A
CD63
FCGR3B
CD14
PTPRC
CD44
CEACAM8
CD33
ENPP3
FUT4
IL3RA
Modality
EE
RE
Timepoint
during 20 min
during 40 min
post 10 min
post 30 min
post 3.5 hr
post 24 hr
Z−Score
5.2
0
−3.8
C
CellMarker Platelets
Modality
Timepoint
CD63
GP9
ITGA2B
SELP
PPBP
GATA2
Modality
EE
RE
Timepoint
during 20 min
during 40 min
post 10 min
post 30 min
post 3.5 hr
post 24 hr
Z−Score
5.3
0
−3.1
D
Curated Monocyte Markers
Modality
Timepoint
TGFB1
FCGR3A
ITGAM
ARG1
SOCS3
IL1B
FCGR3B
TLR4
TLR2
CD14
CHI3L1
IL1RN
FCGR2A
CLEC7A
FCGR1A
STAT1
CX3CR1
IFNG
CD68
IL10
TNF
IRF5
CCR2
HLA−DRB1
CD74
HLA−DMB
HLA−DRA
HLA−DQA1
Modality
EE
RE
Timepoint
during 20 min
during 40 min
post 10 min
post 30 min
post 3.5 hr
post 24 hr
Z−Score
7.8
0
−6.7
E
Curated NK Cell Markers
Modality
Timepoint
GZMB
GZMH
GZMA
B3GAT1
KLRD1
NCAM1
KLRK1
KLRG1
KLRC1
CX3CR1
Modality
EE
RE
Timepoint
during 20 min
during 40 min
post 10 min
post 30 min
post 3.5 hr
post 24 hr
Z−Score
12.1
0
−6.7
F
Curated T Cell Markers
Modality
Timepoint
B3GAT1
KLRG1
CD69
PECAM1
PTPRC
CD44
CDKN1A
SLC7A5
CCR5
PDCD1
CDKN2A
PTK7
SLC3A2
CD3G
CD3E
CD3D
CTLA4
CCR4
CD28
CD27
CCR6
IL7R
CCR7
Modality
EE
RE
Timepoint
during 20 min
during 40 min
post 10 min
post 30 min
post 3.5 hr
post 24 hr
Z−Score
9.6
0
−5.8